ON PAGE

Form Approved
OMB No. 0704-0188

Public rep... gathering... collection... Davis Hig...

1 hour per response, including the time for reviewing instructions, searching existing data sources, ...llection of information. Send comments regarding this burden estimate or any other aspect of this ...ington Headquarters Services, Directorate for Information Operations and Reports, 1215 Jefferson ...ement and Budget, Paperwork Reduction Project (0704-0188), Washington, DC 20503.

1. AGE

3. REPORT TYPE AND DATES COVERED
FINAL 1 July 1992 - 31 December 1992

4. TITLE AND SUBTITLE
A High Thrust Density, C_{60} Cluster, Ion Thruster

5. FUNDING NUMBERS
(C) F49620-92-C-0039

6. AUTHOR(S)
V.J. Hruby

7. PERFORMING ORGANIZATION NAME(S) AND ADDRESS(ES)
Busek Co. Inc.
19 Kearney Road
Needham, MA 02194

8. PERFORMING ORGANIZATION REPORT NUMBER
BCI-029-1

9. SPONSORING/MONITORING AGENCY NAME(S) AND ADDRESS(ES)
USAF, AFSC
Air Force Office of Scientific Research
Building 410
Bolling AFB, DC 20332-6448

10. SPONSORING/MONITORING AGENCY REPORT NUMBER

11. SUPPLEMENTARY NOTES

12a. DISTRIBUTION/AVAILABILITY STATEMENT
Approved for public release,
distribution unlimited

12b. DISTRIBUTION CODE

13. ABSTRACT (Maximum 200 words)

A C_{60} fullerene ion thruster represents a major advance in the evolution of electrostatic propulsion. It could provide up to a factor of 30 increase in thrust density over Xe thruster as well as simultaneous reduction of relative losses by a factor of 5.5. Its basic feasibility has been experimentally verified during the Phase I program. Vaporization and discharge chambers as well as simple acceleration grid were designed and constructed. A set of unique experiments were performed which demonstrated: (1) controllable fullerene vapor generation, (2) stable discharge at approximately 190 volts using 2% thoriated tungsten cathode filament, (3) fullerene acceleration with beam ion energy cost of about 900 to 1000 eV/beam ion at a mass utilization of 70%, (4) no detectable fullerene fragmentation due to vaporization, ionization and acceleration, (5) fullerenes in a highly diffused molecular beam were not detected by FTIR spectroscopy, (6) SST, Mo, BN, $A\ell N$, $A\ell_2O_3$ and quartz do not react with fullerene vapor during limited exposure, and (7) spacecraft contamination by fullerene thruster effluent is comparable to that predicted for lithium. Methods to reduce it were identified.

14. SUBJECT TERMS
fullerene, ion thruster, ion fuel, C_{60}, electric propulsion

15. NUMBER OF PAGES
78

16. PRICE CODE

17. SECURITY CLASSIFICATION OF REPORT	18. SECURITY CLASSIFICATION OF THIS PAGE	19. SECURITY CLASSIFICATION OF ABSTRACT	20. LIMITATION OF ABSTRACT
UNCLASSIFIED	UNCLASSIFIED	UNCLASSIFIED	UL

NSN 7540-01-280-5500

Standard Form 298 (Rev 2-89)
Prescribed by ANSI Std Z39-18
298-102

DISCLAIMER NOTICE

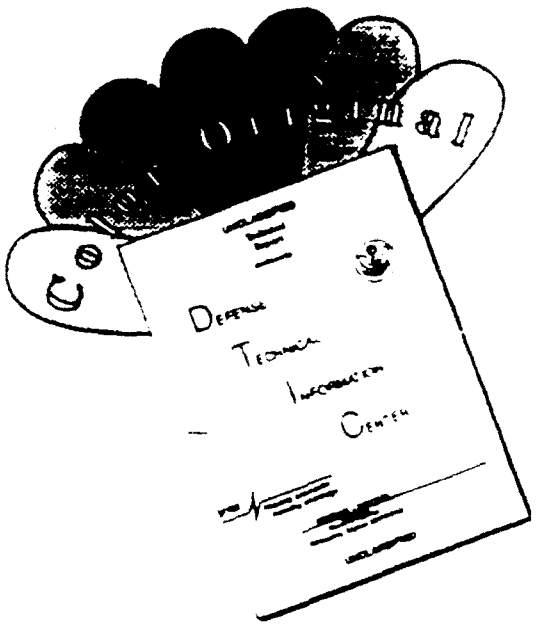

THIS DOCUMENT IS BEST QUALITY AVAILABLE. THE COPY FURNISHED TO DTIC CONTAINED A SIGNIFICANT NUMBER OF COLOR PAGES WHICH DO NOT REPRODUCE LEGIBLY ON BLACK AND WHITE MICROFICHE.

Report No. BCI-029-1

BUSEK

A HIGH THRUST DENSITY, C_{60} CLUSTER, ION THRUSTER

FINAL REPORT

Contract No. F49620-92-C-0039

Prepared for

USAF, AFSC
Air Force Office of Scientific Research
Building 410
Bolling AFB, DC 20332-6448

Prepared by

BUSEK CO. INC.
19 Kearney Road
Needham, MA 02194

28 February 1993

TABLE OF CONTENTS

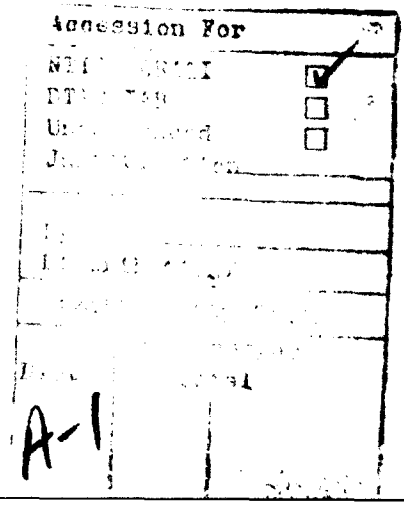

BUSEK

LIST OF ILLUSTRATIONS

LIST OF TABLES

1.0 EXTENDED ABSTRACT

A fullerene ion thruster (FIT) represents a major advancement in electrostatic propulsion. It could deliver up to 30 times larger thrust density than Xe fueled ion thrusters while decreasing the relative losses by a factor of 5.5. To prove the basic feasibility of the FIT concept, Busek designed and constructed balanced beam scale to measure fullerene mass flow, a fullerene vaporization and ionization chamber as well as simple acceleration grid which were used to perform a set of critical and unique experiments. The major accomplishments are:

1) Fullerene compatibility with various metallic and dielectric materials was studied. Milligram quantities of fullerenes were evaporated from SST, molybdenum, alumina, boron nitride, aluminum nitride, and quartz substrates. Substrates and residue of fullerenes were analyzed. No reaction has been found with any materials although some substrates were visually stained. Containment of fullerene solids and vapor in SST vessels should be no problem.

2) FTIR spectroscopy was not able to detect free molecular stream of fullerene vapor but it did detect fullerene condensation coating on IR windows and presence of solvents coming off the fullerenes during heating.

3) Preliminary assessment of spacecraft contamination by fullerene thruster effluent was carried out. The contamination is comparable to that projected for lithium. Concepts to reduce it were suggested.

4) Fullerene vapor generation and control was demonstrated. Samples of up to 9 grams were evaporated from a quartz vessel. Mass flow was measured real time by measuring mass loss rate of the sample and verified by pre and post test sample weight measurements. As much as 7% of the initial sample remained as process residue not vaporizable at 700°C.

5) A discharge in fullerene vapor was established using 2% thoriated tungsten filament in a quartz chamber. Discharge voltage of approximately 190 volts was measured. Lowest discharge voltage obtained was approximately 60 volts which increased to 190 volts in steps of about 30 to 40 volts each time discharge was re-initiated. Graphite coating was found on the cathode as well as possible thorium carbide. Possible explanation for high discharge voltage may be: (1) continuous forming of insulating fullerite layer that must be converted to graphite to maintain discharge, (2) formation of thorium carbide, and (3) high collisional losses, which is however unlikely but no collisional cross section data exist so it cannot be excluded.

6) No fullerene fragmentation occurred due to vaporization, ionization, and acceleration as determined from samples collected in various parts of the system with the exception of an area in the back of the cathode where the deposit was found to be graphitic.

7) An ion beam of about 20 mA was recorded. The beam ion energy cost was estimated to be 900 to 1000 eV/beam ion. Propellant utilization assuming single ionization was estimated to be 70%.

This broad set of unique results briefly described above was achieved by the synergism of two DOD Phase I SBIR contracts. The first is the present, just completed fullerene ion thruster work, and the second is fullerene fueled SPT thruster program currently in progress. Knowledge so far gained in the SPT work is included here to present a more complete picture. It is hoped that this synergism will continue into the next phase of both programs.

2.0 INTRODUCTION AND OBJECTIVES OF THE PRESENT WORK

Space propulsion demands the maximum possible propulsion efficiency be achieved to offset the cost of orbiting the engine and its fuel. For this purpose electrostatic propulsion is very attractive, having excellent efficiency and greatly surpassing the specific impulse of all chemical systems. However, space-charge limitations of the ion acceleration process limit the thrust density to the extent that these engines are presently practical for limited number of missions. Ion thrusters currently use either atomic Xenon, or Mercury as a propellant, due to their combination of molecular weight and ionization characteristics. Other fuels have been examined to increase thrust density to levels that would lead to an attractive thruster with wider applicability. Atomic clusters were found to have the most promise as a result of their large effective molecular weight. Heretofore, problems with cluster stability during acceleration have so far prevented their use in ion thrusters.

Fullerene, C_{60}, is a recently discovered form of carbon that possesses a wide variety of unusual properties. Its extreme stability under impact and at high temperatures plus low first ionization potential make it an excellent candidate for an ion thruster fuel. A C_{60} ion thruster could provide up to a factor of 30 increase in thrust density over the current atomic fuels of choice (Xe, Hg) as well as a simultaneous reduction of relative losses by a factor of 5.5. This thrust density increase would result in a reduction in required accelerator grid areas to a size that is economical and practical to construct even for megawatt sized thrusters. A C_{60} fuelled ion thruster would be a major advance in ion thruster development.

The overall objective of the Phase I effort was to demonstrate the feasibility of C_{60} fueled thruster and justify continued DOD support in Phase II.

Five (5) issues were identified in the Phase I proposal. These are:

1. Vapor generation and control
2. Electrode poisoning (function of insulating layer on electrodes by C_{60} deposition) and discharge voltage
3. Fragmentation of C_{60} upon ionization
4. High electron affinity of C_{60} (formation of negative ions)
5. Plume deposition and effects

The specific objectives of this effort was to resolve the first three issues and perform preliminary study of the remaining issues. This was successfully accomplished as will be discussed in subsequent sections.

3.0 BACKGROUND AND MOTIVATION FOR THE PRESENT WORK

Inter grid space charge limits the thrust density of ion thrusters. The Child-Langmuir space charge limited current equation is

$$j=\frac{4\sqrt{2}}{9}\varepsilon_o\left(\frac{e}{m_i}\right)^{1/2}\frac{V_a^{3/2}}{d^2} \qquad [1]$$

where V_a is the accelerating potential, d is the grid spacing and m_i is the ion mass. As this equation shows, increasing m_i, at fixed V_a tends to reduce the current density. However, a more likely scenario is that the specific impulse and hence the ion exit velocity (c), would be kept constant, since an optimum value of c exists for each given mission and power supply. In that case, the accelerating voltage would be proportional to m_i, since

$$V_a=\frac{m_i c^2}{2e}$$

and the current density (Eq. [1]) is seen to increase as m_i.

The grids act as a very selective filter, extracting ions in preference to neutrals from the partially ionized chamber gas. If we assume only ions are extracted. The mass flow rate per unit grid area is

$$\frac{\dot{m}}{A}=j\frac{m_i}{e}$$

Multiplying times c gives the thrust density which combined with Eq. [1] yields

$$\frac{F}{A}=\frac{2}{9}\varepsilon_o\left(\frac{m_i}{e}\right)^2\frac{c^4}{d^2} \qquad [2]$$

This shows the principal advantages of using high mass ions: the thrust density can be made higher as m_i^2, thus mitigating one of the principal disadvantages of ion thrusters.

Extension of the analysis carried out above leads to an expression relating thruster beam power per unit grid area to the thrust density of Eq. [2]. This expression is

$$\frac{P_i}{A}=\frac{1}{2}\left(\frac{F}{A}\right)c \qquad [3]$$

As an example, consider an interplanetary mission with a thruster beam power of 10 MW, c ≈ 50,000 m/sec and grid spacing d ≈ 1 mm. Equations [2] and [3] then say that for Xe, the grid area is 18.3 m^2 and for C_{60} it reduces to 0.61 m^2. The later is practical, the former is not. In fact, it may be advisable to reduce the thrust density for other reasons and still maintain practical size grid. Thus, C_{60} opens new doors for electrostatic propulsion.

Another advantage is the relative reduction of power losses. These losses arise from a variety of sources (ionization work, need to re-ionize ions that strike chamber walls before extraction, electron kinetic energy rendered to the anode, etc.). In general, the energy loss per ion tends to be independent of propellent used, since it is closely associated with the ionization energy, which varies relatively little (although it is to be noted that C_{60} has lower ionization energy than Hg and Xe). The losses per ion are usually quoted as a voltage ΔV_L, such that $\Delta V_L \times I_{beam}$ = Energy Loss Rate. The useful ion work is 1/2 $m_i c^2$, and so the efficiency is

$$\eta = \frac{\frac{1}{2} m_i c^2}{\frac{1}{2} m_i c^2 + e\Delta V_L} = \frac{1}{1 + \frac{2e\Delta V_L}{m_i c^2}}$$

It is clear that higher m_i leads directly to higher efficiency. For example, using ΔV_L = 200 V (a conservative estimate) Fig. 3.1 shows the thruster efficiencies with Xe, Hg and C_{60} used as propellants. The advantage of fullerene is most striking in the specific impulse range between 1000 and 2000 seconds, where many space missions optimize, and where the conventional propellants give unacceptably low efficiencies (as well as low thrust densities, (see Eq. [2]). The dramatic thrust density and efficiency impovements with C_{60} fuel are shown below in Table 3.1.

TABLE 3.1

PROPELLANT COMPARISON FOR c = 50,000 m/sec, d = 1 mm, ΔV_L = 200 volts
$V_{aXe}/V_{aC_{60}}$ = $mi_{Xe}/mi_{C_{60}}$

PROPELLANT	m_i (g/mol)	V (Volt)	F/A (N/m^2)	P_{jet}/A (W/m^2)	η
Xe	131	1700	21.8	5.46×10^5	0.89
C_{60}	720	9340	659	1.65×10^7	0.97

In general, the best propellant for an ion thruster would have a high molecular mass, low first ionization potential and high maximum cross-section for 1st ionization (but the reverse properties for 2nd and higher levels of ionization) and it should be straight forward to store and handle without creating problems of materials compatibility or human safety. Mercury is one prime candidate but it has a relatively low 2nd ionization threshold and is toxic. Cesium is similar but worse, and has been only used in contact ionization thrusters. Spacecraft contamination by condensation of plume-derived atoms (or molecules) on external surfaces is a generic

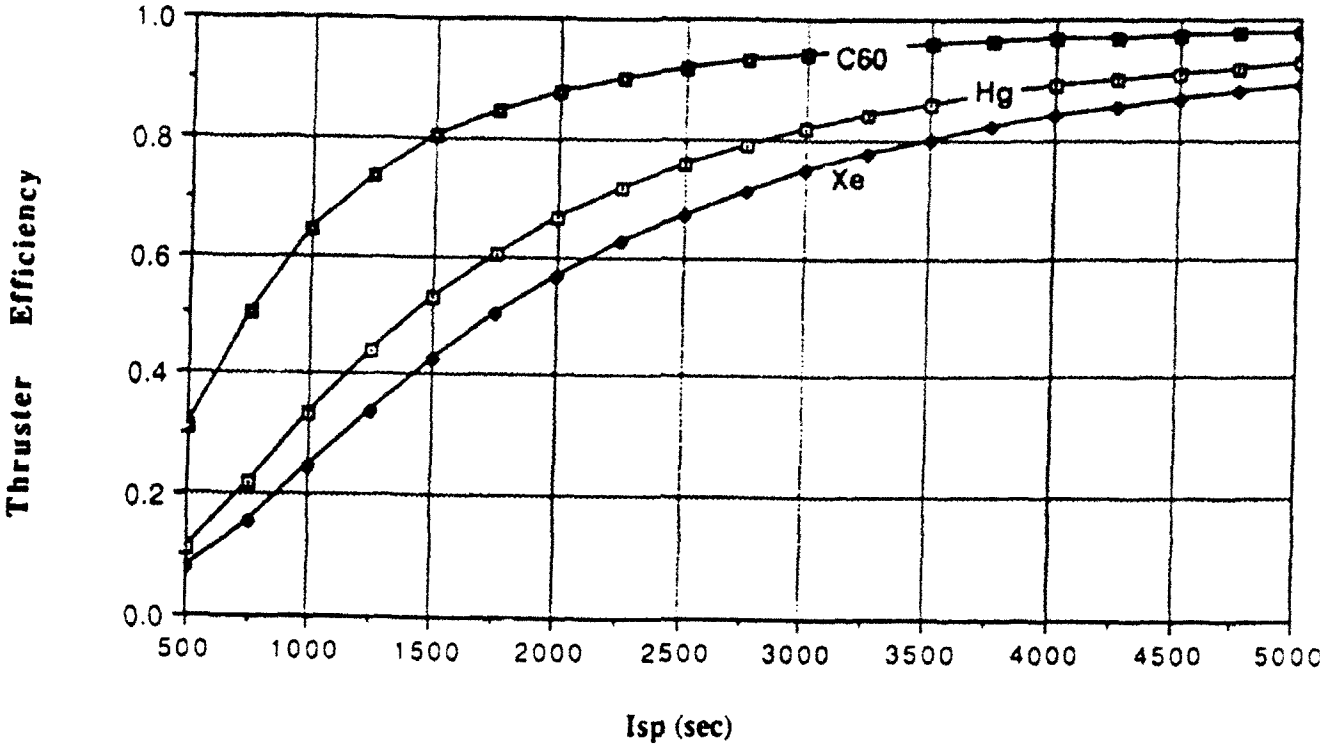

Fig. 3.1 The C_{60} Greatly Improves Ion Thruster Efficiency in the Range of I_{sp} Where Most Missions Optimize (1500 to 2500). At I_{sp} = 1500 the C_{60} thruster has double the efficiency of Xe fueled thruster.

problem with liquid metals (e.g., mercury), causing a trend toward alternative, safer propellants. Molecular gases are usually rejected because of the multiplicity of ionic and excited species their discharges can generate. This is where C_{60} should be a notable exception. The noble gases are thus a natural choice, and especially Xenon which is the heaviest and easiest to ionize of the naturally occurring noble gases. Argon has also been considered because of its lower cost. A survey of electric propulsion can be found in Ref. 1.

Table 3.2 gives a compilation of physical and operational properties of these propellants, with some comments as to their impact on thruster operation. Much of the material comes from the excellent discussions in Refs. 2 and 3. The overall performance with Xe is very similar to that with Hg, although the efficiency at a given thrust level is slightly better in Hg.[2]

The most probable initial use of ion propulsion is for north-south station keeping of geosynchronous communication satellites. An early study of that application[4] showed that the on-board batteries that are normally used to power the satellites during periods of shadow could be used to operate ion thrusters for about one hour daily without adversely affecting satellite operation. More recent studies of ion propulsion for this application[5,6] have confirmed that a significant net performance improvement can be achieved by replacing, or even augmenting, chemical propulsion systems with high-specific-impulse ion propulsion. The performance improvement would translate into a reduction in vehicle launch weight and lower launch cost, an increase in the amount of revenue-producing equipment, or an extension of the maneuver lifetime of the spacecraft.

For example, analyses performed by Hughes have shown that the maneuver lifetime of INTELSAT-VI, the world's largest communication satellite, could be increased from its present 14 years to nearly 23 years by using xenon ion propulsion to augment the chemical bipropellant propulsion system. The baseline system, and the status of the technology, is described in the work of Beattie, et al.[7] Though the station keeping application is emphasized, several recent studies[8,9] have shown that high-power versions of the baseline xenon ion thruster or its derivatives, can offer tremendous performance advantages for other, more demanding applications such as orbit raising and maneuvering. A similar study for the INTELSAT VII satellite is reported by Day, et al.[10]

PROPERTY	FUEL				COMMENT
	Hg	Ar	Xe	C60	
1st ionization potential (eV)	10.43	15.8	12.13	7.5+/-0.2	C60 is best,lower ionization losses?
2nd ionization potential (eV)	29.2	27.6	33.3	12	higher 2nd leads to fewer double ions
3rd ionization potential (eV)	63.4	45	65.5	?	propably high enough in all
1st excitation potential (eV)	4.8	11.7	8.39	?	C60 very electronegative (2.7+/-0.1eV)
2nd excitation potential (eV)	4.6(Metast)	13.2	8.28(Metast)	?	effective hollow cathodes for Hg, C60effects ?
3rd excitation potential (eV)	5.4(Metast)	14.1	9.4(Metast)	?	effective hollow cathodes for Hg, C60effects ?
Atomic(or molecular) Mass(Amu)	200.59	39.9	131.3	720.6	C60 the best
Boiling(or sublimation) T(degC)	356.58	-189.2	-107	550	C60 requires the highest T (drawback)
Storage Conditions	Liquid 13.6 g/cc	Compr. Gas or Cryogenic Liq	Near Critical (0.5g/cc at 35C and 60Bar)	Crystaline Solid	Ar requires bulkier tank
Chemical Activity (Toxicity)	High	None	None	None ?	Ar and Xe safe, Cu, Al, common brazes OK
Cost	Moderate	Low	High	? likely high	may be issue in large systems
(Relative) Sputtering Yield	1	4	2	?	higher errosion in Ar,Xe despite fewer 2nd ions,C60 effects ?
Propellant Flow Control	Simple, via vaporizer, T-cont	More complex thru plenum, control or servo needle valve		?, vaporizer	heavier propellant system for Ar,Xe despite elimination of heaters, C60 system unknown
Power Processing		No need for heaters on fuel fuel lines and vaporizer		?, similar to Hg	Higher reliabilty with Ar, Xe also some loss reduction, C60 should be most efficient
Theoretical Thrust Density (relative)	0.077	0.0031	0.033	1	C60 has from 13 to 322 times greater thrust density, should make very compact system
Theoretical Efficiency at Isp=2000 (relative	0.759	0.324	0.646	1	C60 is from 30 to 300% more efficient without taking into account lower ionization potential

TABLE 3.2

FUEL PROPERTIES AND THRUSTER PERFORMANCE

(Majority of this table was reprinted from AIAA Handbook on Electrical Propulsion by Prof. Martinez-Sanchez, to be published in 1992)

4.0 FULERENE COMPATIBILITY STUDY

Initially we envisioned that the entire experimental flow train wetted by fullerene vapor will be made from stainless steel (SST). However, Dr. Lorents of SRI (our fullerene consultant) indicated potential interaction of SST with fullerenes.(11) He found it impossible to vaporize all fullerenes in his SST container even at 700°C. The remaining material was analyzed using laser desorption in a mass spectrometer and seemed to contain only C_{60} but yet it was not soluble in toluene. It was suggested that there is some thermally activated process that chemically bonds some of the fullerenes together and decreases their vapor pressure. This process might of course be catalyzed by the SST container. Another phenomena observed at SRI was that vaporization rate depended on the number of reheat cycles of the sample. With a new fullerene sample to be vaporized they obtained expected mass flux at 500°C but each time it was reheated it required higher temperature to obtain the same mass flux until finally reaching 700°C.

Because of this experience we performed an experiment to determine if there is interaction between fullerene, SST 316, Boron Nitride (BN), Alumina ($A\ell_2O_3$), Aluminum Nitride ($A\ell N$), quartz, and Molybdenum (Mo). Two samples of each material in the form of small 1" x 1" x 1/8" to 1" x 2" x 1/8" coupons were placed into a vacuum furnace. Approximately 50 to 100 mg of fullerene mix (C_{60}/C_{70}) was placed on one of each pair of the coupons leaving the other as control specimen. The oven was heated to 750°C in 50 minutes held for 60 minutes and allowed to cool down. Apparent reaction/contamination of $A\ell_2O_3$ with fullerenes is shown in Fig. 4.1. The coupon on the left had no fullerenes on it during heating while the coupon on the right did. The fullerene residue and SST. BN, $A\ell_2O_3$ coupons were then sent to SRI for mass spectrometric analysis. The other coupons showed no discoloration of any kind, were untouched by the fullerenes and therefore not sent for further analysis.

The mass spectrometry was done in the SRI Surface Analysis by Laser Ionization (SALI) system using 532 nm laser light to desorb the sample material and 118 nm photoionization of the desorbed neutrals followed by Time of Flight mass spectrometry. A schematic of the SALI system is shown in Fig. 4.2. Mass spectra were taken on both the residual powder material left after the heating experiment and on the substrates from which the fullerenes were vaporized. The residual material had a small amount of fullerenes in it and was contaminated with hydrocarbons which may be pump oil or pump oil fragments. Despite discoloration of the coupons no fullerenes were found on any of the substrate samples. The mass spectra of the residuals from the alumina coupon show the existence of C_{60}, C_{70} and a string of higher fullerenes (Figs. 4.3, 4.4, and 4.5). These spectra clearly show the C_{60} to be heavily depleted in the sample since the ratio of C_{60}/C_{70} and C_{60}/higher fullerenes is much higher than is normally seen for the starting material. In the starting material there typically is 15-20% of C_{70} and 1-2% of C_{76}, C_{78} and C_{84} whereas in this sample the ratios appear to be of the order of 50%, and 5-10% respectively. The large peaks at 356 and 430 amu were not identified. All of the samples showed these peaks and SRI has never seen these peaks in their fullerene samples. They may be forepump or diffusion pump oil contamination. The lower masses below 200 are typical fragment masses from hydrocarbon contamination.

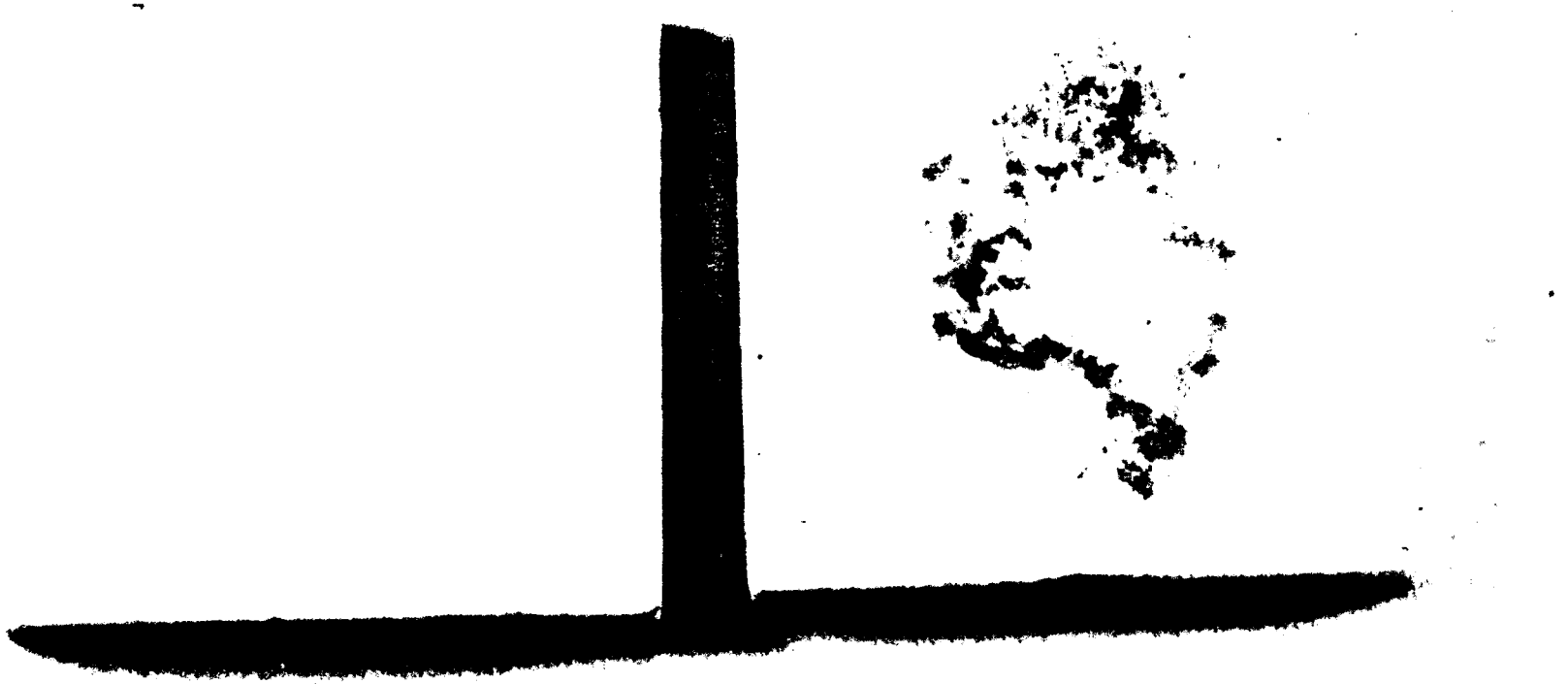

Fig. 4.1 Photo of Al_2O_3 Coupons. Sample on left is a control sample. Sample on right had fullerenes on it that were vaporized at 700 C

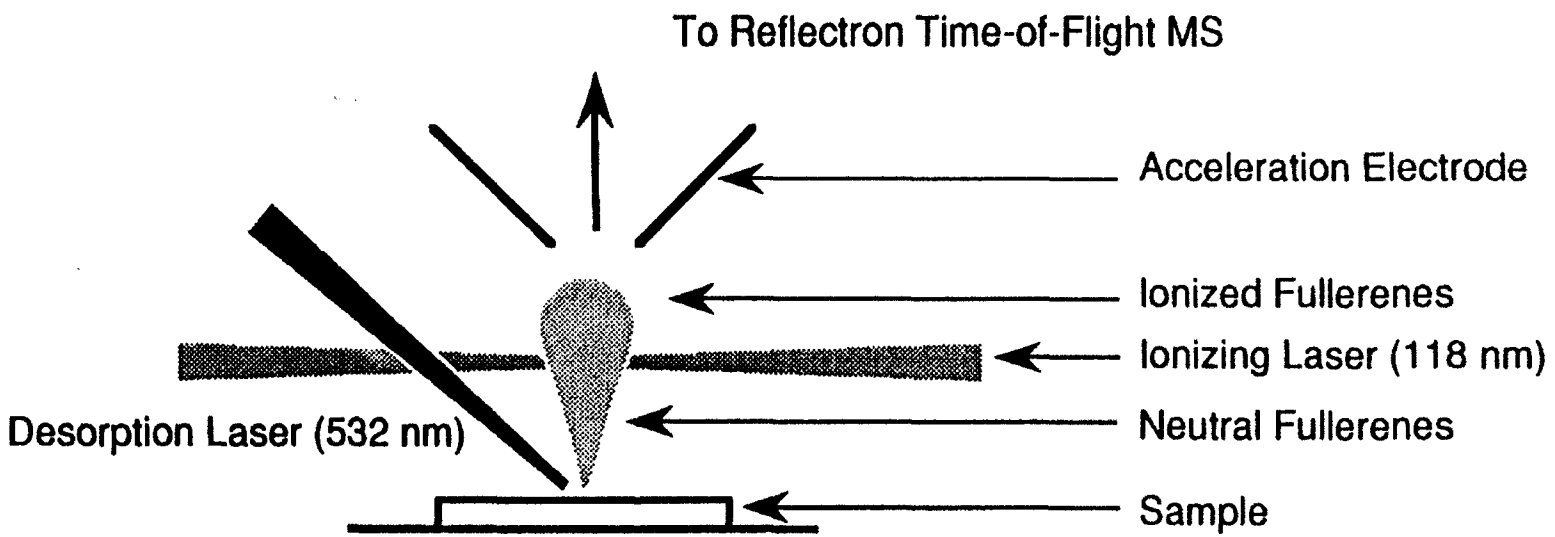

Fig. 4.2 Laser Desorption Postionization Mass Spectrometry (SALI) Schematic

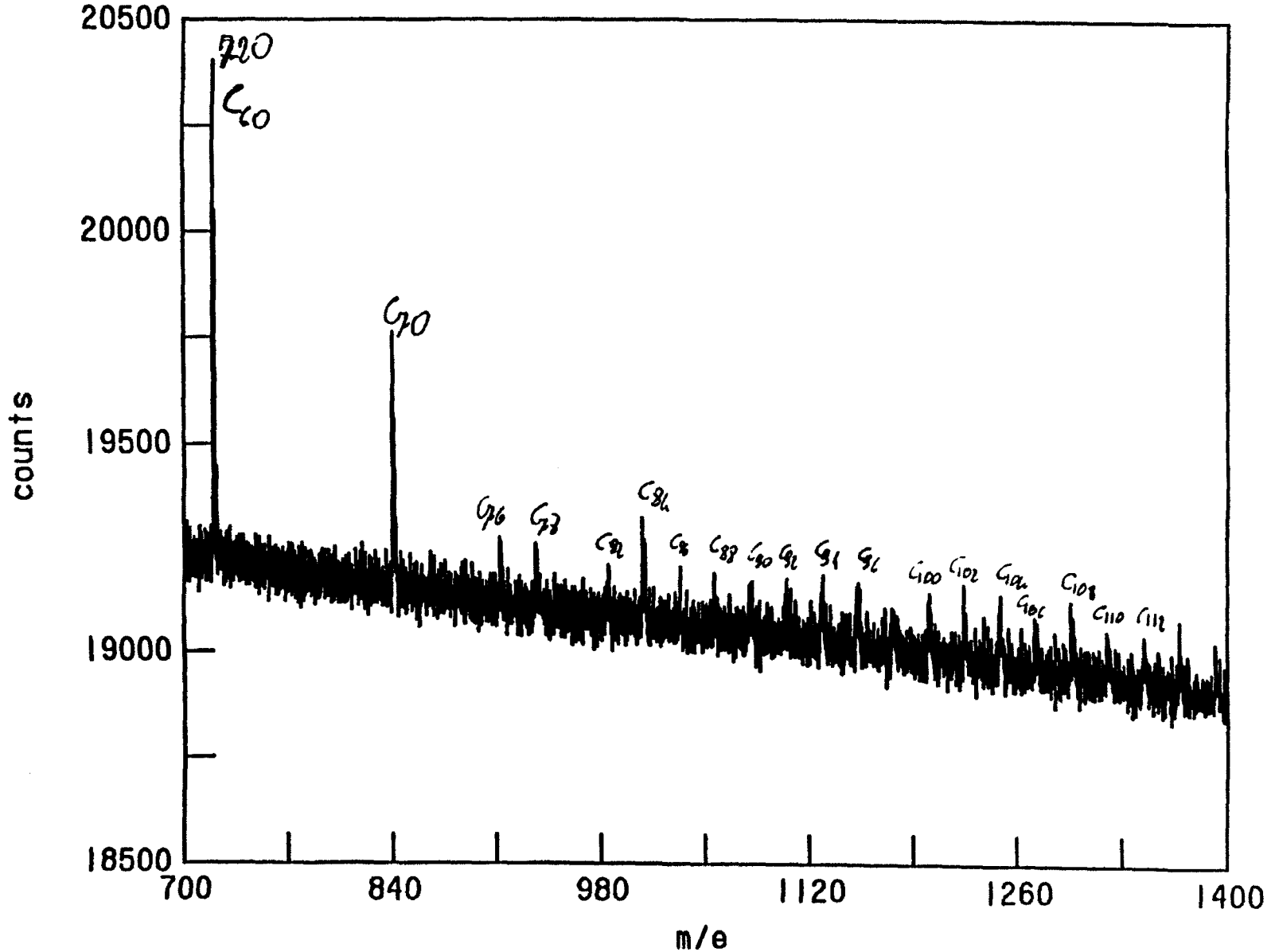

se2505, residual fullerenes on alumina

Fig. 4.3 SALI Spectra of Residual Fullerenes on Alumina Sample for amu Range of 700 to 1400

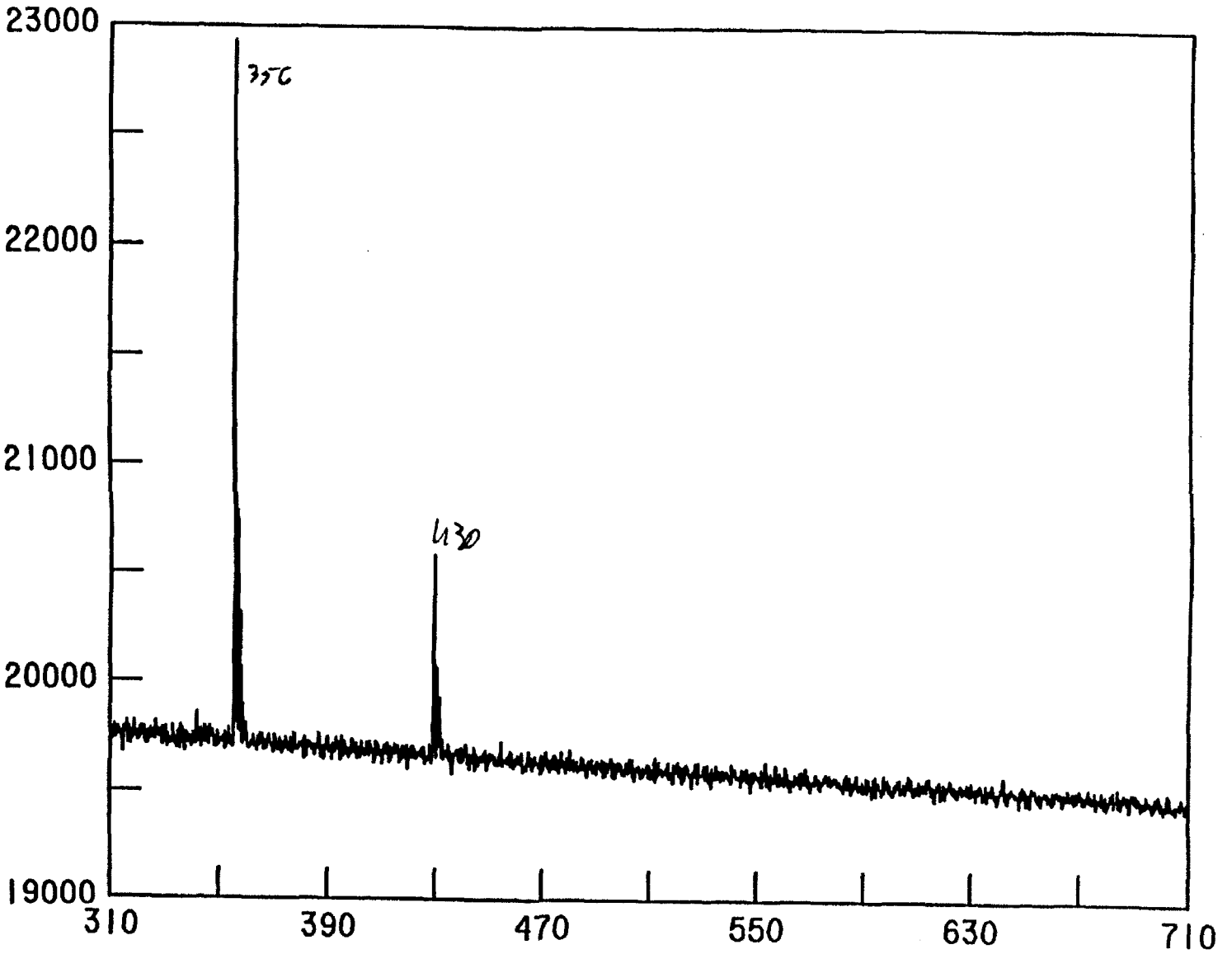

Fig. 4.4 SALI Spectra of Residual Fullerenes on Alumina Sample for amu Range of 310 to 710

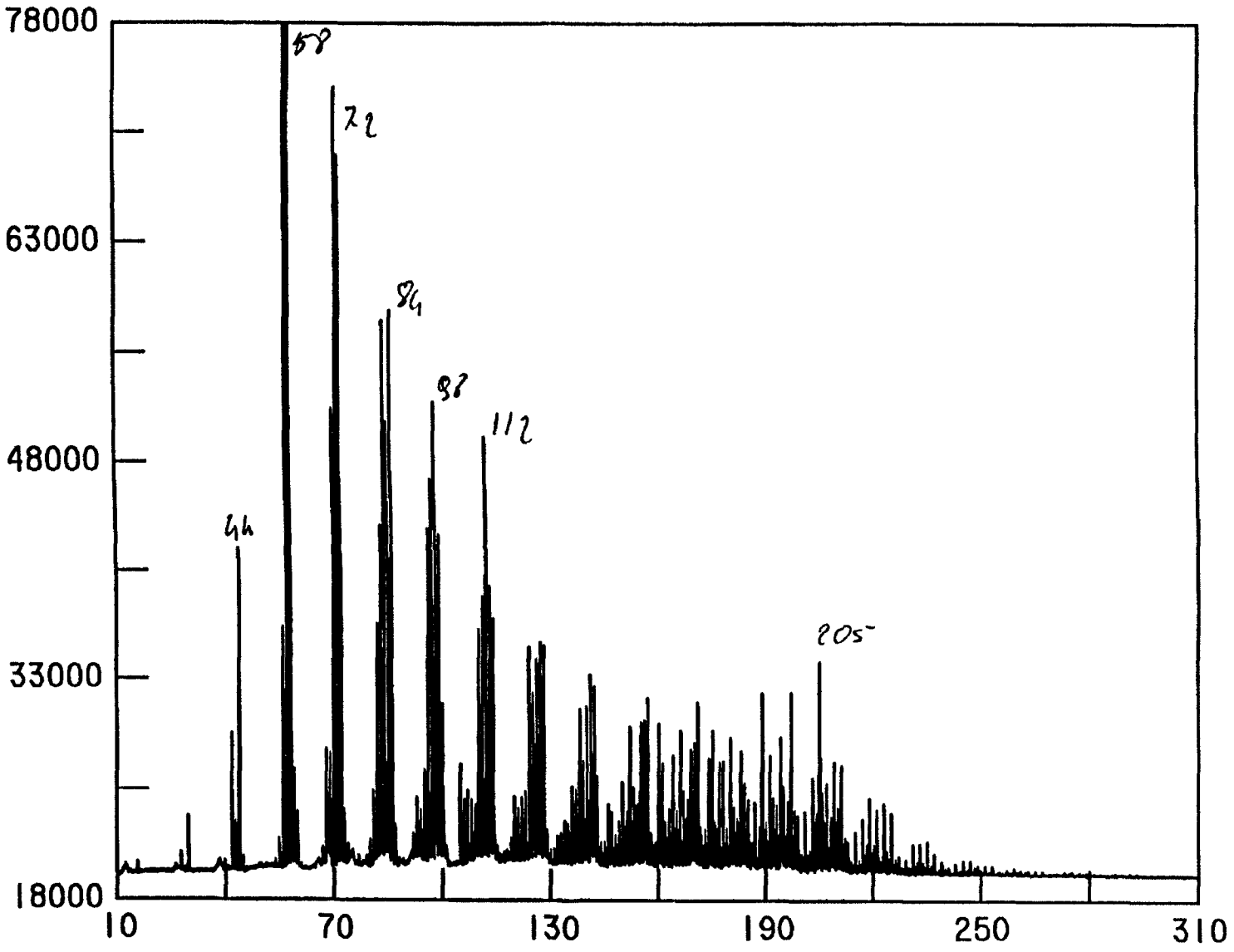

se2515, residual fullerenes on alumina

Fig. 4.5 SALI Spectra of Residual Fullerenes on Alumina Sample for amu Range of 10 to 310

In addition to the potential importance of contamination there are several conclusions from this experiment.

1) Mo, Quartz and AℓN exhibited no reaction or discoloration and hence they are the preferred materials to use in the fullerene vaporizer. For these reasons and to be able to observe the internal content of the fullerene flow train, quartz was selected for the vaporization and the ionization chambers.

2) SST and others discolored but none of them showed contamination by fullerene. Thus aside of the reservations stated above could be used as well.

3) The composition of the fullerene residues showed depletion of C_{60} which indicates that the C_{60} in mixed C60/C70 samples vaporizes first which is consistent with vapor pressure data. This means that vapor mass flow from mixed fullerene sample will be sensitive to temperature as well as time as the composition and hence vapor pressure changes. At 700°C the vapor pressures of C_{60} and C_{70} are about equal and was one of the reasons 700°C was selected as the nominal operating point of the fullerene flow train (to be described later). Additional consequences of using mixed fullerenes are variations in discharge voltage and current due to the differences in ionization and excitation cross-sections. These difficulties clearly point to the need to perform critical experiments with pure C_{60} samples which are five times more expensive than mixed fullerenes.

5.0 SELECTION OF OPERATING TEMPERATURE/PRESSURE

The peak vapor mass flow rate was selected to be 5 mg/sec. Converted to ionic current it represents 3.3 Amps. Converted to ionic current it represents 3.3 Amps. The design issues were operating temperature of the vaporization chamber to deliver this mass flow which determines its size and the material of construction. Each of these is discussed in turn.

Figure 5.1 shows a curve fit of C60 and C70 vapor pressure data versus its temperature. The data were obtained from Abrefah[12] and are shown superimposed on the curve fit. No data exists above 600°C. The curve fit has the functional form

$$p = p_r e^{-\frac{\Delta Hs}{RT}} \qquad [4]$$

where p is pressure, p_r is a constant given by "best" fit, ΔH_S is the sublimation energy, R is the gas constant, and T is temperature. Table 5.1 shows p_r and ΔH_S for C_{60} and C_{70}. The vapor mass flow is given by[12]

$$\dot{m} = pA\sqrt{\frac{Mw}{2\pi RT}} \qquad [5]$$

where A is the flow area which can also be viewed as the minimum vaporization surface by the subliming solid.[13] Combining the two equations, solving for A and calculating the corresponding tube or orifice diameter necessary to transport the vapor at $\dot{m}$ = 5 mg/sec yields the graph shown in Fig. 5.2. For operating temperature below 600°C the orifice or fuel supply tube is too large to be practical (D > 40 mm). Thus we selected our initial experimental orifice to be 10 mm in diameter and selected vaporizer operating temperature range from 650°C to 800°C. The upper limit is given as a temperature above which C_{60} fragmentation may result.[14]

TABLE 5.1

C_{60} AND C_{70} VAPOR PRESSURE RELATED CONSTANTS

	C_{60}	C_{70}
Pr (mTorr)	4×10^{10}	1.4×10^{12}
ΔHs (cal/mole)	38,000	45,000
Mw (g/mole)	720	840

The minimum required vaporization chamber volume was given by the maximum selected test duration (1 hour) at $\dot{m}$ = 5 mg/sec (typical fullerene powder density is 1.5 g/cm^3). Based on that we selected the vaporization chamber volume to be about 100 cm^3. Approximately 15% of its volume will be occupied at maximum charge by the fullerene powder.

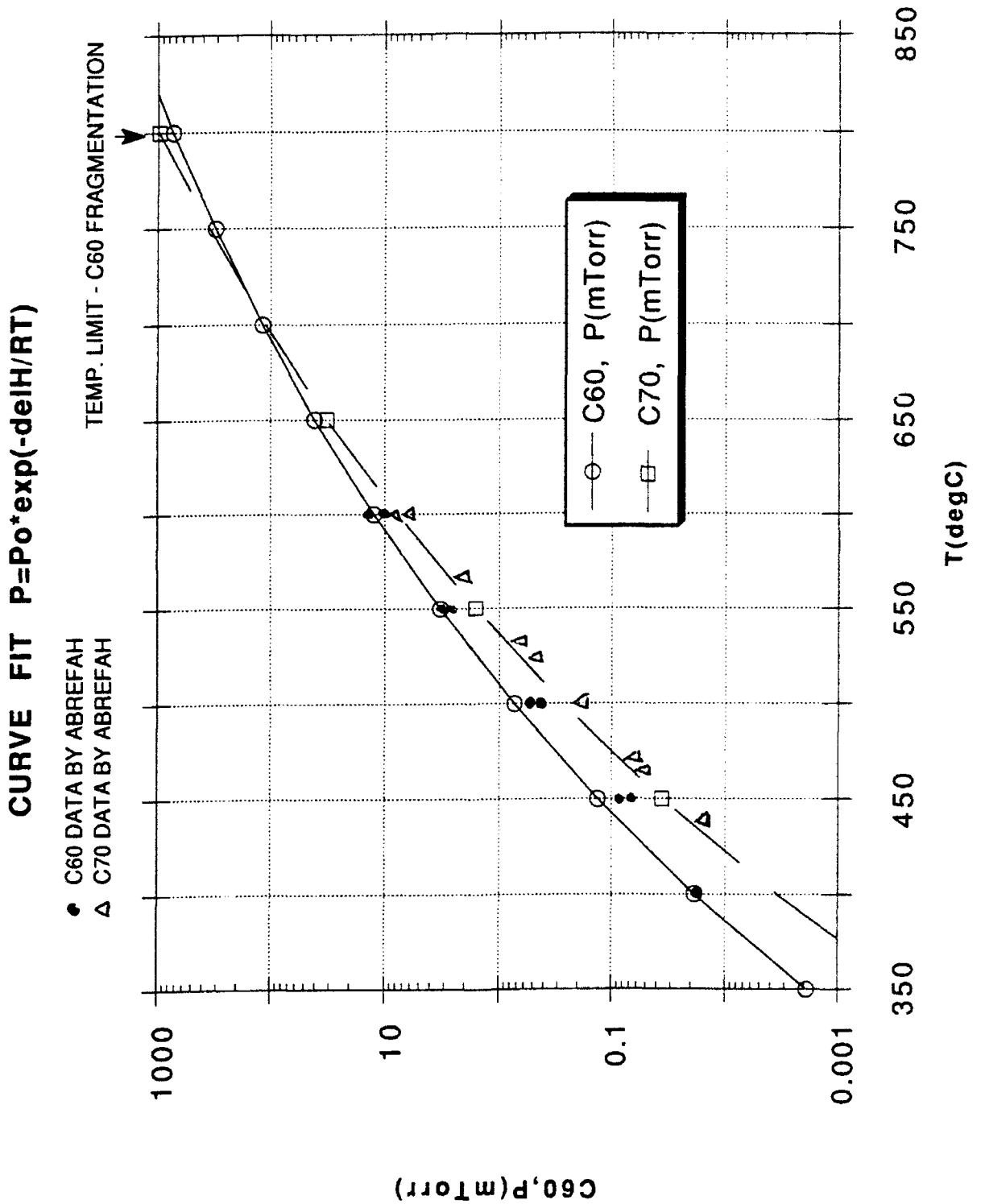

Fig. 5.1 C60 and C70 Vapor Pressure. Curve Fit to Data from Ref. 12

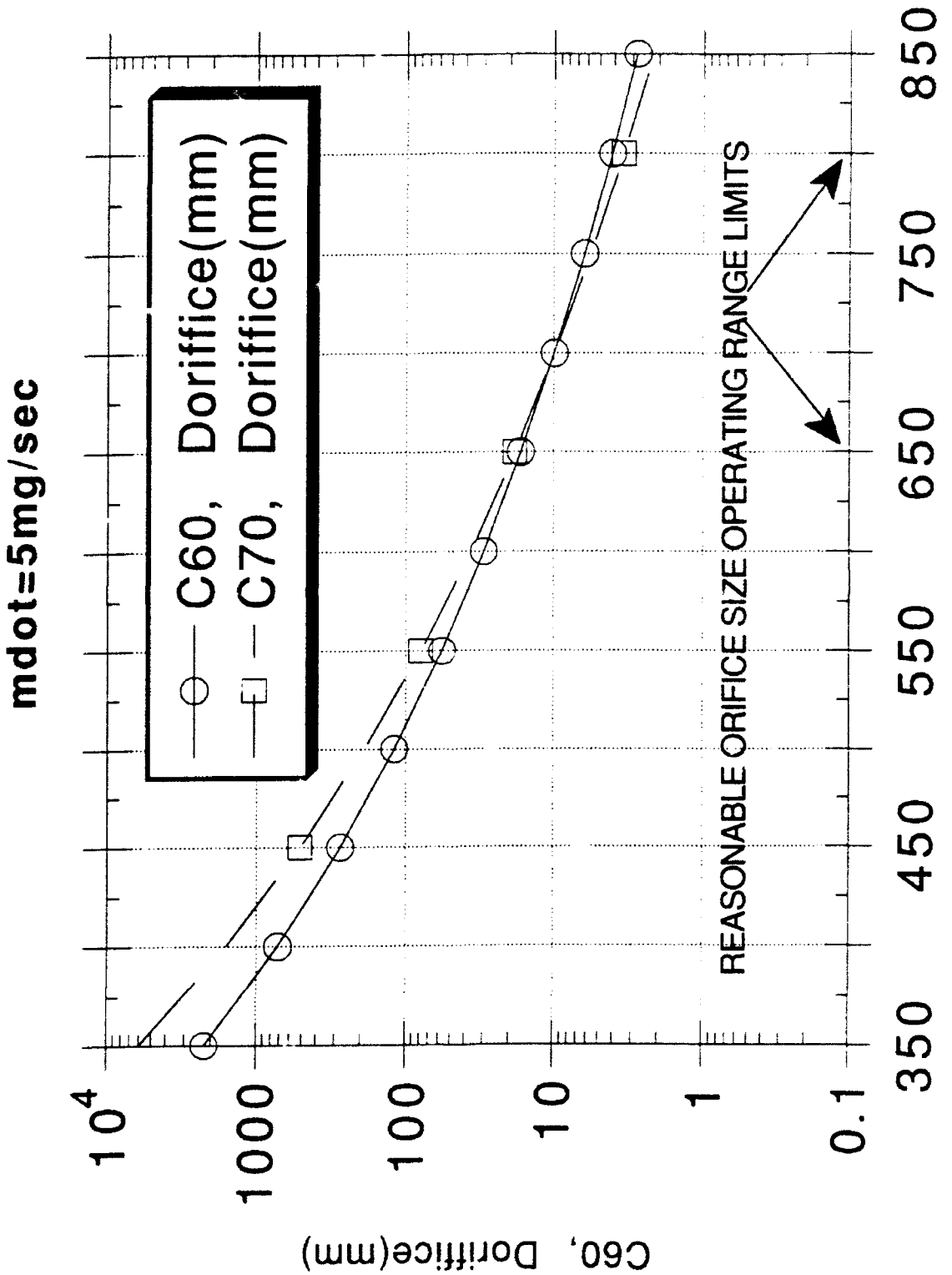

Fig. 5.2 Orifice Size for 5 mg/sec Fullerene Mass Flow Versus Vapor Temperature

6.0 EXPERIMENTAL FACILITY AND APPARATUS

6.1 Flow Train Description

The fullerene fueled ion thruster experiment is housed in our 4 ft. diameter space chamber as depicted in Fig. 6.1. A photograph of the tank is shown in Fig. 6.2. The experimental apparatus is contained with the block labeled "oven" (see Fig. 6.1) where the entire fullerene exposed flow train could be heated up to 800°C. This flow train consisting of fullerene vaporization chamber, flow orifice, discharge/ionization chamber plus the accelerating grids is shown in Fig. 6.3. A photograph of these components made of quartz is shown in Figs. 6.4(a), (b), and (c). The oven and its content are mounted on a water cooled balanced scale platform to measure the apparatus weight change rate as the fullerenes evaporate giving a real time fullerene mass flow.

The fullerene in the form of a loose powder is loaded into the vaporization chamber prior to the experiment, typically up to 10 grams at a time. When heated they flow through a choked orifice into the ionization/discharge chamber where the neutral molecules get ionized by electron bombardment from a hot filament tungsten cathode. Voltage applied on the grid at the discharge chamber exit accelerates to positive ions outward. Exiting ions or neutrals are condensed on either a collector/target plate or in a condenser tube as shown in Fig. 6.1. This prevents condensation of the fullerenes on the balanced beam scale and corresponding errors in the weight change measurements.

The designs of the fullerene hot flow train, the oven, the balanced beam scale and vaporizer and ionizer are described in Sections 6.2, 6.3, and 6.4 respectively. The design of the hardware is dictated by the selected operating regime, principally sublimation temperature and by the materials of construction.

6.2 Oven Design

The fullerene experiment is contained within an electrically heated oven shown schematically in Fig. 6.5. It is designed to heat the fullerene flow train uniformly to a maximum of 900°C. At 750°C it operates at 110 volts and 18 amps with two SST heat shields around its OD. The temperature is maintained by a programmable controller with feed back to a dc power supply. A portion of its length is occupied by the fullerene vaporization chamber and a portion by the fullerene ionization chamber. The vaporization chamber must be heated to higher temperature to establish a pressure vapor gradient between it and the downstream discharge chamber. We elected however, to heat the whole flow train uniformly to avoid complications and to ensure that nowhere along the flow train is a cold area where the fullerenes could condense. In addition to heat, the downstream half of the tungsten wire spiral provides axial magnetic field that diverges similar to the Hughes "J" series thrusters.[15] The magnetic field on the oven axis is given by

$$B = \frac{\mu_o IN}{L}$$

where N is number of turns, L is coil length, I is current and μo is its permeability. With 18 amps in the coil the critical magnetic field is approximately 30 Gauss.

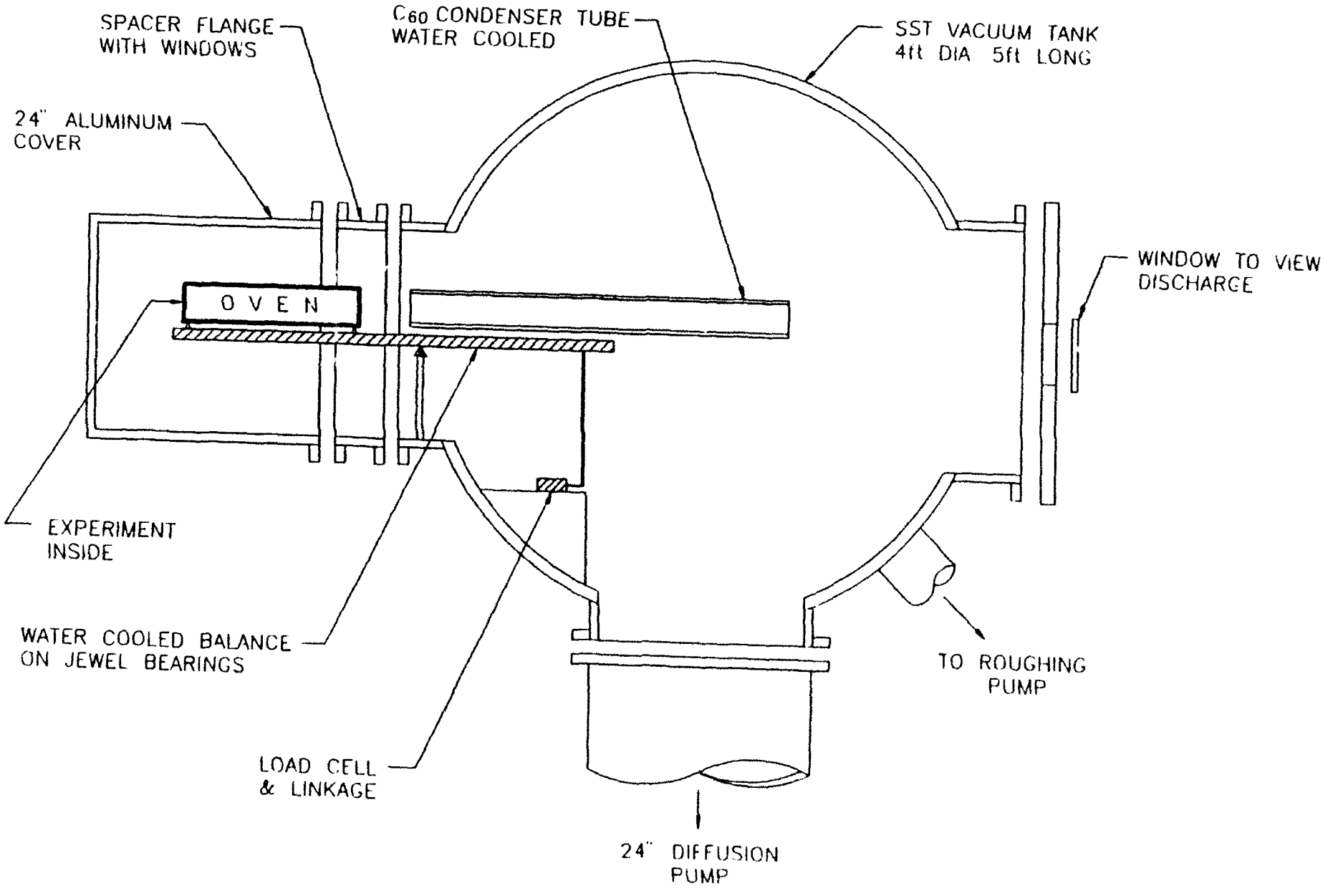

Fig. 6.1 Overall Vacuum System Schematic - C_{60} Fullerene Thruster Experiment

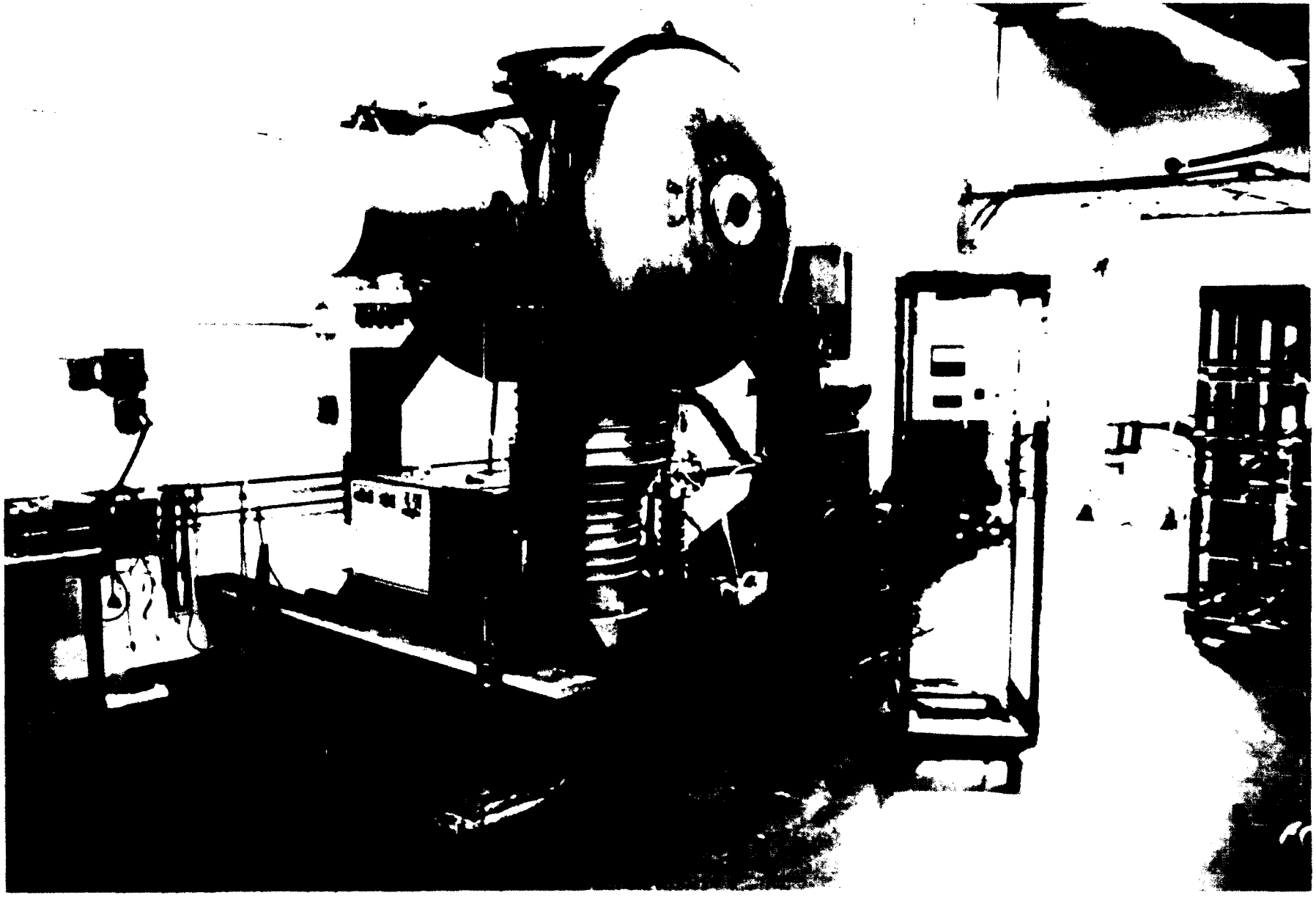

0039

Fig. 6.2 Large Throughput Vacuum Facility

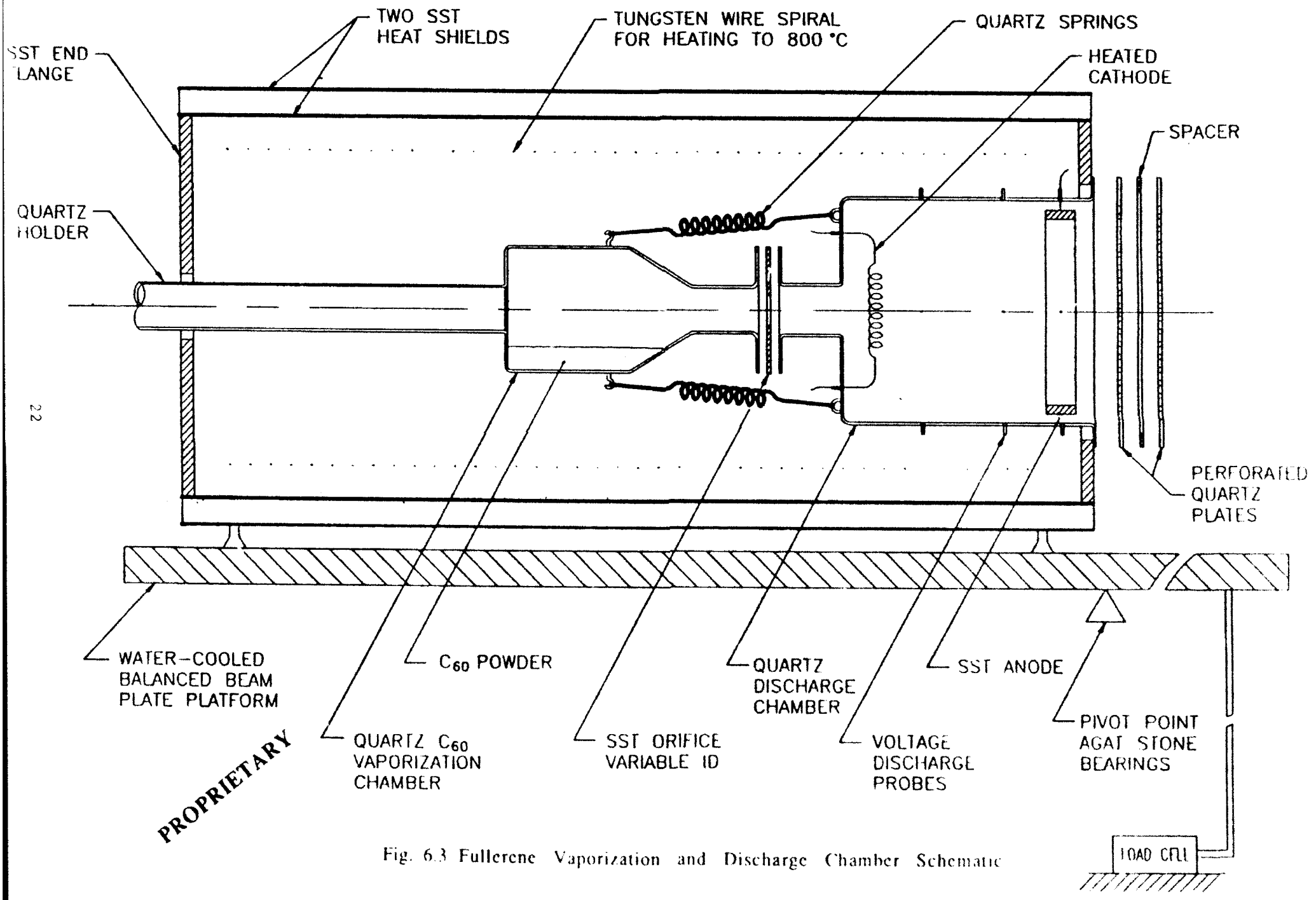

Fig. 6.3 Fullerene Vaporization and Discharge Chamber Schematic

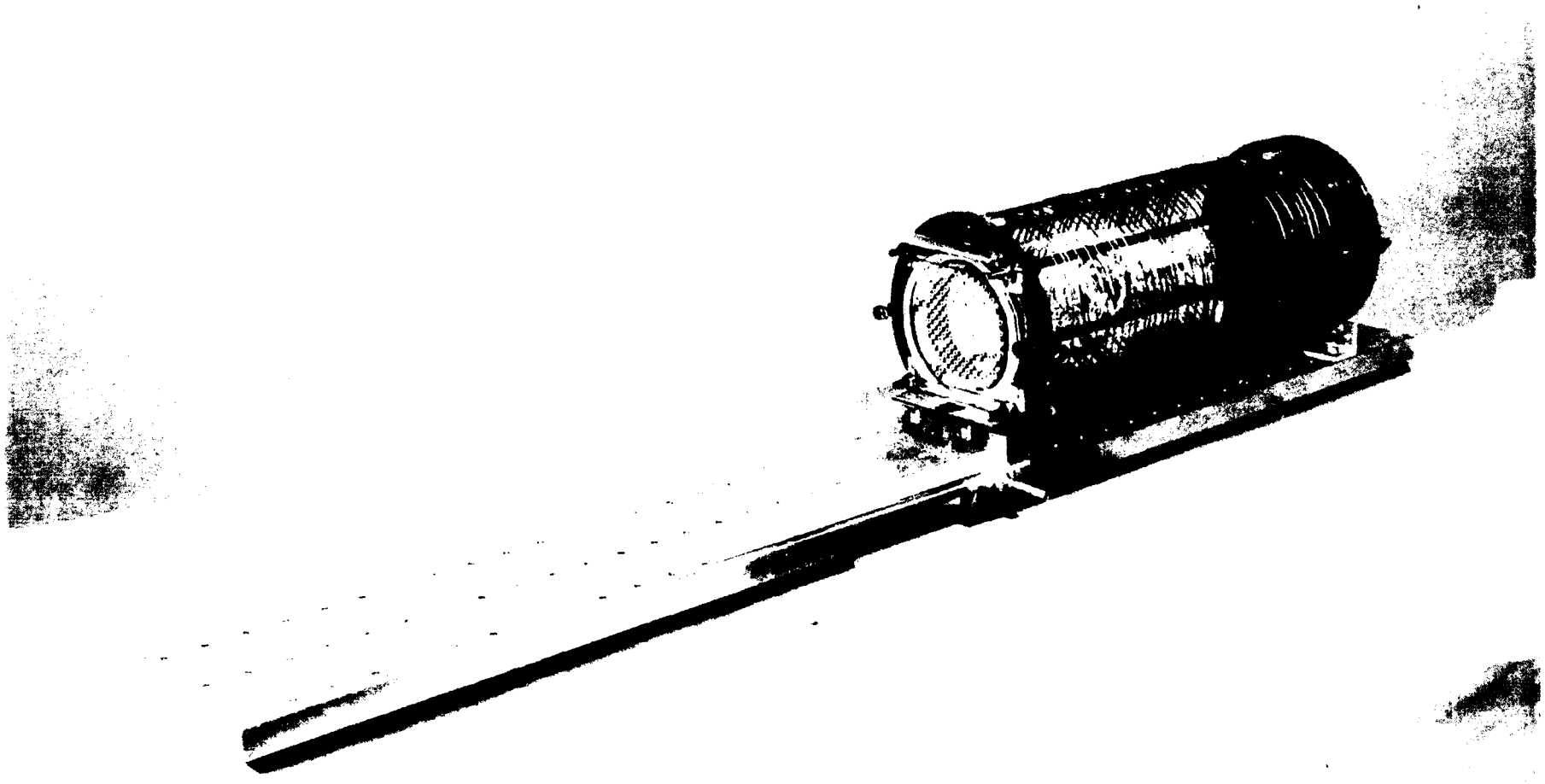

0057

Fig. 6.4(a) Fullerene Thruster Experiment Mounted on a Water Cooled Platform of the Balanced Beam Scale

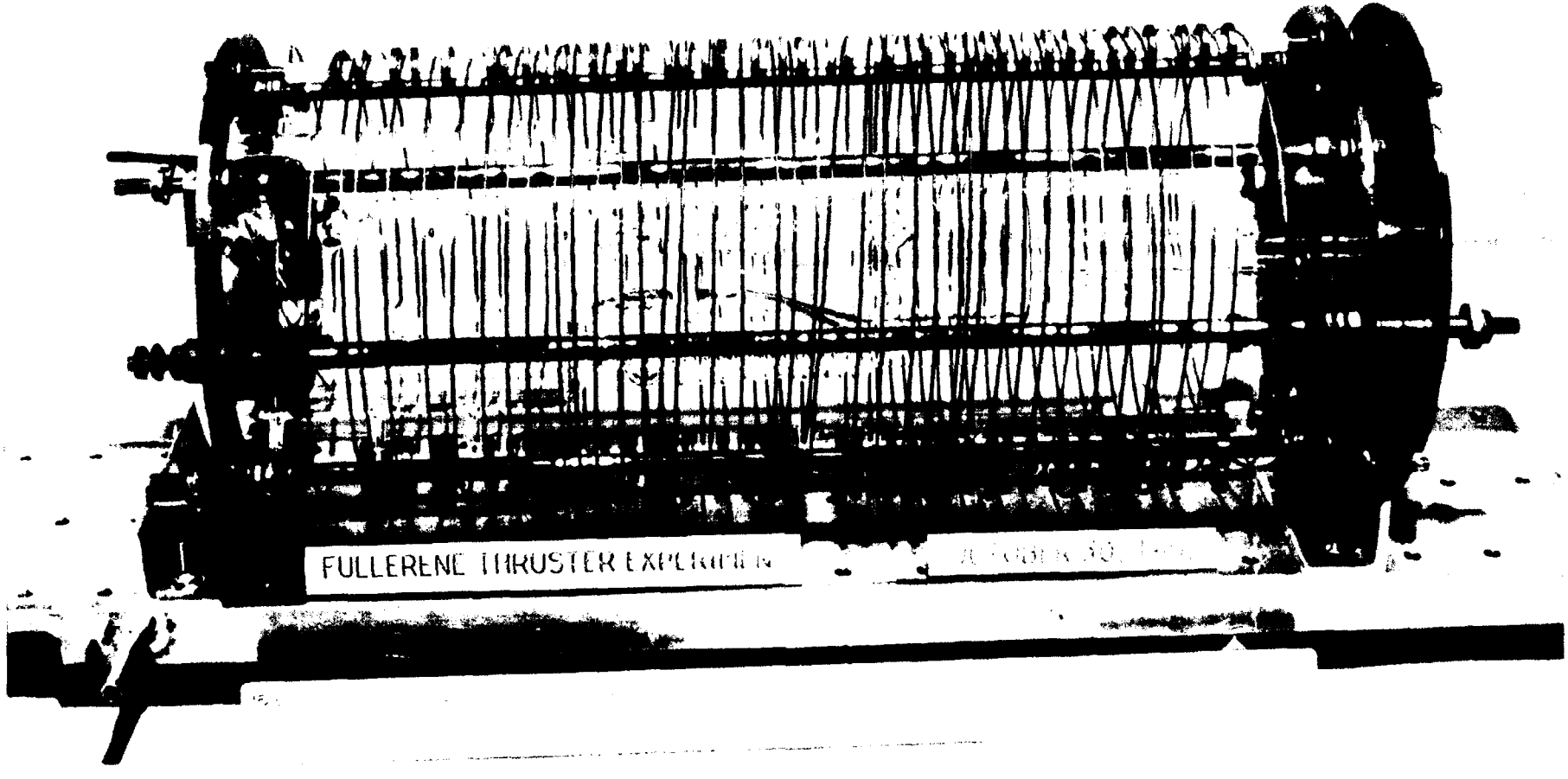

0058

Fig. 6.4(b) Fullerene Vaporization and Ionization Chamber Made of Quartz Inside a Spiral Wound Heater (oven)

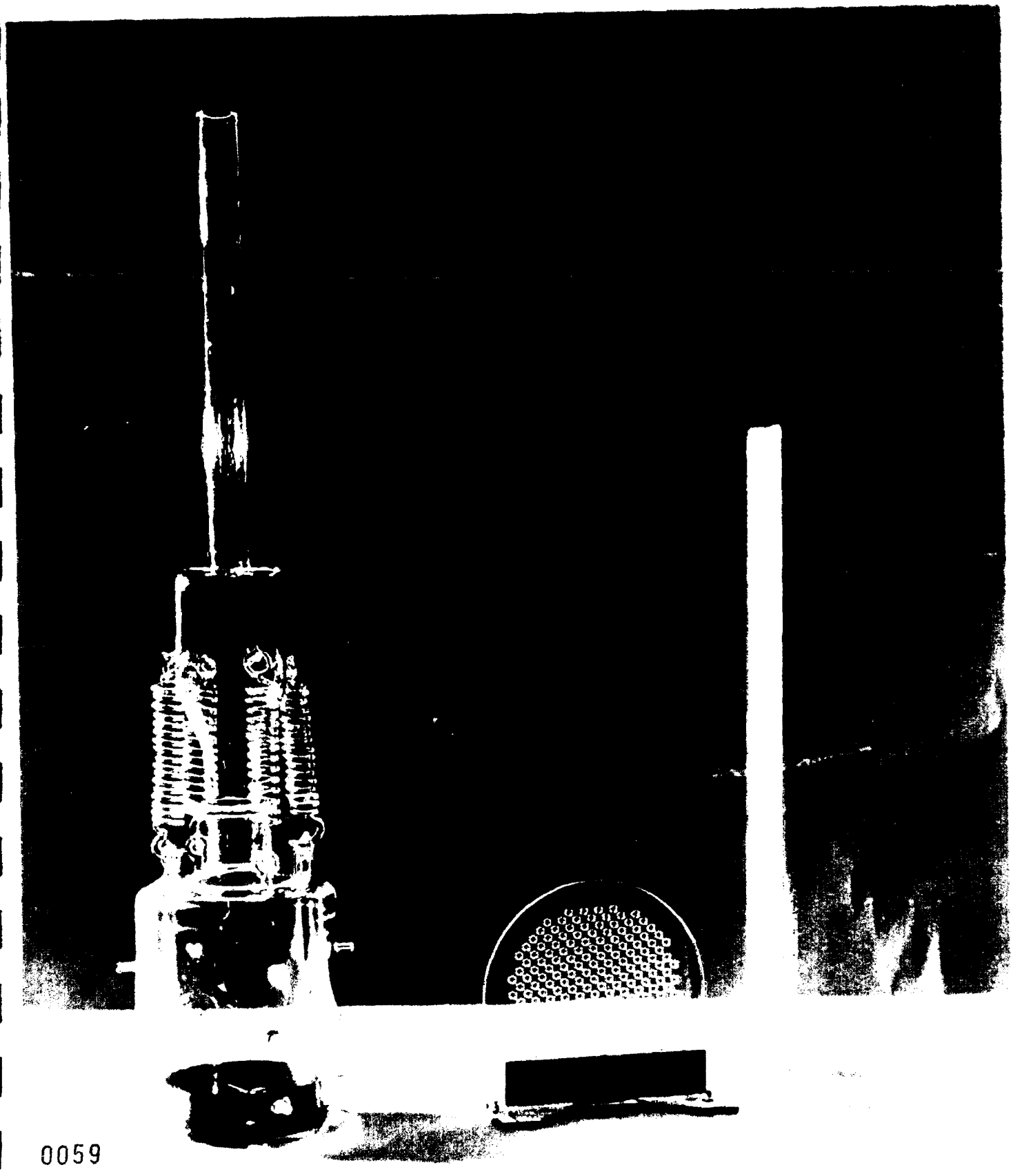

0059

Fig. 3-2. Quartz Vaporization and Ionization Chamber Held Together by Coil Springs

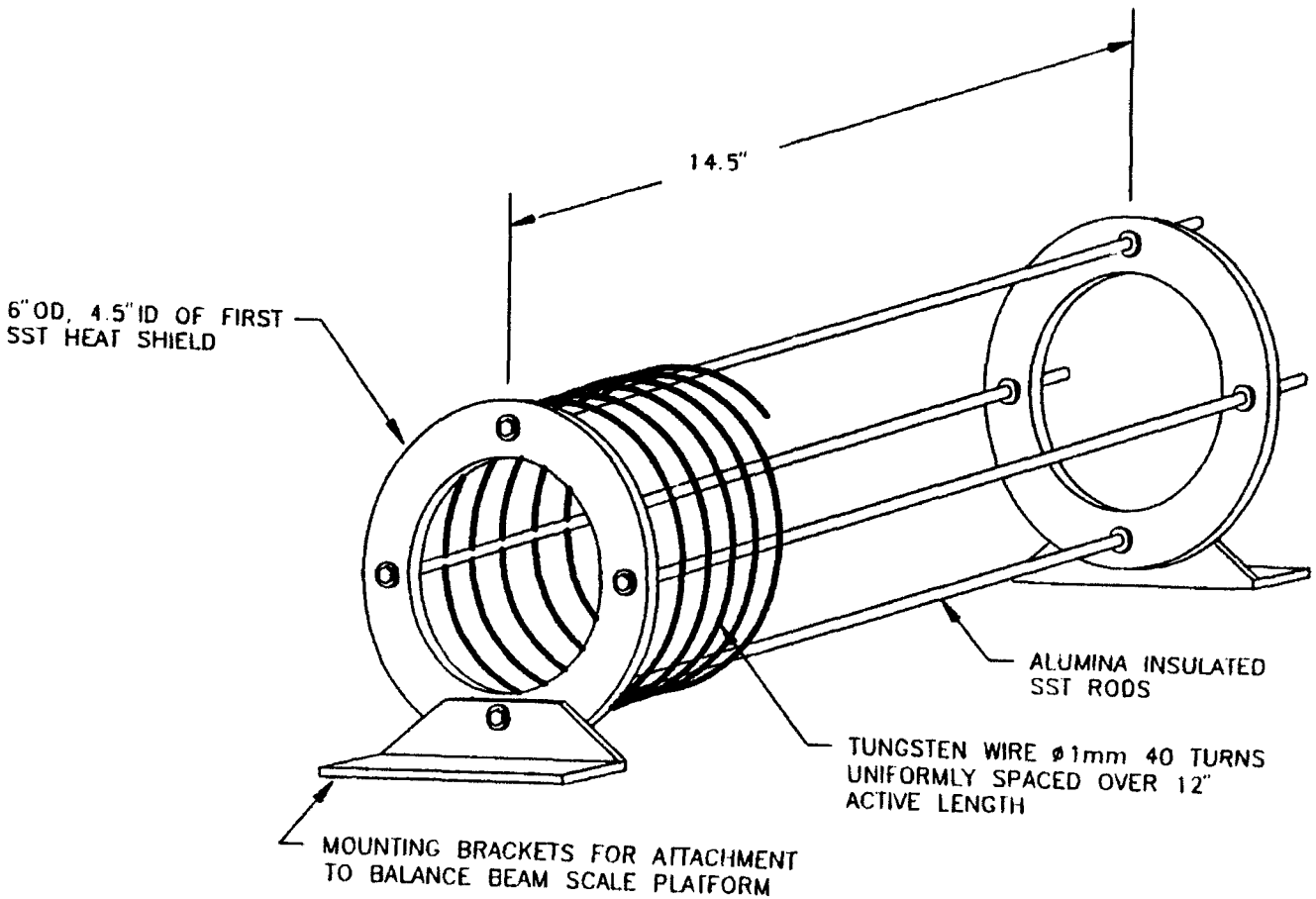

Fig. 6.5 Schematic of the Experimental Oven

6.3 Balanced Beam Scale Design

Critical to the successful application of fullerenes as electrostatic thruster propellant is a predictable and real time adjustable fullerene vapor mass flow rate. This rate is of course dependent on the vapor pressure and hence temperature of the fullerenes (assuming equilibrium between the solid and vapor phase). As pointed out earlier there is no vapor pressure data in the temperature range necessary for thruster operation. Thus we constructed a scale to measure mass loss rate of the solids as a function of the vaporization chamber temperature.

The scale is shown schematically in Fig. 6.6. The oven, inside which is the fullerene vaporization chamber, the ionization chamber and accelerating grids, is mounted on the left side of the pivot and counterbalanced by weights on the right side. In this manner starting with a few grams extra on the right side we can use 50 gram load cell to measure fraction of a gram weight change of an oven plus the fullerene experiment which weighs several pounds. The platform is made of aluminum and is water cooled to maintain its dimensional stability and prevent distortions during heating. All connections to the experiment (water, power and thermocouples) are made near the pivot point to minimize their influence on the weight change. The pivot consists of hardened tool steel shaft with a knife edge on both ends resting on Agat "V" blocks. The scale was calibrated using standard weights and proved linear up to about 25 grams weight change. The development of this scale was one of the most difficult undertakings in this project. It worked well when cooled but remained sensitive to temperature transients in the oven, because its expansion and contractions with temperature that varied from room to 800°C resulted in shifting of the center of gravity and false indications of weight change. Good weight loss rate measurements were performed only after oven temperature stabilized.

6.4 Vaporizer, Ionizer And Accelerator Design

The schematic of the experimental flow train and its installation into the oven was shown in Fig. 6.3 and a photograph of its components in Fig. 6.4(a), (b), and (c). For reasons specified in the previous section all components of the fullerene wetted flow train were made of quartz including the grid/accelerator plates. The dimensions of these components, the vaporization/discharge chamber, ionization chamber and the grids/accelerator plates are shown in Figs. 6.7, 6.8 and 6.9 respectively. During initial experiments a stainless steel orifice plate with various size orifices was inserted between the vaporizer and the discharge chamber. Later during the experimental program the SST orifice plate was replaced by a quartz orifice fused into the neck of the vaporizer. In order to maintain seal at the vaporizer/ionizer interface at high operating temperature the two chambers were compressed by four quartz springs. Quartz is the only material that retains spring qualities and remains flexible from room to the operating temperature.

The ionization/discharge chamber contains centrally located tungsten filament cathode made of 0.5 mm dia., 2% thoriated tungsten wire. The anode is made of SST ring that stands off the quartz wall. The intent of this stand off was to minimize the possibility of electrically shorting along the walls from the cathode leads to the anode which we thought could occur if the fullerenes break down to soot and deposit on the walls. Based on short duration tests described later this does not appear to be a problem.

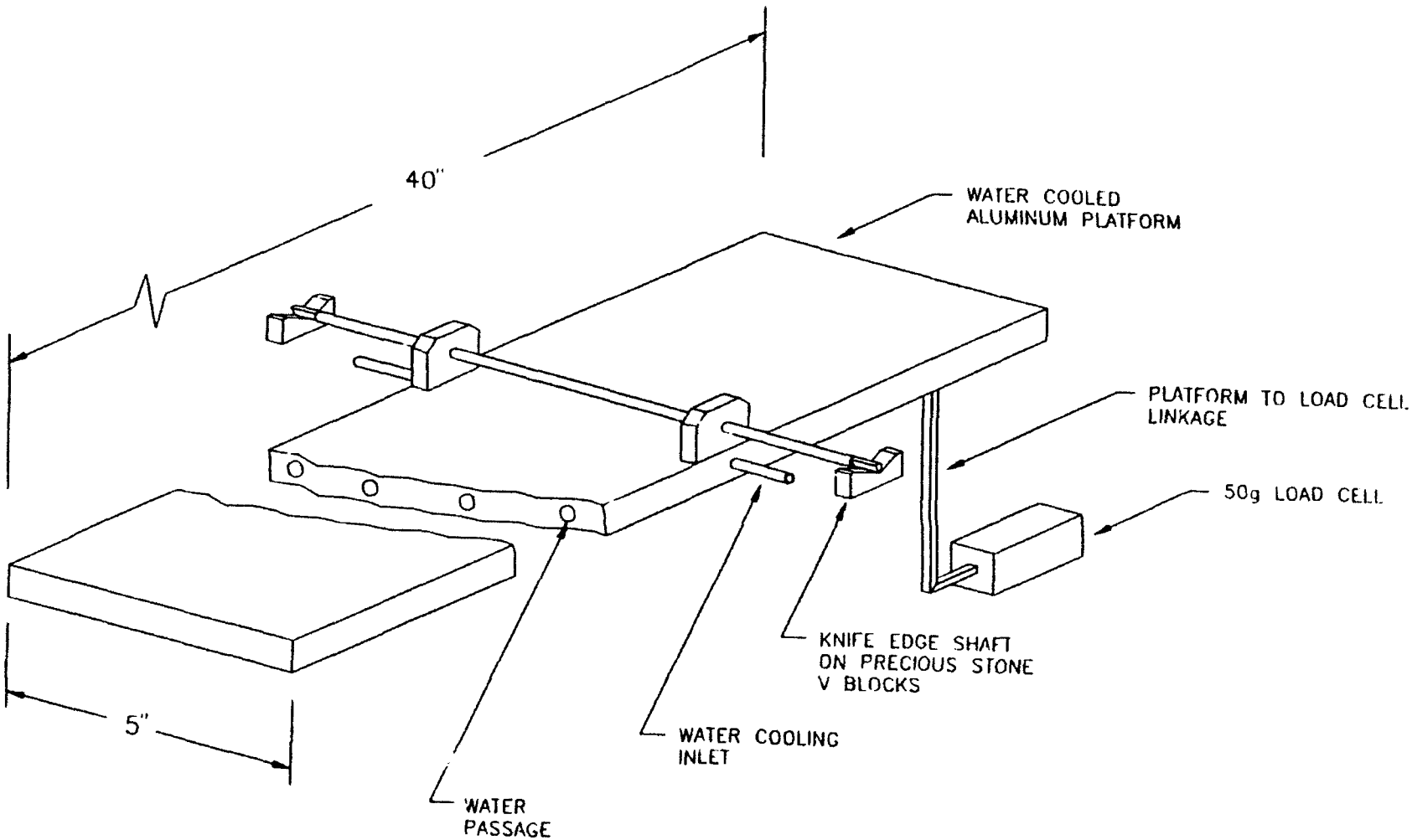

Fig. 6.6 Fullerene Balanced Beam Scale Experiment Schematic

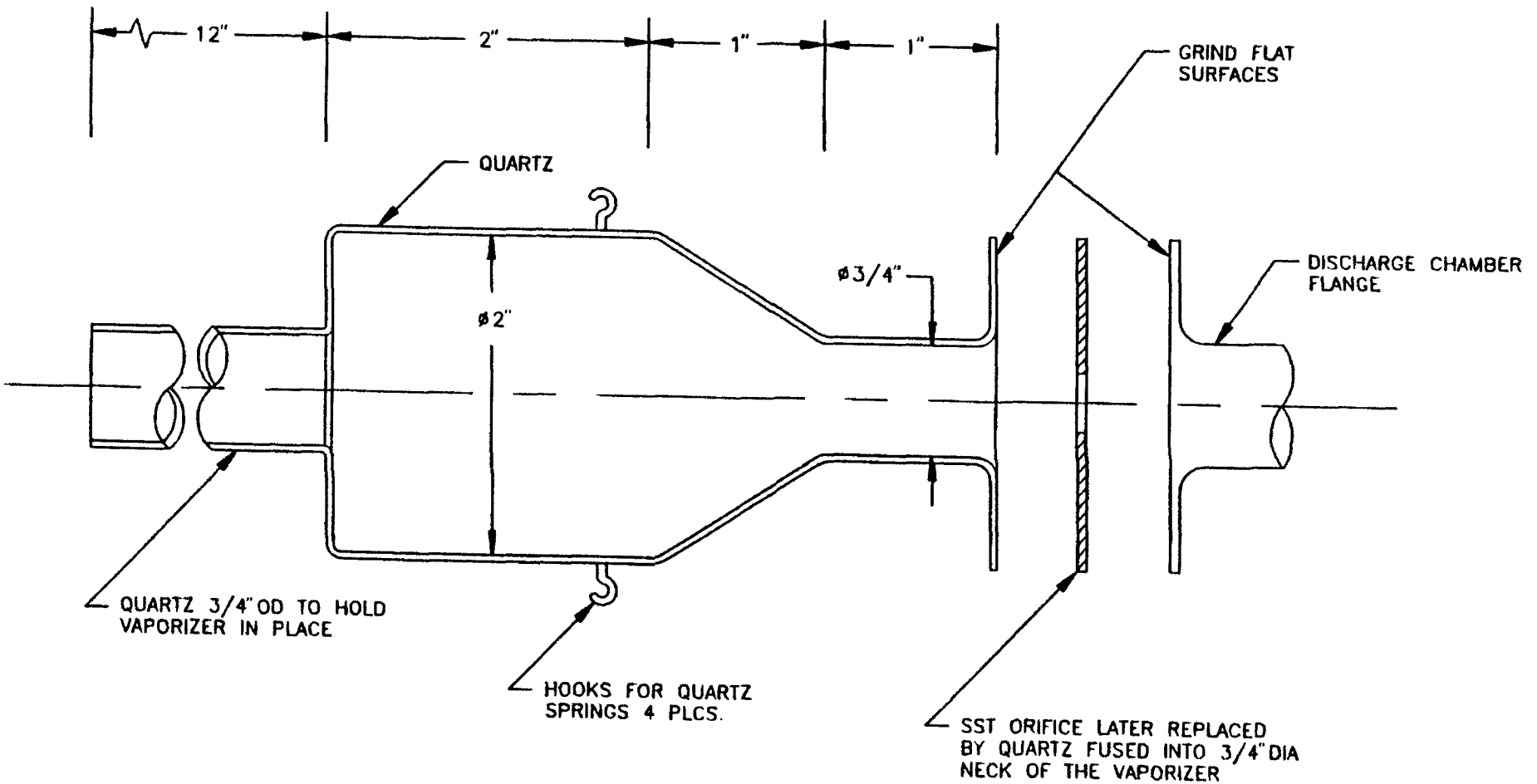

Fig. 6.7 Fullerene Vaporization Chamber

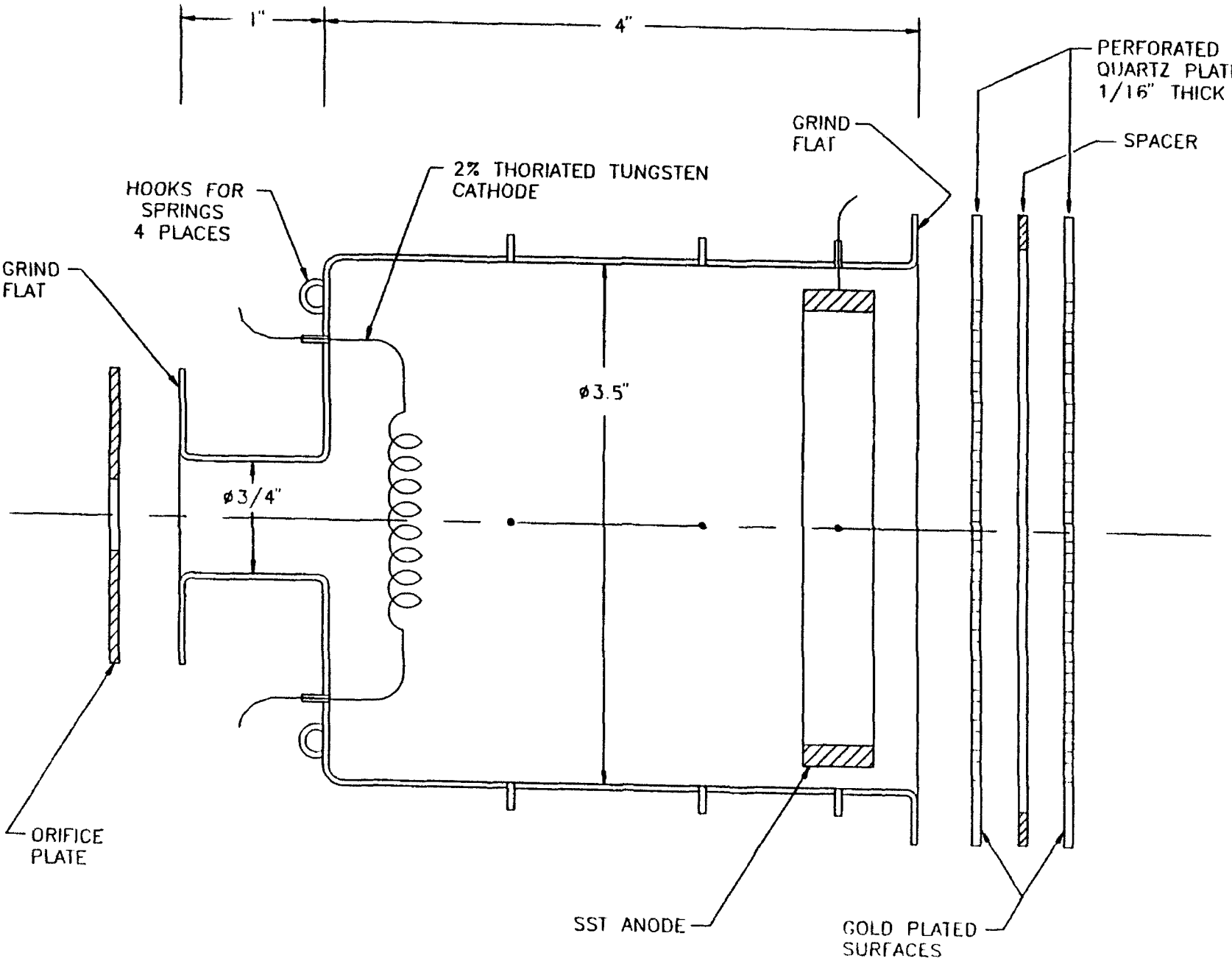

Fig. 6.8 Fullerene Ionization Chamber and Acceleration Grids

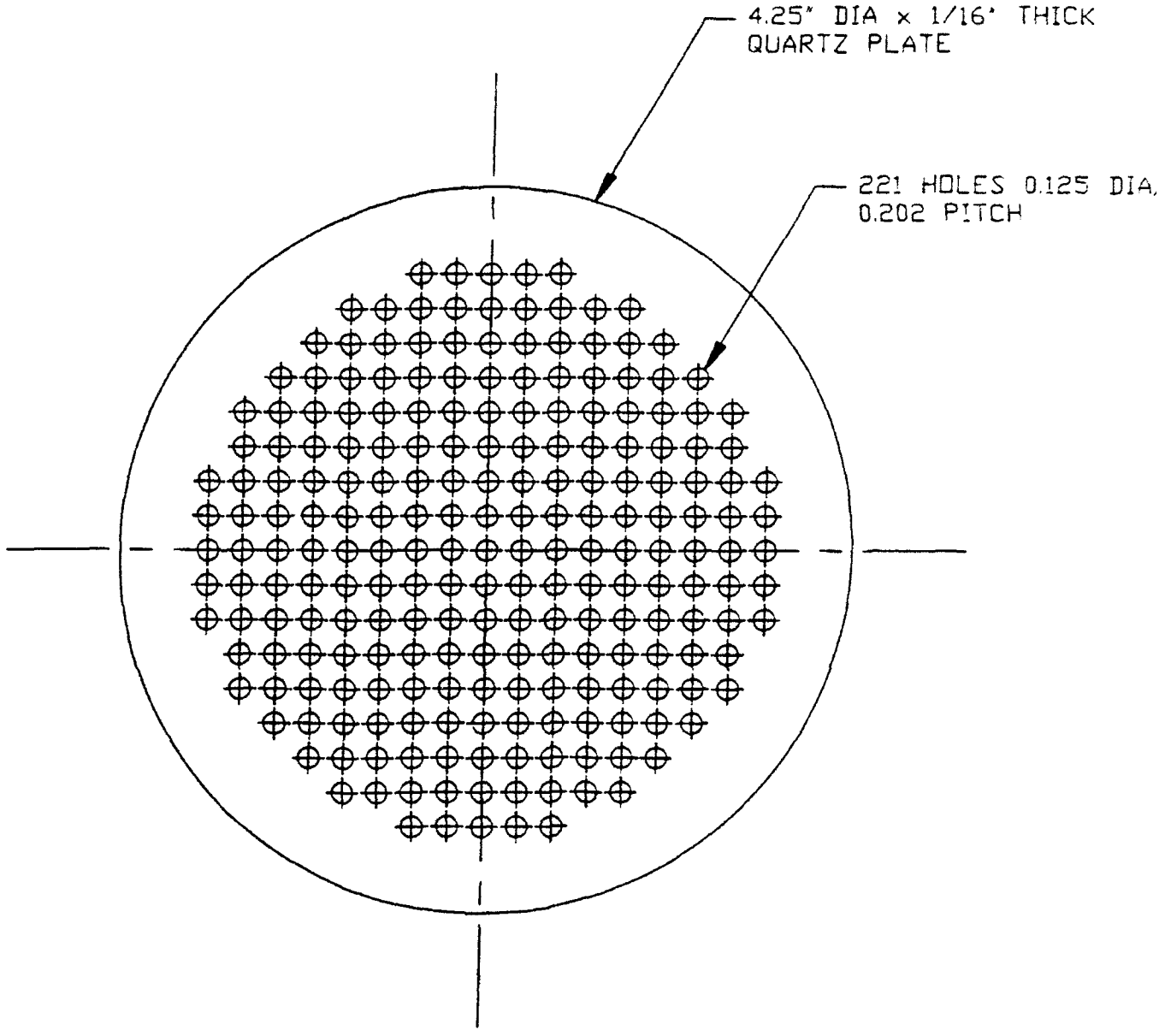

Fig. 6.9 Fullerene Accelerator Grid (made of quartz)

The quartz accelerator grids shown in cross-section in Fig. 6.8 and in plain view in Fig. 6.9 are clamped to the exit flange of the discharge chamber. The internal faces of the grids are gold plated to provide high voltage equipotential surfaces for acceleration of charged ions. There are 221 of 0.125" holes in each plate which provides about 30% open area. Because optimization of the acceleration process was not the objective of this effort, no attention was paid to the ion focusing optics to avoid complexity and increased cost.

The quartz grid plates were replaced by metal grids during the experimental program for several reasons. The first was excessive inter grid current leakage when the system was at temperature which exceeded the capacity of our high voltage power supply. By making the grids metal we had greater freedom in designing a high voltage stand off capability. The second reason was heat transfer within the grids. The gold surfaces on the quartz acted as excellent heat reflectors (essentially high quality gold backed mirrors) which decreased the temperature of the outer grid (located just outside of the oven) to below condensation points of fullerenes. This caused an unacceptable fullerene build up on both sides of the outer/accelerating grid.

The metal grids that replaced quartz later during the experimental program had the same hole pattern. The inner/screen grid is made of 0.003" thick Mo sheet and the outer of 0.012" thick SST sheet. Their juxtaposition designed to minimize current leakage at high voltage is shown in Fig. 6.10.

6.5 Electrical System and Instrumentation

The electric schematic is shown in Fig. 6.11. The quantities recorded on a strip chart recorder are listed in Table 6.1. During mass flow rate experiments the strip chart was also recording load cell output. The balanced beam scale was locked in position and the load cell was disabled during ionization and acceleration experiments because the number of power connections to the balanced beam scale made weight change determination impossible.

The oven was controlled by a programmable controller that could maintain any temperature ramp or hold within a few degrees. All other power supplies were controlled manually.

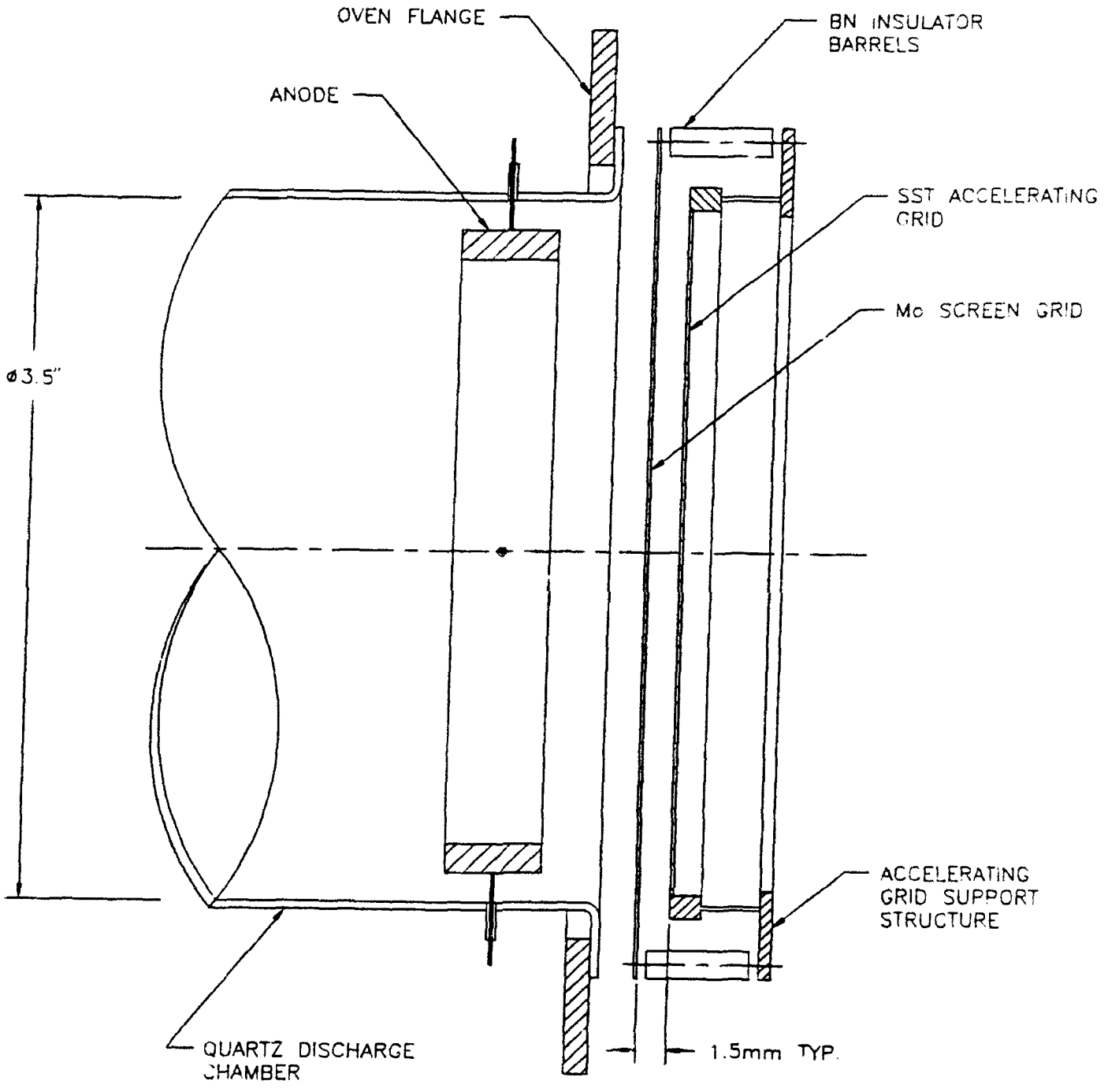

Fig. 6.10 Metal Accclerating Grid Arrangement

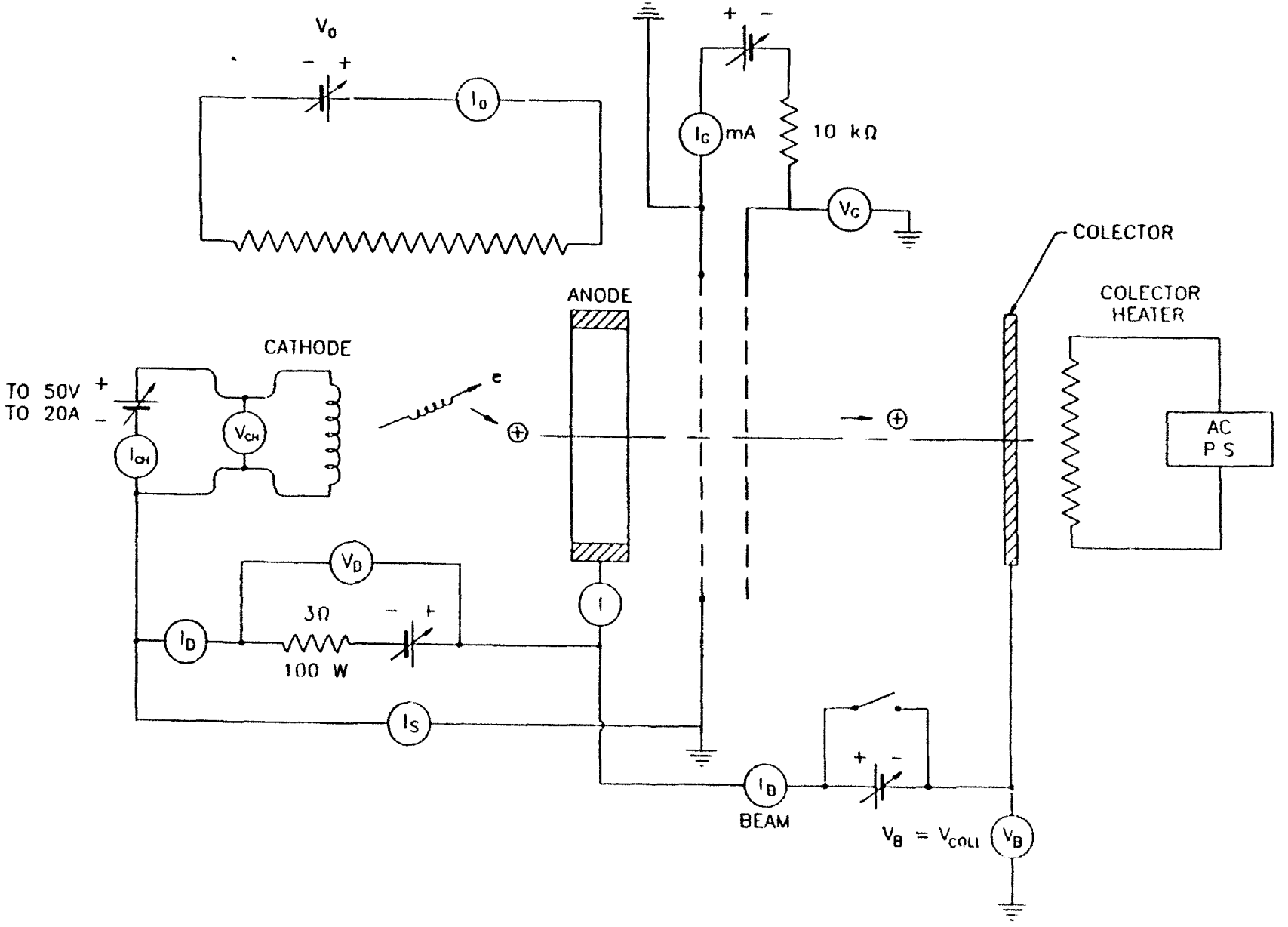

Fig. 6.11 Fullerene Ion Thruster Electrical Schematic

TABLE 6.1

RECORDED DATA - FULLERENE THRUSTER

CHANNEL	QUANTITY MEASURED	INSTRUMENT/ SENSOR	ZERO	SCALE LEFT	SCALE RIGHT
2	Temperature Oven	TC	Full Left	0	1000°C
3	Grid Current, I_G	1Ω, 10 mV	Center	- 2 mA	+ 8 mA
4	Collector/Beam Current, I_B	I Probe	Center	+ 1.25 A	- 1.25 A
5	Cathode Heating Current, I_{CH}	Shunt 20 A/50 mV	Full Right	+ 20 A	0
6	Anode/Discharge Current, I_D	Shunt 10 A/50 mV	Center	- 5 A	+ 5 A
7	Cathode Heating Voltage, V_{CH}	V Probe	Full Right	50 V	0 V
8	Tank Pressure	VAC Gauge	Full Right	-	10^{-3} Torr
9	Grid Voltage	200:1 Divider to Ground	90% Right	- 1800 V	+ 200 V
10	Beam/Collector Voltage, V_B	200:1 Divider to Ground	80% Left	+ 400 V	- 1600 V
12	Anode/Discharge Voltage, V_D	3:1 Divider to Ground	90% Left	- 30 V	+ 270 V

7.0 EXPERIMENTAL RESULTS

7.1 Fullerene Mass Flow Measurements

Fullerene mix of typically 80% C_{60} and 20% C_{70} in the form of loose powder was inserted into the vaporizer. The ratio of C_{60} and C_{70} is important because each has slightly different vapor pressure and hence will evaporate at different rates at a given temperature. Typically the fullerene mix quantities ranged from 4 to 9 grams. The vaporization chamber was attached to the ionization chamber by the quartz springs as described earlier and the two chamber assembly was inserted into the oven where it was supported on both ends on the oven flanges. The orifice, initially SST, and later quartz fused into the vaporizer exit tube were used. The fullerenes were weighed prior and post each run to determine net weight loss and compare it to load cell rate measurement. The load cell gave unreliable readings during oven temperature transients and proved to be reliable at conditions with steady state temperature.

We conducted four tests devoted to mass flow measurements. Table 7.1 shows the results. The first three tests were performed with three different SST orifices and a constant temperature of approximately 700°C which is where the extrapolated vapor pressure data for C_{60} and C_{70} roughly coincide. There was a 30°C spatial temperature nonuniformity as measured by two thermocouples at two different locations in the oven separated by about 5" axially and 4" radially. After completion of all tests there was some residue left in the vaporizer. The fraction vaporized ranged from 99.6 to 93.3% which is consistent with SRI experience described previously. The flow rate in the first three tests was measured from the slope of the load cell output and compared to the pre and post test weight change. These agree with ±8% which gives us confidence in the difficult to perform rate measurement. Once temperature in the oven stabilized the mass flow rate was steady and constant. However, comparing it to the theoretical flow rate based on extrapolated vapor pressure data (Table 7.1) the measured flow rates were substantially higher and the discrepancy was increasing with decreasing orifice size. Moreover, the measured flow rate did not scale proportionally to the orifice flow area. For example, by decreasing orifice diameter from 0.34" to 0.188", the measured mass flow decreased only by a factor of 0.55 instead of by a factor of 0.22 as the area ratio implies. We searched for the reason of this anomaly and determined, based on SST orifice depositions, that at the operating temperature the seal around the orifice opened up and in effect increased the flow area. This was the reason why the theoretical versus measured flow rate discrepancy increased with decreasing orifice size because the leak area started to dominate the orifice area. To eliminate any issue of poor seal around the SST orifice we fused a quartz orifice into the exit neck of the vaporizer with a fixed hole diameter of 0.140" (~ 3.55 mm). With this arrangement we performed a single test and ran it at three different oven temperatures. This is the 12/15/92 test. We still measured substantially higher (factor of 6) flow rates than theoretical but the integrated mass flow rate measurements and the pre and post test weight differential agree within 16% as shown in the bottom part of the table under the title "Mass Closure." Considering that this test took over three hours, over which the flow was integrated, the 16% discrepancy is very reasonable. Thus the data can be considered valid which in turn implies higher vapor pressure than that extrapolated from published data. Back calculating the necessary vapor pressure necessary to flow the 2.22 and 4.08 mg/sec of fullerenes using the equation

TABLE 7.1

SUMMARY OF MASS FLOW DATA

run date	C60/C70 batch source ID	Toven on controler (degC)	Toven on Strip chart TC (degC)	p vapor theoretical at Toven (Torr)	mdot theoretical (mg/sec)	Orifice D (inches)	total m loaded (grams)	m left in vaporizer (grams)	% vaporized	delta m (grams)	mdot from delta m (mg/sec)	mdot from slope (mg/sec)	delta mdot (mg/sec)	delta mdot (%)
				WITH SST ORIFICE PLATE BETWEEN VAPORIZER AND IONIZER										
11/12/92	SRI	700	730	0.214 for C60 0.224 for C70	8.18 9.26	0.394	9.67	0.04	0.996	9.63	13.20	12.20	1.00	0.08
11/17/92	SRI 7/23-7/27	700	730	0.214 for C60 0.224 for C70	1.87 2.11	0.188	6.00	0.4	0.933	5.60	6.20	6.74	-0.54	-0.08
11/18/92	SRI	700	730	0.214 for C60 0.224 for C70	0.43 0.48	0.090	3.80	0.2	0.947	3.60	too short test	3.86	N/A	N/A
				WITH QUARTZ ORIFICE FUSED INTO VAPORIZER EXIT NECK										
12/15/92	ULVICK IND.	530	530	0.002 for C60 0.001 for C70	0.010 0.005	0.14				N/A	N/A	0	N/A	N/A
		680	675	0.070 for C60 0.060 for C70	0.391 0.368	0.14				N/A	N/A	2.22	N/A	N/A
		700	695	0.107 for C60 0.099 for C70	0.529 0.527	0.14				N/A	N/A	4.08	N/A	N/A
SUMMARY FOR	12/15/92					0.14	9.5	0.14	0.985	9.36				
				MASS CLOSURE FOR 12/15/92										
			TIME AT TEMP (minutes)	TEMPERATURE (degC)	MDOT theory (mg/sec)	MDOT from slope (mg/sec)	DISCHARGED M (grams)	INITIAL M (grams)	DELTA (grams)	DELTA (%)				
			140	530	0.007	In the noise	N/A	9.5						
			34	675	0.380	2.22	4.53							
			14	695	0.528	4.08	3.43							
		TOTALS	188				7.96	9.5	1.54	0.16253				

$$p = \frac{\dot{m}}{A}\sqrt{\frac{2\pi RT}{Mw}}$$

we get 404 mTorr and 751 mTorr respectively. Figure 7.1 shows this data superimposed on the curves extrapolated from data by Abrefah.[12]

A possible explanation is inaccurate temperature measurement. The two thermocouples within the oven agreed within 5°C during this test. They are located outside of the quartz vaporizer in a space between it and the tungsten heating wire. It is hard to imagine that they could be about 60°C below the actual fullerene temperature within the vaporizer, which is what it would take to put the data on the projected curve. Another possibility is solvents coming off the mix which is unlikely because we did not see the normal corresponding tank pressure increase. The tests are difficult and expensive to perform and we have expended approximately $5000 worth of fullerenes just on these flow rate tests and hence could not repeat them on a Phase I SBIR budget. There is however, no question that the mass flow rate measurement is reasonably accurate and reproducible and verified by the weight difference of the fullerenes between the initial and final weight. A three hour duration test demonstrated that the vapor flow is steady and controllable from rates of near zero to 2.2 and 4.1 mg/sec.

Samples collected after the 11/12/92 test from various locations within the system were sent out for analysis to SRI. These samples were from vacuum tank walls, ionization chamber, vaporization chamber, and fullerene condenser located downstream of the ionizer exit (see Fig. 6.1).

Each of these samples was dissolved in toluene and subjected to a HPLC analysis for C_{60} and C_{70}. All of the samples except for the vaporizer residue were completely soluble and the vaporizer residue was partially soluble. Furthermore the ratio of C_{70} to C_{60} in the soluble samples was about 20% in all samples which is what is normally found in the original extract. Therefore one can conclude that the fullerenes that have been vaporized from the thruster and collected in various parts of the system are exactly the same as the original fullerene mixture and have not been degraded in any way. They could in fact be used over again in future tests. The composition of the nonsoluble part of the vaporizer sample was not determined.

These unique tests demonstrated controllable fullerene vapor generation rate and that controlled vaporization does not affect their molecular weight (no fragmentation). Back calculated vapor pressure data are higher than anticipated from extrapolated low vapor pressure data obtained from literature.

7.2 Discharge and Acceleration Experiments

For the first set of discharge experiments we used the gold plated quartz grids (see Fig. 6.8), electrically connected approximately as shown in Fig. 6.11. The collector plate indicated in Fig. 6.11 was approximately 5" downstream from the grid and instead of being heated it was water cooled to insure condensation of all fullerenes so that following establishment of discharge, the condensed fullerenes on the collector can be examined for possible fragmentation.

During the first test the cathode filament was heated to approximately 2400°K and discharge voltage up to 200 VDC was applied without observing any discharge

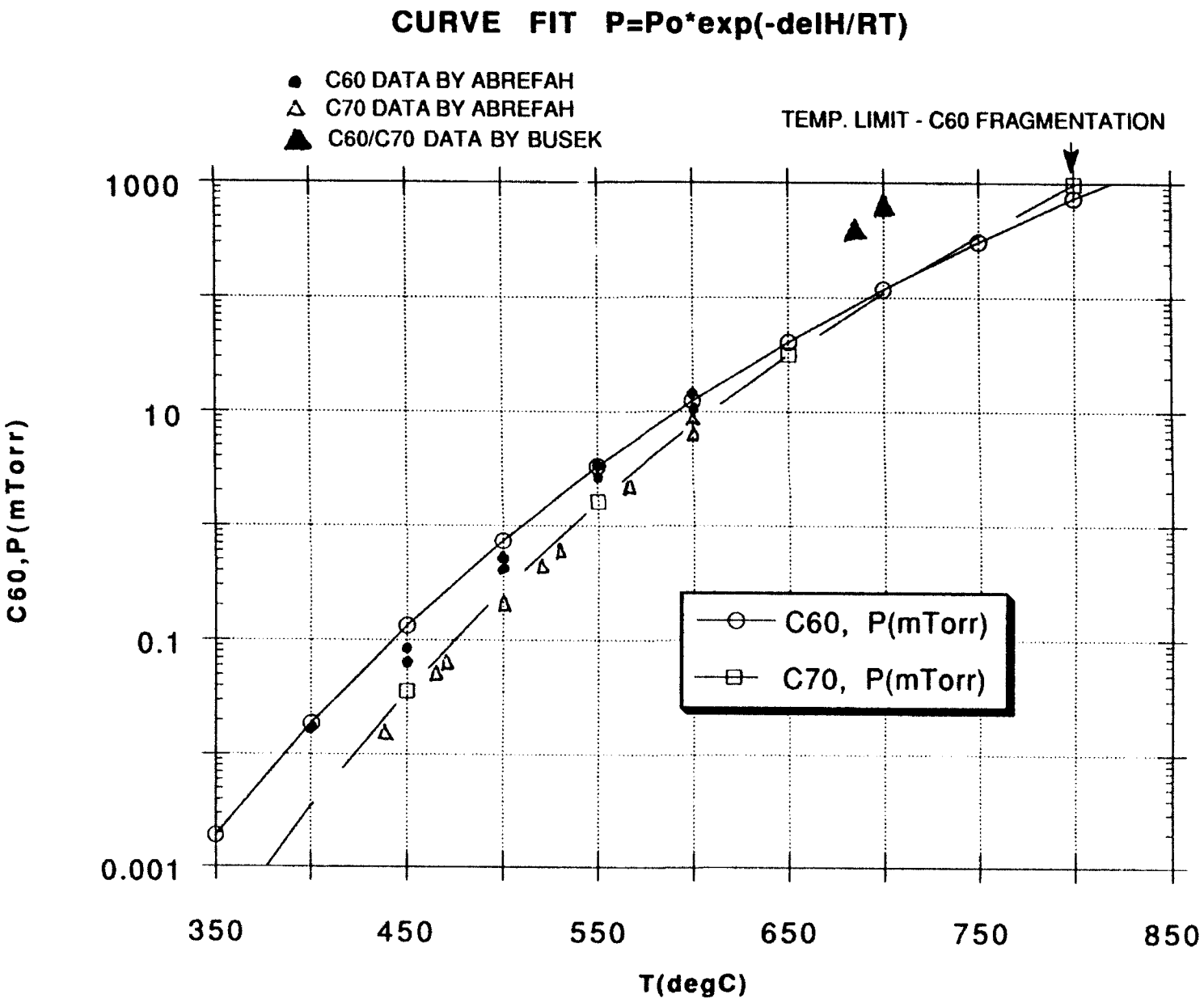

Fig. 7.1 Fullerene High Temperature Vapor Pressure Data were Calculated from Measured Mass Flow. The high temperature data obtained by Busek fall above the curve extrapolated from low temperature data by Abrefah.[12]

current. There may have been a few milliamperes which the shunt used at the time would not pick up. This was puzzling because we expected a discharge voltage of the order of 40 volts. Therefore, in order to verify the experimental set up we allowed the oven to cool to room temperature, back filled the tank with nitrogen to an estimated pressure of a few mTorr inside the ionization chamber and established discharge. Its V-I characteristic is shown in Fig. 7.2. The current is limited by the cathode emissivity as expected, revealing insensitivity to the discharge voltage. This proved that there is nothing wrong with the experimental set up.

Cathode emissivity in nitrogen is shown in Fig. 7.3 where we plot the discharge current versus the cathode filament heater current. (The cathode was a spiral of 0.020" dia., 2% thoriated tungsten wire). Typical exponential emissivity (discharge current) is revealed. The exact temperature of the cathode was not determined because of unknown voltage drops of leads and connections leading to the cathode. Estimated temperature is 2500°K to 3000°K. As noted in this figure the discharge voltage was kept approximately constant at 50 volts. However, to first start the discharge the required voltage was 84 volts. This was a cathode filament that was previously exposed to fullerenes. Subsequently we replaced the cathode with a new filament never exposed to fullerenes and started the discharge at 32 volts. Table 7.2 compares the first start and second start voltage for new and fullerene exposed cathodes. It clearly indicates that some sort of cathode poisoning occurred even after a very short exposure to fullerenes which persisted and maintained higher than normal discharge voltage.

Using the cathode previously exposed to fullerenes (test #010593) and proven by using it in an N_2 discharge described above, we established a discharge in fullerenes. The oven temperature was approximately 700°C which, based on previously discussed data, was giving fullerene mass flow of about $\dot{m}$ = 4 mg/sec. The estimated discharge chamber pressure (based on tank pressure measurement) was 1 to 5 mTorr. To start the discharge, 250 volts of applied voltage was required with a cathode heating current of I_{CH} = 15.0 Amps and cathode voltage of V_{CH} = 36 volts. When the discharge started the I_{CH} dropped from 15 A to 14.2 Amps reflecting the discharge current draw. The V-I of this discharge is shown in Fig. 7.4.

After the initial start the discharge voltage was gradually increased to 270 volts, with a small corresponding increase in discharge current which is the standard shallow V-I characteristic of cathode current limited discharge. From 270 volts the voltage was turned down back to 250 volts with no effect on the discharge current. Then the cathode heater current (I_{CH}) was increased from 14.2 Amps to 14.5 Amps which doubled the discharge current. The discharge power supply was then turned off and turned back on within approximately 1 minute. The applied voltage was gradually increased until the discharge restarted which occurred at 192 volts. These observations together with data in Table 7.2 provide strong evidence of cathode poisoning phenomena which results in low emissivity and high discharge voltage - approximately six times higher than expected.

The cathode filament disintegrated during post test inspection. The total estimated exposure to fullerenes was about 30 minutes. The filament diameter increased from 0.020" diameter to 0.025". Examined under optical microscope the surface of the filament was covered with hemispherical protrusions typically 0.005" in diameter which appeared to consist of carbon. Because the cathode is crucial to successful application of the fullerene ion thruster we conducted a thorough exami-

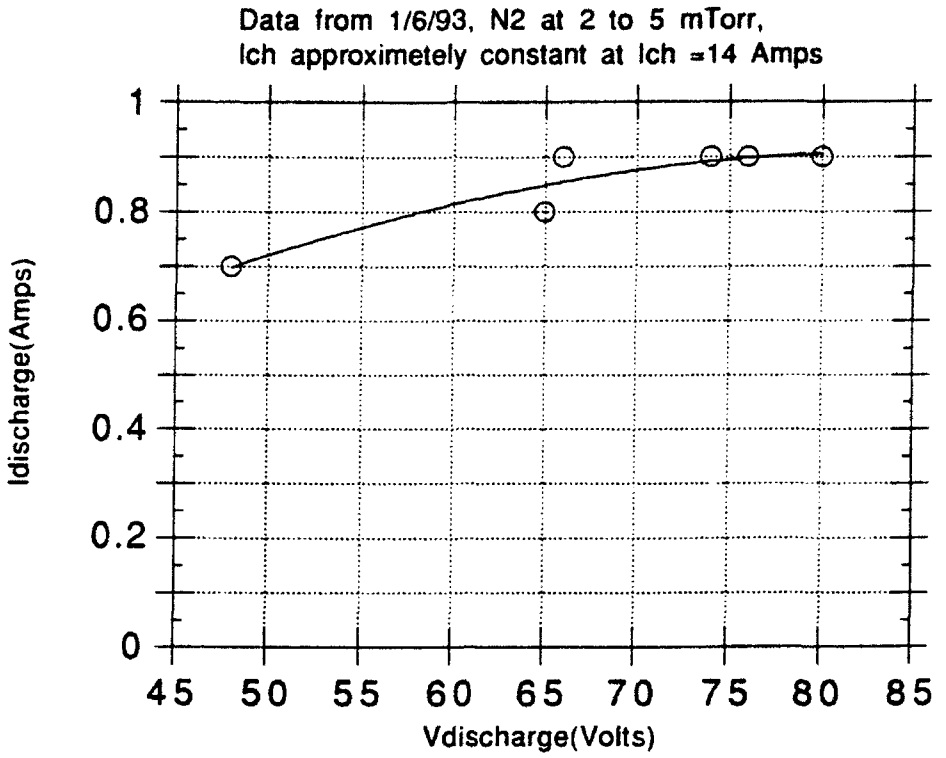

Fig. 7.2 V-I Characteristic of a Nitrogen Discharge

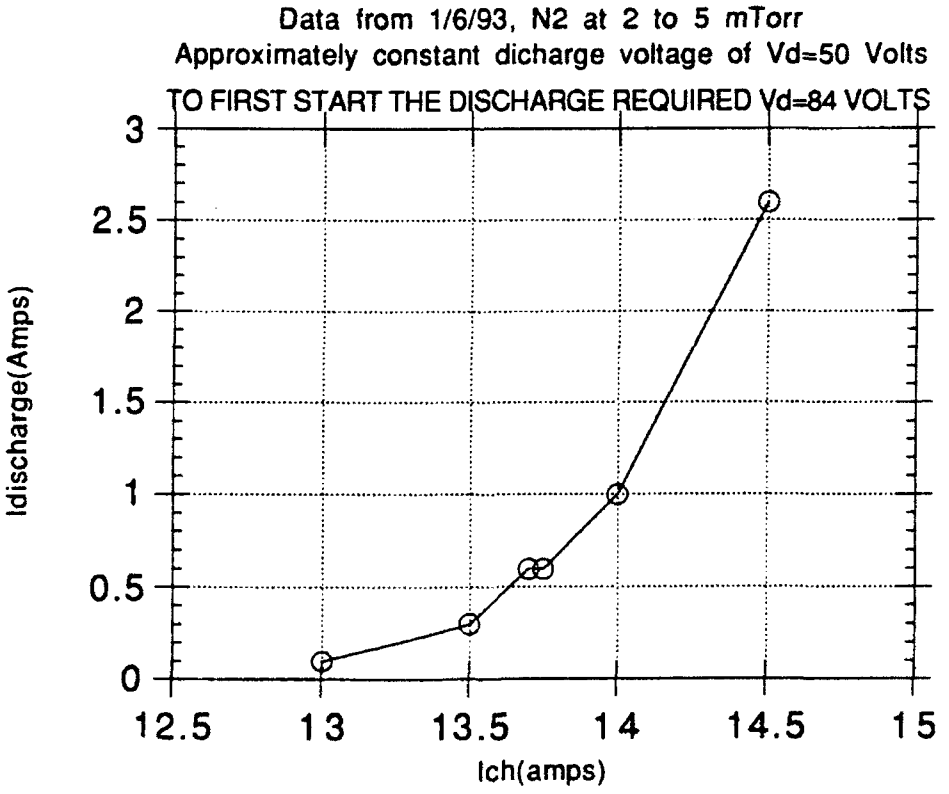

Fig. 7.3 Nitrogen Discharge Current Dependence on Cathode Filament Heating

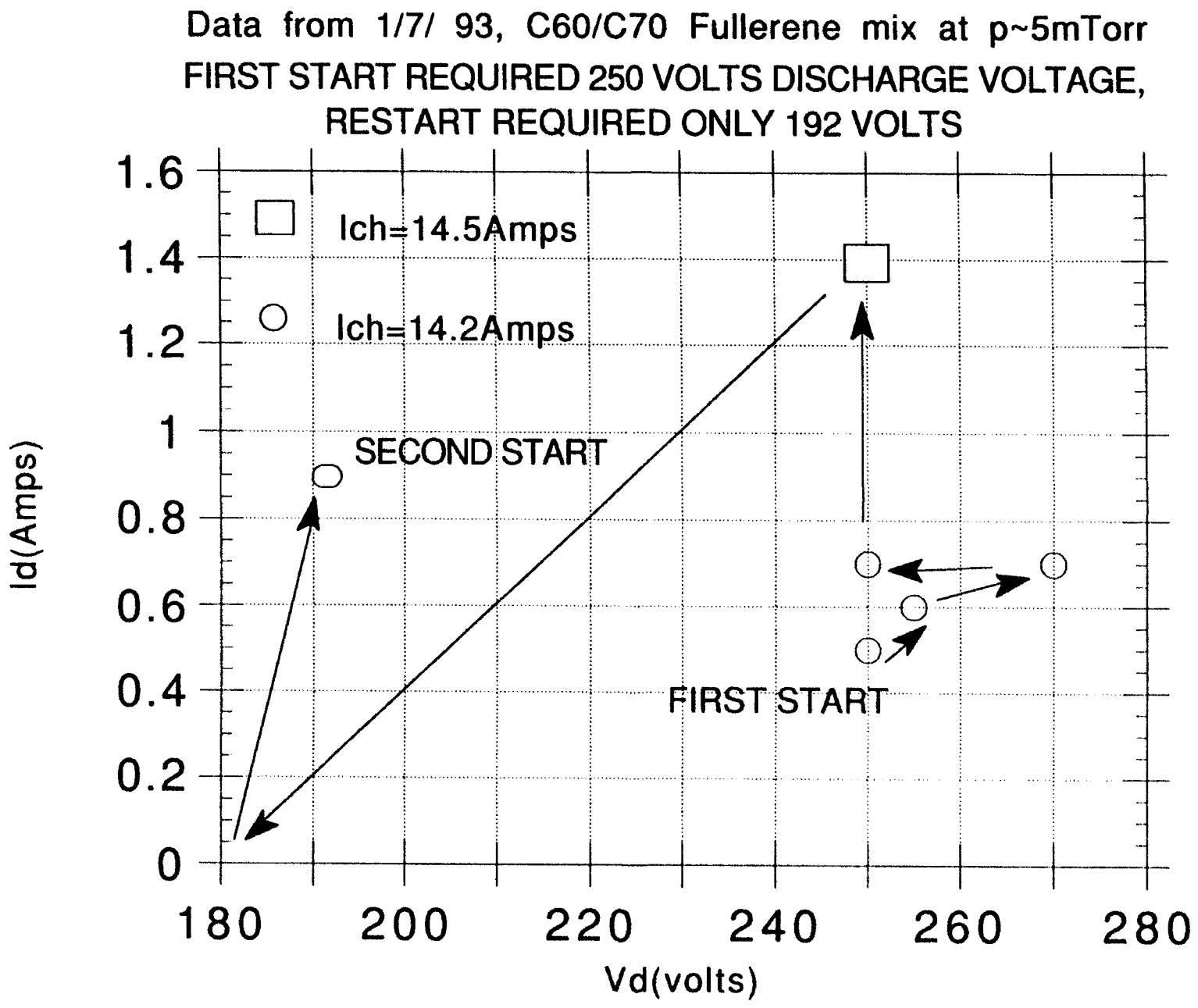

Fig. 7.4 V-I Characteristic of Fullerene Discharge

nation of this as well as one other cathode filament. The results of this examination are in Section 8.0 entitled, "Discussion."

TABLE 7.2

STARTING VOLTAGES OF NITROGEN DISCHARGE FOR NEW AND FULLERENE EXPOSED CATHODE FILAMENT

	V_D FIRST START	V_D SECOND START
New (test 1/21/93)	32	28
Exposed to Fullerenes (test 1/6/93)	84	48

During the same tests we attempted to accelerate the positive ions using the quartz grids described previously. These shorted shortly after we applied voltage even though at room temperature they tested to 2 kV without leakage before and after the test. Fullerenes, which are dielectric, were found to be condensed on both the screen and the accelerating (outer) grids and on the collector plate located downstream of the grids. Figure 7.5 is a photo of the accelerating grid showing the deposition of the fullerenes not only on the grids but also on portions of the vacuum tank. Unlike previous tests that were performed without discharge inside the ionization chamber we found a deposit in the back of the cathode. This film was electrically conductive and adherent to the quartz walls of the chamber. Because condensed fullerenes are electrically nonconductive this layer consisted of fullerenes that fragmented under heat and discharge conditions to graphite. Deposits in all other parts of the experiment on the tank walls were nonconductive. There were no deposits on the anode. The following sample deposits from the various locations were submitted for analysis.

L14 Ion Chamber
L15 Collector Plate
L16 Inner Grid, Internal Face
L17 Outer Grid, Internal Face
L18 Outer Grid, External Face

Each of these samples was dissolved in carbon disulphide (CS2) which is a stronger solvent than toluene and subjected to a HPLC analysis for C_{60} and C_{70}. The sample L14 was insoluble in CS2 and L16 was only partially soluble. L15, L17, and L18 were completely soluble. The ratio of C_{70} to C_{60} in the soluble samples was in the normal range of 20-25% in all samples. This indicates that portions of the ionization chamber were overheated most likely due to the combination of discharge Joule dissipation and radiated heat by the high temperature cathode filament. All of the L14 samples came from an area upstream of the cathode filament. All samples collected outside of the discharge chamber exhibited no fragmentation due to discharge and retained the original C_{60}/C_{70} split. This is one of the salient results of this study.

For the next test we replaced the gold plated quartz grids with metal grids (see Fig. 6.10) and installed new cathode filament. The tank was pumped down to the 10^{-6} Torr range and power was applied to the discharge chamber, grids, collector

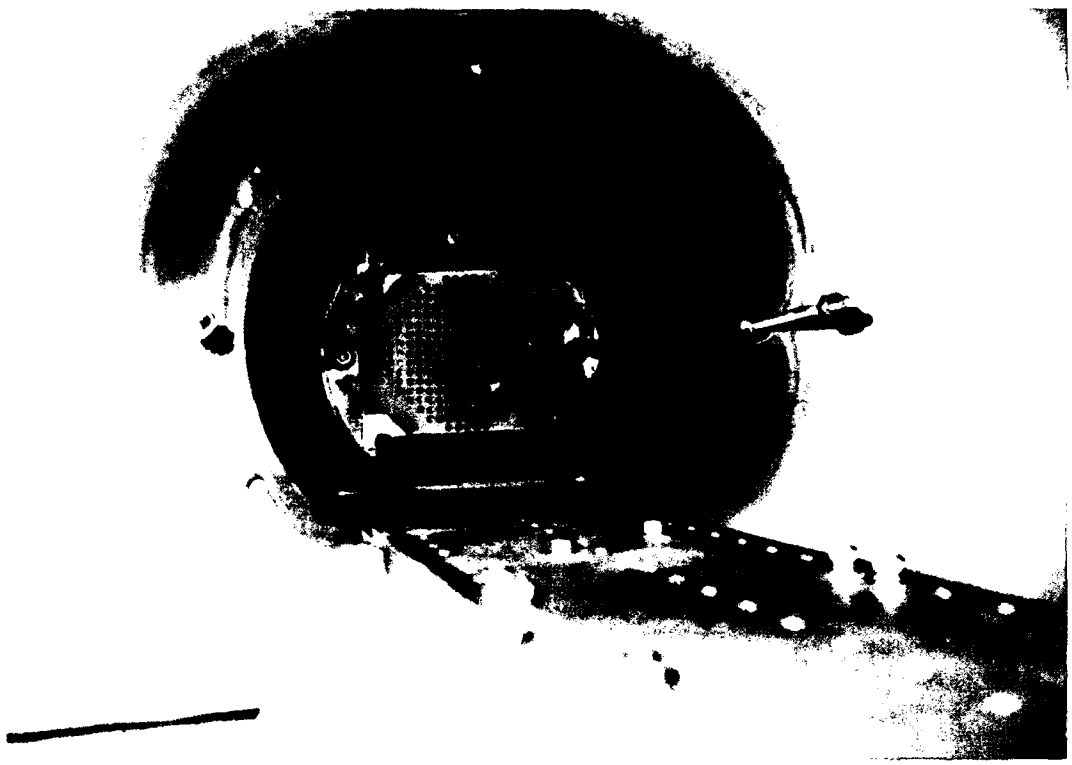

Fig. 7.5 Outer Face of the Accelerating Grid Shows a Layer of Condensed Fullerenes

plate and the cathode filament. The respective voltages were (see schematic, Fig. 6.11) V_D = 50 volts, $V_G \cong$ 1000 volts, $V_{collector} = V_{Beam} \cong$ 1000 volts, V_{CH}=33 volts drawing I_{CH} = 14.8 Amps.

At these conditions the oven heater was turned on and its programmable controller was set to reach 650°C within approximately 5 minutes and hold it constant. When fullerene vapor started to flow the grid voltage collapsed and fluctuated between 280 volts and 400 volts depending on the grid current (of the order of 0.5 to 0.2 mA) which is a consequence of our poorly regulated power supply. The collector voltage held steady at 1000 volts. Discharge was not detected until V_D was manually increased to about 60 volts. At that point the discharge power supply with a preset current limit tripped because the current limit was exceeded. Its magnitude was unknown and our recording equipment (Beckman Strip Chart Model 2500) sampling once every 6 seconds did not catch it. The same repeated itself at several times while we were increasing the current limit set point until $V_D \approx$ 136 volts. At that point the discharge current of I_D = 160 mA and beam/collector current of I_B = 18 mA was recorded. The V_D was turned off and brought up again to determine where the next ignition point occurs. At $V_D \cong$ 170 volts the discharge started and next time it started at $V_D \cong$ 195 volts drawing a discharge current of 250 mA. At that point we wanted to increase the discharge current by increasing the cathode heater current (hence, emissivity) to $I_{CH} \sim$ 15.6 Amps and the cathode failed terminating the test.

It is to be noted that we measured approximately the same discharge voltage in our first test after a second discharge start (see Fig. 7.4). This confirms that, with a tungsten filament cathode, a stable discharge in fullerene vapor requires 190 volts.

Upon disassembly the unheated collector was coated with a film of strongly adhering fullerene layer indicating impact by energetic ions rather than simple condensation observed in previous tests. The layer was highly resistive. Two probes placed 1 cm apart on the cooled surface of SST collector indicated resistance range of 10^7 to 10^8 ohms, hence there is no question about the fullerene/fullerite nature of the layer. The layer was too thin and too adherent to scrape and analyze, however its resistive nature indicates that the fullerenes did not fragment during their ionization as well as acceleration process or due to impact upon the collector. This corroborates the data repeated earlier which were obtained from the analysis of nonaccelerated deposit on the collector. Thus, this test fulfilled one of the major objectives of the Phase I research which was to confirm that fullerenes do not fragment upon ionization or acceleration.

The data described above were used to estimate the key ion thruster performance numbers that are summarized in Table 7.3. This data must be taken as very preliminary and provide just an initial idea of future prospects. An important parameter, the ion beam energy cost is high (ε = 915 volts) relative to xenon ion thruster which for similar discharge size and cusp magnetic field is of the order of 200. Analysis performed by Torres[16] predict that same sized fullerene thruster with cusp magnetic field should have ε = 177 volts. The principal reason for the high measured ε is of course high discharge voltage. This is a crucial issue which will be examined in Section 8.0 entitled, "Discussion."

Another important parameter is the propellant utilization which came out surprisingly high. This may be due to double ionization or just inaccuracies in the measurement of the beam current as well as in the estimated total propellant mass

flow. Torres[16] however, predicted high fullerene propellant utilization (Fig. 7.6) which gives credence to the data. Clearly these tests must be repeated with better instrumentation and longer test times which, due to the cost of fullerenes, were necessarily limited by the Phase I SBIR budget.

These tests demonstrated the first discharge in pure fullerene vapor and first fullerene ion thruster data were obtained. The discharge voltage was higher than expected. Detectable fragmentation of fullerenes did not occur.

TABLE 7.3

SUMMARY OF EXPERIMENTAL CONDITIONS AND RESULTS

Cathode Heater Voltage	V_{CH} (Volts) = 33.0
Cathode Heater Current	I_{CH} (A) = 14.9
Discharge Voltage with Respect to Ground	V_D (Volts) = 136
Discharge Current	I_D (mA) = 160
Collector Voltage WRT Ground	$V_{coll.}$ (Volts) = 1000
Collector/Beam Ionic Current	I_C (mA) = 18
Inter Grid Voltage	V_G (Volts) = 4000
Actual Discharge Voltage	V_{DA} (Volts) = V_D - V_{CH} = 103
Beam Ion Energy Cost	$\dot{\varepsilon}_{(volts)} = \frac{V_{DA} \cdot I_D}{I_C} = 915$
Mass Flow Based on Beam Current Assuming Single Ionization	$\dot{m}_c = \frac{I_C \dot{m}_i}{q} = 0.14 mg/sec$
Estimated Mass Flow Based on Temperature Measurement and Corresponding Vapor Pressure	$\dot{m}_t = 0.2 mg$
Fullerene Vapor Pressure in Vaporizer	T_{vapor} (°C) ≅ 650
Pressure in Discharge Chamber Estimated on the Basis of Tank Pressure	P_D(Torr) ~ 10^{-4}
Estimated Propellant Utilization Assuming Single Ionization	$\eta_p = \frac{\dot{m}_c}{\dot{m}_t} = 0.7$

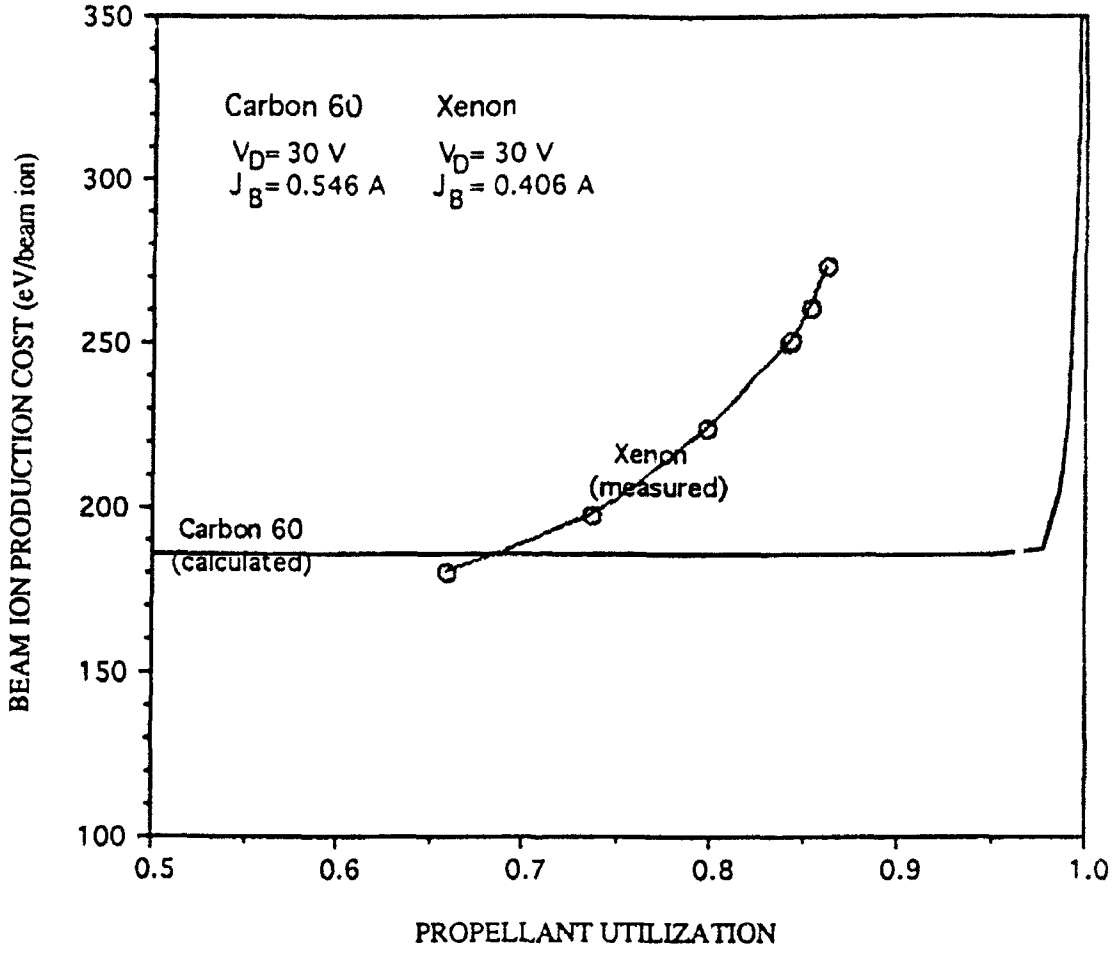

Fig. 7.6 Beam Ion Production Cost for the Hughes 13 cm Lab-Model Thruster Using Xenon and C_{60} for the Propellant Gas. V_D = 30 V

(Reprinted from Ref. 16)

8.0 DISCUSSION OF CRITICAL ISSUES

There are at least two crucial issues that must be resolved before a successful fullerene ion thruster can be constructed. The first is the magnitude of the discharge voltage and its relation to suspected cathode poisoning and other possible causes. The second is propellant feed, dependency of propellant vapor generation on heat cycling and unusable fraction of the propellant, i.e., the fraction that cannot be vaporized at 700°C which according to our measurements could be as much as 7%.These are discussed below.

8.1 High Voltage Causes and Cathode Phenomena

The high measured discharge voltage could be the result of several phenomena including:

1) Poisoning of the cathode and formation of insulating layer

2) Insulating layer on anode

3) Large C_{60} excitation cross sections

4) High negative C_{60} ion density

These are discussed in reverse order below.

The negative ion formation has been predicted to be negligible by Torres.[16] No data exists as yet on C_{60} excitation cross sections. Torrez predicted large excitation cross section, however its ratio with measured ionization cross section is about the same as the ratio for Xe and hence looks reasonable as shown in Table 8.1 below.

TABLE 8.1

COMPARISON OF Xe VERSUS. C_{60} IONIZATION AND EXCITATION CROSS SECTIONS

CROSS SECTION	Xe	C_{60}
$\sigma_{ionization}$ (m^2) at 30 eV	3.9×10^{-20}	55×10^{-20}
$\sigma_{excitation}$ (m^2) at 30 eV	3.5×10^{-20}	45×10^{-20} (predicted)
Ratio of σ_i/σ_e	1.11	1.22

Larger than predicted excitation cross section could of course mean larger inelastic energy losses by the electrons as they collide with the fullerenes. The average energy of the discharge electrons is a balance between the energy gain from the imposed anode to cathode voltage and the energy they lose in collisions in

which they excite the fullerene rotational, vibrational and electronic states. When the inelastic losses are high, higher voltage must be applied. This scenario, however is not consistent with the observed initial discharge established at 60 volts which increased in steps of 30 to 40 volts at each discharge restart until it stabilized at 190 volts. If the large excitation cross section was responsible for the high voltage the voltage would be independent of the number of restarts. This evidence points to electrode problems.

No layer has been visually observed on the anode and electrical continuity checks indicate no such layer exists, hence anode is not responsible for the high discharge voltage. That leaves the cathode.

Two cathode filaments were operated in fullerene vapor. One failed after test completion (1/7/93) during apparatus disassembly and will be identified as F1. It was exposed to fullerene vapor after cathode heater current and the oven heat was turned off thus a possibility exists that fullerene vapor simply condensed on it. The second filament (F2) failed due to cathode heater/discharge over-current during the test and was exposed to fullerenes for much shorter time than filament F1. Both filaments were analyzed using scanning electron microscope (SEM). Photos in Figs. 8.1 and 8.2 clearly reveal a thick deposit on the filament. In some areas it is as much as 0.002" (0.05 mm) thick. Figure 8.1(a) shows sections of the filament and a break in the wire (0.020" in dia.) showing the bare tungsten metal. Figure 8.1(b) shows a close-up area of the surface layer. Figure 8.2(a) shows another break surface and with the surface deposit on it and Fig. 8.2(b) shows a close-up of this deposit taken from the top photos. It shows a layered structure of the deposit. The surface of the deposit is nearly pure carbon as shown in Fig. 8.3 obtained from EDAX spectrometer. Some contamination of the carbon, which is not fullerenes but graphite because it is highly electrically conductive, is revealed as evidenced by weak counts of oxygen, tungsten, and possibly silver which may be scatter from the sample mounting paste. The EDAX spectrum of the bare metal is shown in Fig. 8.4 There appears to be a small contamination of carbon on the metal and little thoria (initially 2% thoriated W). That small carbon contamination alone can poison the cathode emissivity and explains why we had to run the cathode very hot.

Analysis of the second cathode filament (F2) that had a shorter exposure to fullerenes revealed much thinner coating. An SEM close-up of a typical surface of this filament is shown in Fig. 8.5. Portions of this cathode appear nearly free of deposits and portions reveal very light coating. Of particular interest are the portions that appear not coated because these areas should have high emission and low cathodic voltage drop. The filament was purposely fractured in that area and Fig. 8.6(a) shows a portion of the fracture while Fig. 8.6(b) show a close-up of the outer layer. Figure 8.6(a) reveals radially oriented recrystallization about 100 μ deep. Figure 8.6(b) shows a dark layer about 2 microns deep that appear as a contaminated metal. Figure 8.7 shows the EDAX spectra of the coated and the relatively coat free (metallic looking) portion of the surfaces shown in Fig. 8.5. As expected the coated portion shows much higher carbon content. Oxygen contamination is similar in both areas. Unexpected result was strong presence of thoria in the coated layer with much less of it in the uncoated metallic area. To confirm it EDAX spectra was taken of the interior and the outer layer of the fractured surface shown in the photos of Figs. 8.6(a) and 8.6(b). This spectra, shown in Fig. 8.8, confirms strong presence of thoria in the 2 μm thick carbon contaminated layer (not exterior coating) while showing depletion of thoria in the interior (30 μ radially inward from the surface). This interior was also showing low carbon and oxygen content. Based on these spectra it appears that fullerene ions bombarding the cathode penetrate at least 2 μ

Fig. 8.1(a) SEM Photo of 2% Thoriated Cathode Filament (F1) Showing Thick Layer of Carbon

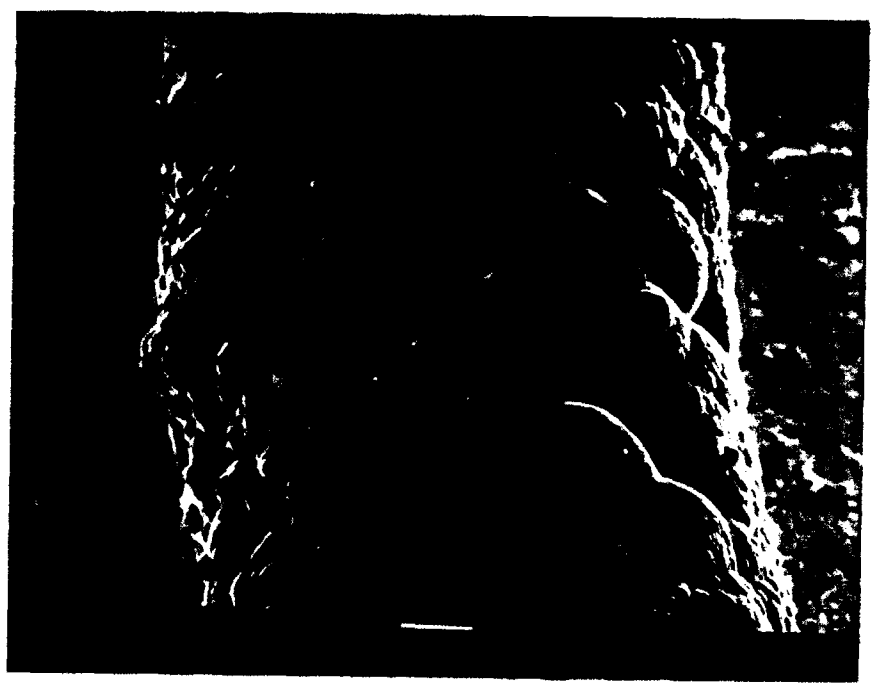

Fig. 8.1(b) Close Up of Carbon Layer on Filament F1

Fig. 8.2(a) SEM Photo of Fractured End of Filament F1

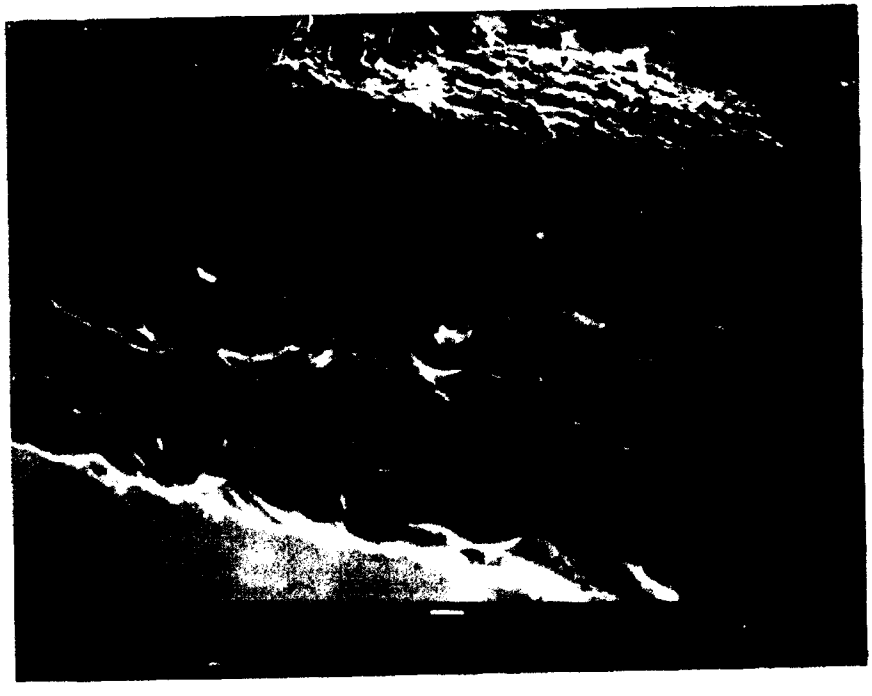

Fig. 8.2(b) Close Up of the Fractured End of Filament F1 Showing the Layered Structure of the Carbon Deposit

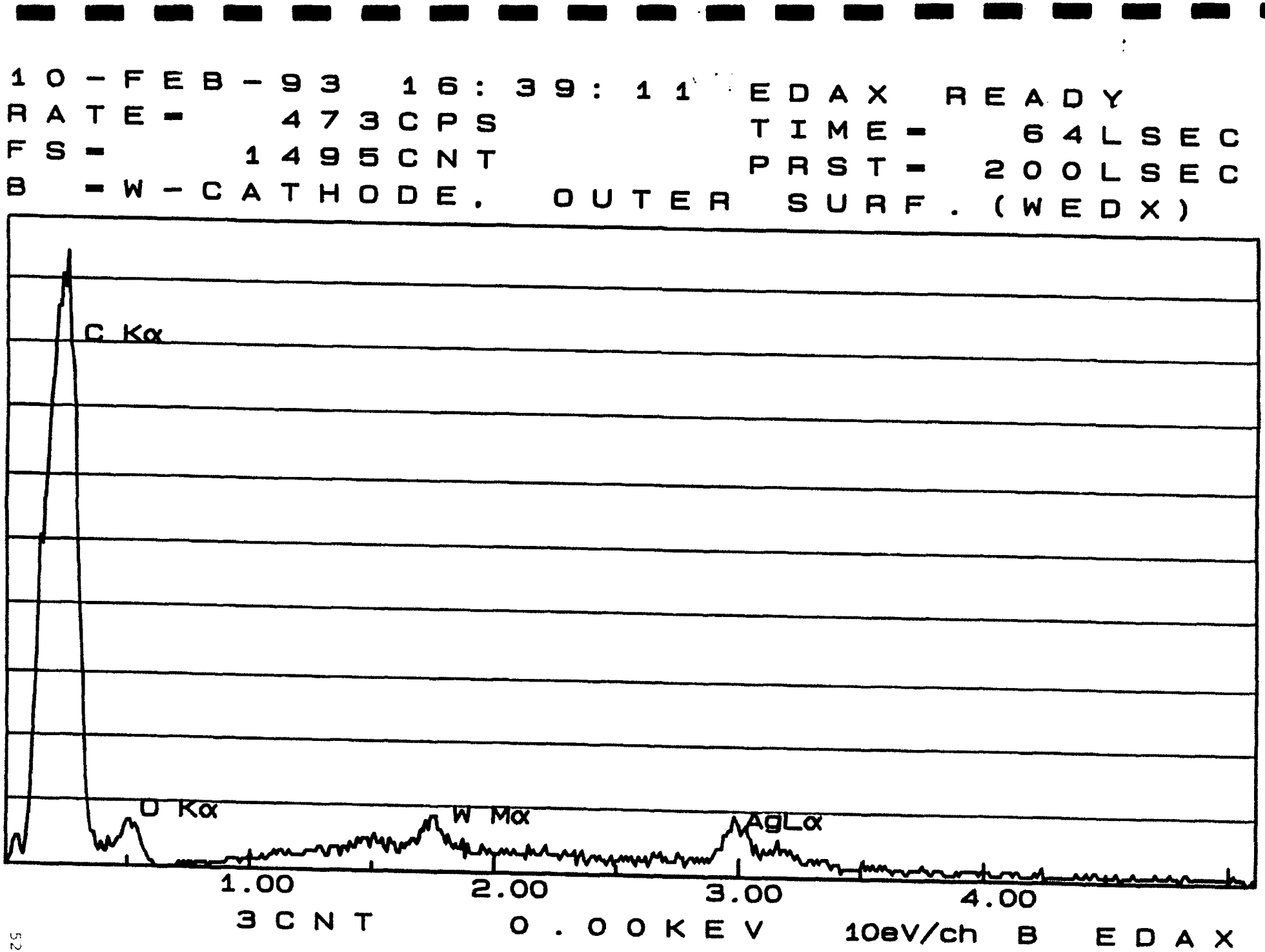

Fig. 8.3 EDAX Spectrum of the Outer Surface of the Layer Shown in Fig. 8.1(b)

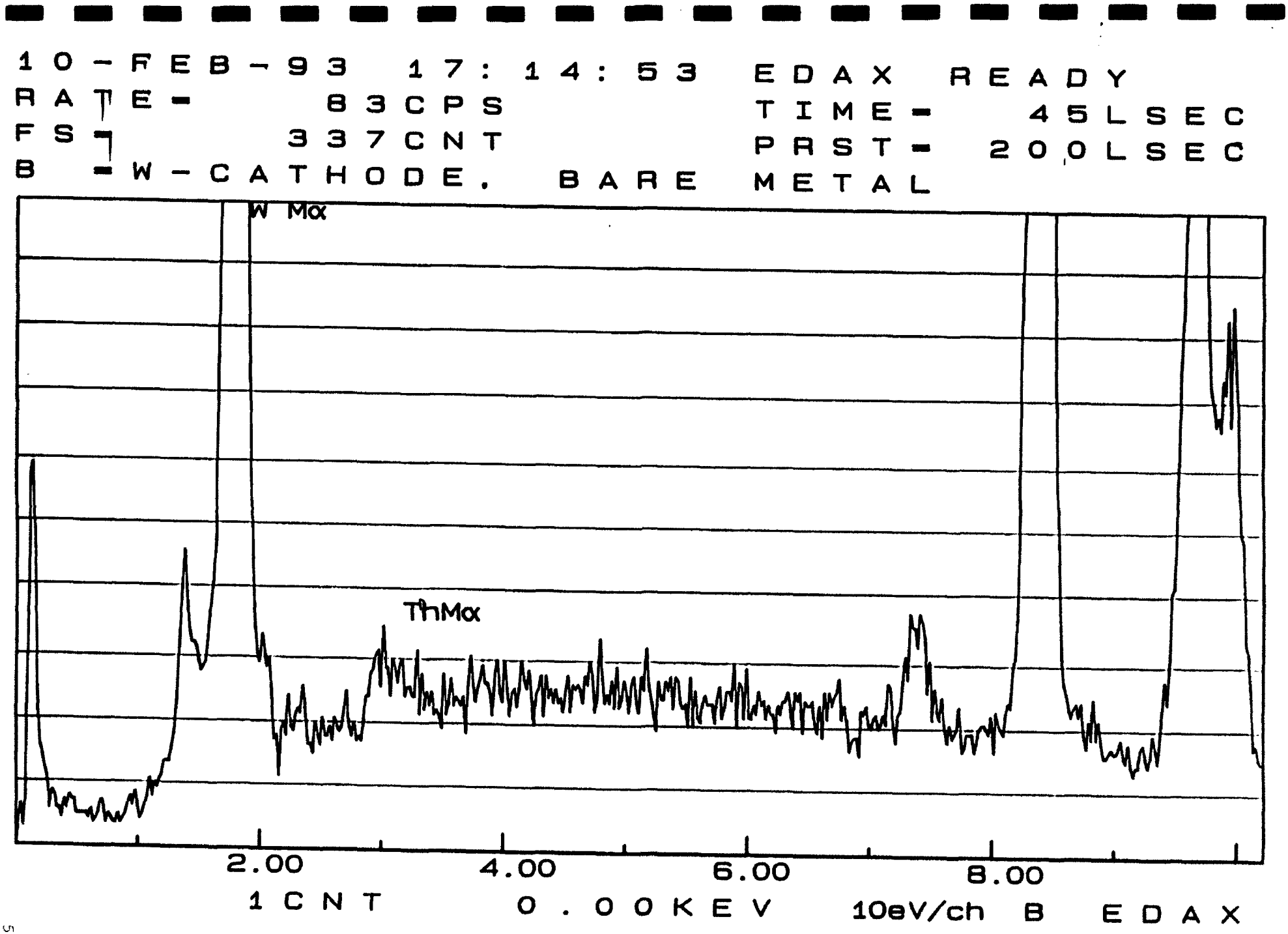

Fig. 8.4 EDAX Spectrum of the Interior of the Fracture Shown in Fig. 8.2(b)

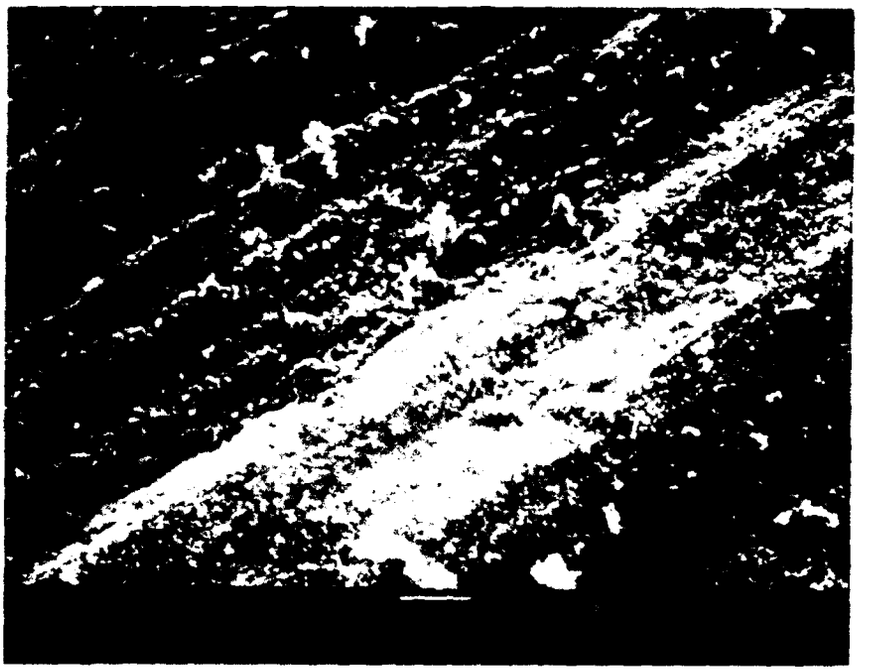

Fig. 8.5 SEM Close Up of the Surface of 2% Th/W Cathode Filament F2 Showing Coated and Metallic Surfaces

Fig. 8.6(a) SEM Photo of the Fracture in Filament F2 Showing Recrystallization of Outer Layer that is about 100 Microns Thick

Fig. 8.6(b) SEM Close Up of the Fracture Showing a Contaminated Layer About 2 Microns Thick

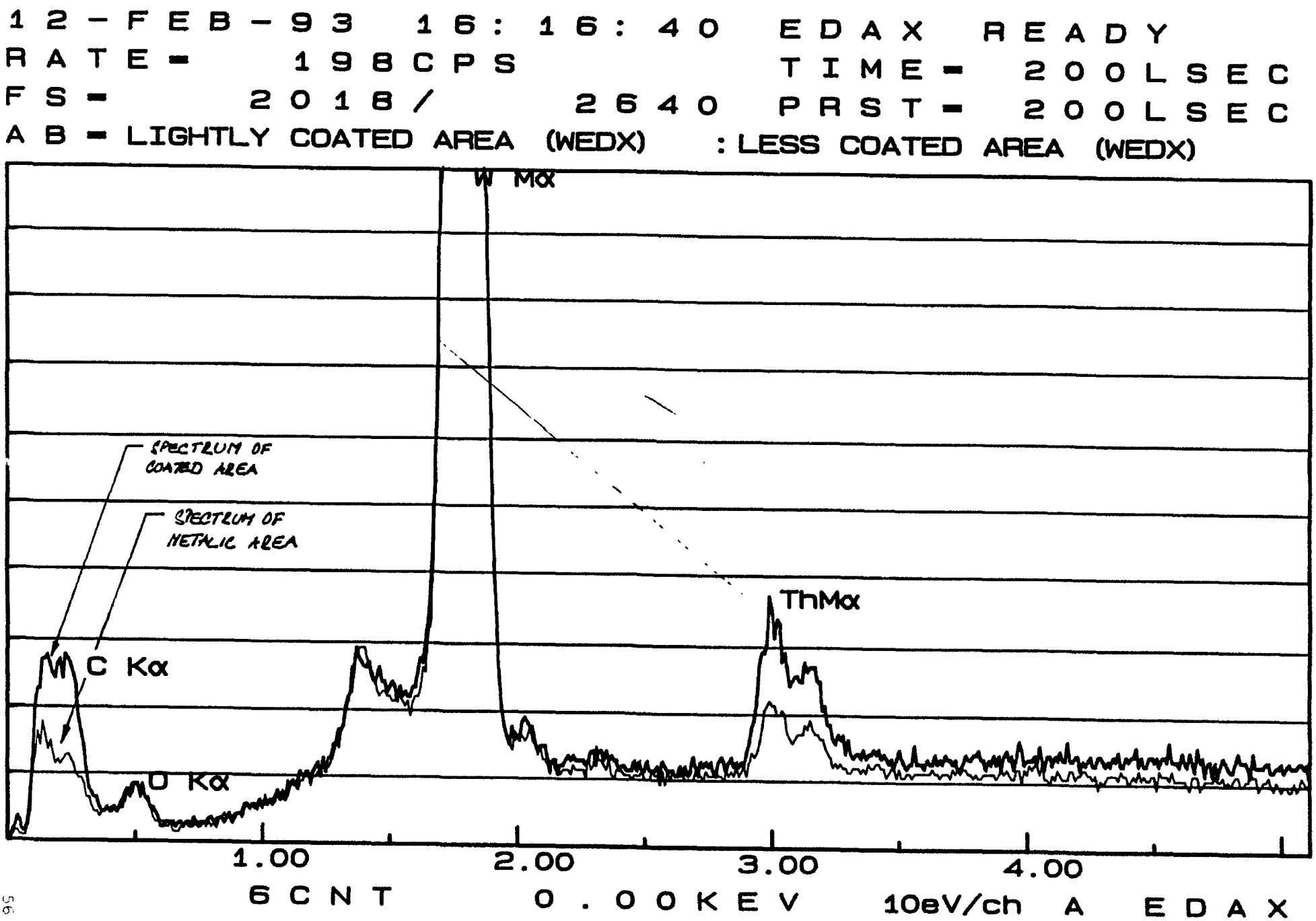

Fig. 8.7 EDAX Spectrum of the Coated and Metallic Surfaces in Fig. 8.5

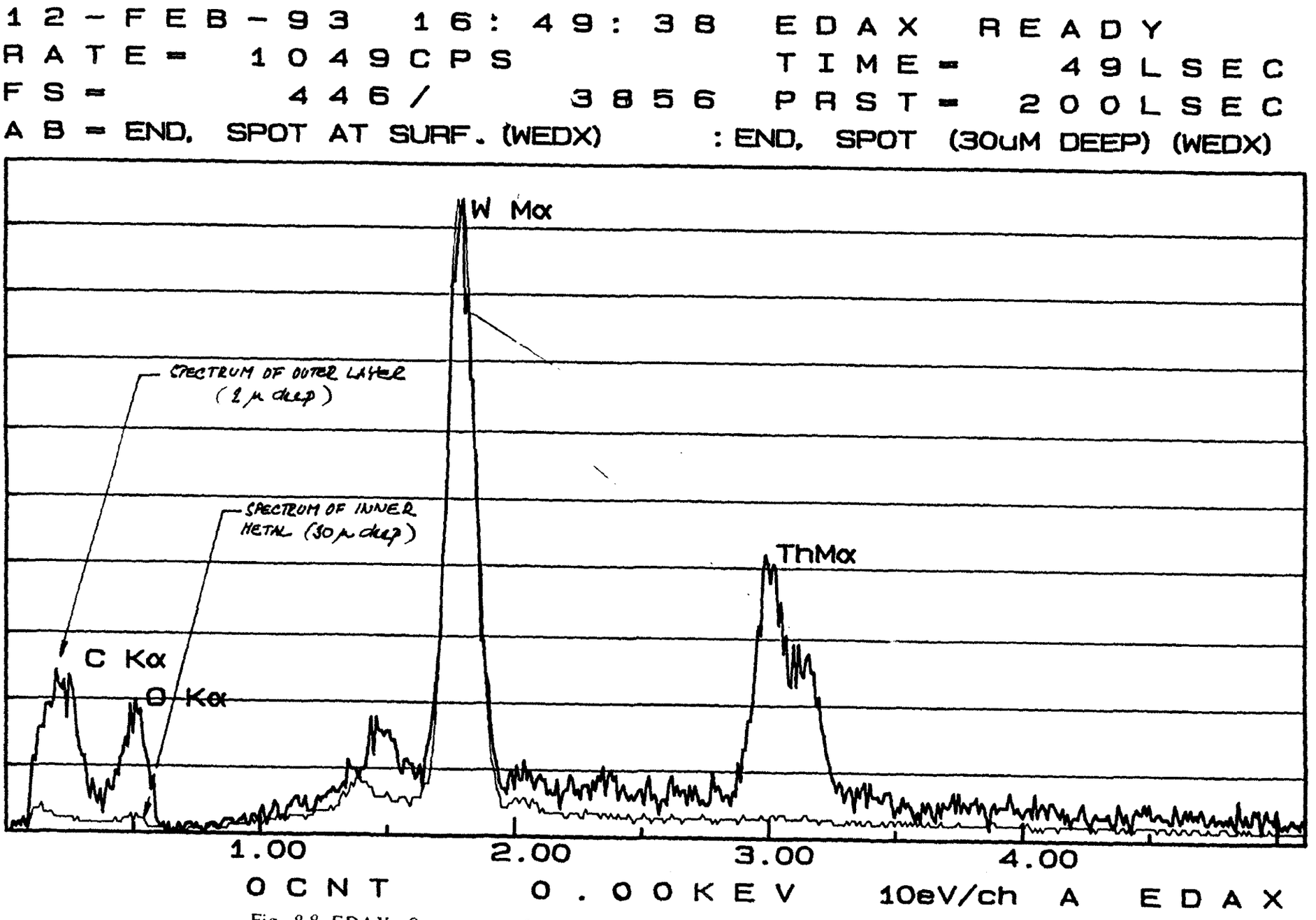

Fig. 8.8 EDAX Spectrum of the Contaminated Outer Layer (2 microns thick) and Interior (30 microns deep) of the Fractured Cathode Filament F2 Shown in Fig. 8.6(b)

into its surface and react with thorium to form thorium carbide. This clearly poisons the cathode emissivity and may be at least partially responsible for high discharge voltage.

The mechanism of formation of the layer is postulated as follows. When cathode first starts emitting, some fullerene ions will be accelerated toward it and bombard it. This poisons the cathode and initiates building of a graphitic layer because the tungsten is hot and breaks down the fullerenes to graphite. This builds up continuously until the graphite surface temperature (heated by the Joule dissipation of the discharge current) reaches a point where the graphite vaporization and effusion rate balances the flux of fullerenes forming the deposit. This also explains why every time a discharge is established and turned off it takes higher voltage to reinitiate it until it reaches equilibrium at approximately 190 volts discharge voltage. It is unlikely that the coating is uniform and therefore emission will occur in small spots on the cathode. Here the emission is likely to be space charge limited adding to the voltage necessary to sustain the discharge.

It appears likely that even a tungsten hollow cathode (HC) normally used in ion thrusters will have the same problem because it operates at temperatures of the order of 1100°C[17] which may be sufficient to start forming graphitic layers. A possibility is to test alternative materials that have high work functions but do not react with fullerenes. Graphite cathode should also be tested because it would be self replenishing with fullerenes and hence have long life. This cathode would require high temperature to emit but since the discharge chamber must be heated anyway, the cathode heat would not be a loss. Another option is to run hollow cathode on Ar or Xe but this could decrease the thruster performance, and increase grid erosion (due to different mass to charge ratio). Another option is to use ionization by Electron Cyclotron Resonance (ECR) discharge[18,19] instead of by electron bombardment. However, testing of alternative cathodes on fullerene vapor must be performed before discarding dc ionization.

8.2 Fullerene Feed System

A spacecraft with fullerene fueled ion thrusters performing a low to GEO transfer and station keeping may have on board hundreds of kilograms of fullerenes. How to store the propellants and how to feed it into the vaporizer is a challenging engineering problem. Several approaches can be considered which defer depending on the amount stored and hence, the spacecraft mission.

Fundamentally they can be divided into: (1) heating the entire fuel storage in which case the storage tank becomes the vaporizer, or (2) heating small portions of the propellant in a small vaporizer that is fed incrementally or continuously from the storage tank.

Both approaches have drawbacks and advantages. The obvious disadvantage of the first approach is that one is heating large volume (of the order of 0.6 m^3 for 1000 kg of propellant) which implies large heat loss and large thermal inertia.

The second approach where one can consider feeding pelletized fuel using gun-like magazines requires complex mechanical system with a hermetic seal in between the vaporizer and the storage tank so that fullerene vapor does not flow back into the storage tank where it would condense. The hermetic seal would have to be basically a high temperature valve operating at up to 700°C so that condensation

does not occur within it, which could freeze it up and plug the conduit. The pros and cons of these approaches are summarized in Table 8.2. To decide which is preferable (and to search for alternatives) requires detailed analysis which is beyond the scope of this work. However, option 1 is more appealing especially for systems that store only a few tens of kilograms of fuel because it's a passive system.

TABLE 8.2

FUNDAMENTAL OPTIONS FOR FULLERENE STORAGE AND VAPOR GENERATION

CONFIGURATION	PROS	CONS
OPTION 1 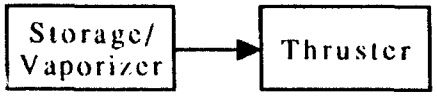	- Passive System - No mechanism to incrementally feed propellant - Hence, more reliable	- Large volume/mass to heat - Larger heat losses - Large thermal inertia
OPTION 2 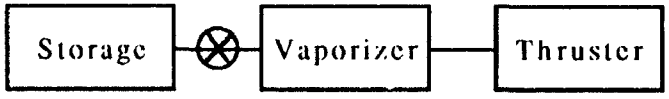	- Low power to vaporizer due to low volume/losses	- Complex mechanical feed system - Requires high T valve between storage and vaporizer - System failes if valve fails to close - Possibility of unvaporizable fullerene residue accumulation in vaporizer

9.0 FULLERENE PRODUCT DETECTION BY FOURIER TRANSFORM INFRARED SPECTROSCOPY

9.1 INTRODUCTION

The goal of the work described below was to detect C_{60}/C_{70} fullerene vapor concentration and possible fragmentation of the fullerenes in free molecular stream of fuller ? vapor inside a heated enclosure. Since fullerene vapors only exist in large concentrations at high temperatures (600-900°C), it is preferable to detect them by using optical measurement techniques that avoid contact with this extreme environment. Fourier Transform Infrared Spectroscopy (FTIR) is the optical technique used in this work, chosen because it can take an entire mid infrared (IR) spectrum simultaneously. The mid IR region of the spectrum is notable for the fact that almost all vapors have unique absorbance spectra in this region. FTIR spectrometry is a widely used analytical tool at present[20] that uses transmission through a sample, or emission from a sample (at high temperature) to detect the simultaneous concentration of many chemical species. FTIR spectrometry is not a dispersive technique; it employs the fourier transform of light interference between closely parallel moving mirrors to deconvolve a spectrum from a raw signal called an interferogram.[20]

The commonly available fullerenes (C_{60} and C_{70}) have strong absorption signatures in the mid IR region of the spectrum with relatively large absorbance values as shown in Figure 9.1.[21] C_{60} has four principle absorbance peaks, centered at 528, 577, 1183, and 1429 cm^{-1}; the 528 and 1429 cm^{-1} peaks are the strongest. The emission of C_{60} in the IR[22] and the UV/visible absorption of C_{60}[23] has also been measured. Since it is a molecule of high symmetry the peaks are few in number, but there are a sufficient number of sufficiently strong peaks to assure identification of the material if it is present even in small quantities. The reason for this is the fingerprint nature of spectra identification. While many compounds (and noise) can contribute to the absorption at a particular wavelength, absorption at 3 or 4 distinct and prespecified wavelengths in calibrated amounts allows measurement of the concentration of the absorber to high accuracy even in the presence of large amounts of noise or other material.

9.2 Apparatus and Procedures

A Bomem MB-155 Michelson Mid IR FTIR Spectrometer was used for measurements in the fullerene facility at Busek Inc. This spectrometer has high IR throughput, fine resolution, and wide frequency range. The spectral range of the spectrometer is from 500 to 6500 cm^{-1}, and it has selectable resolution from 1 to 128 cm^{-1}. For this work the spectrometer was used in transmission mode: IR radiation is generated by a hot source in the spectrometer, collimated, passed through the moving mirror system, and manipulated by external optics through the sample volume and into the slaved detector.

Figure 9.2 shows the geometry of the optical arrangement including the spectrometer, IR beam optics, IR detector, and fullerene facility vacuum chamber. The IR output beam was deflected and focused by a parabolic mirror segment through the two KBr windows mounted on the vacuum chamber and then collected by a second parabolic mirror whose focus is on the IR detector. The spectrometer was mounted on a platform unattached to the vacuum chamber at the same height as the fullerene

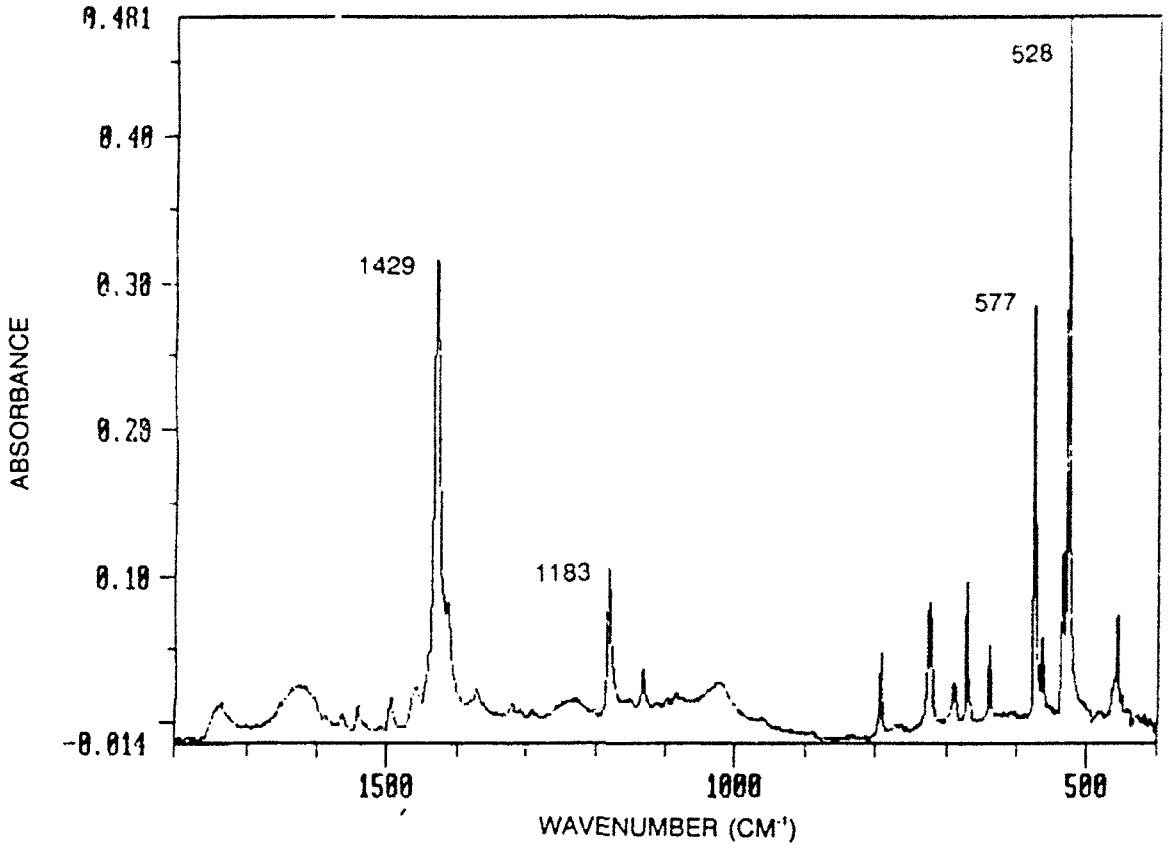

Fig. 9.1 Infrared Spectrum of the DEE-Washed Toluene Extract of HTLP Soot. The sample is pressed into a KBr pellet. C_{60} and C_{70} peaks are identified. Resolution = 2 cm^{-1}.

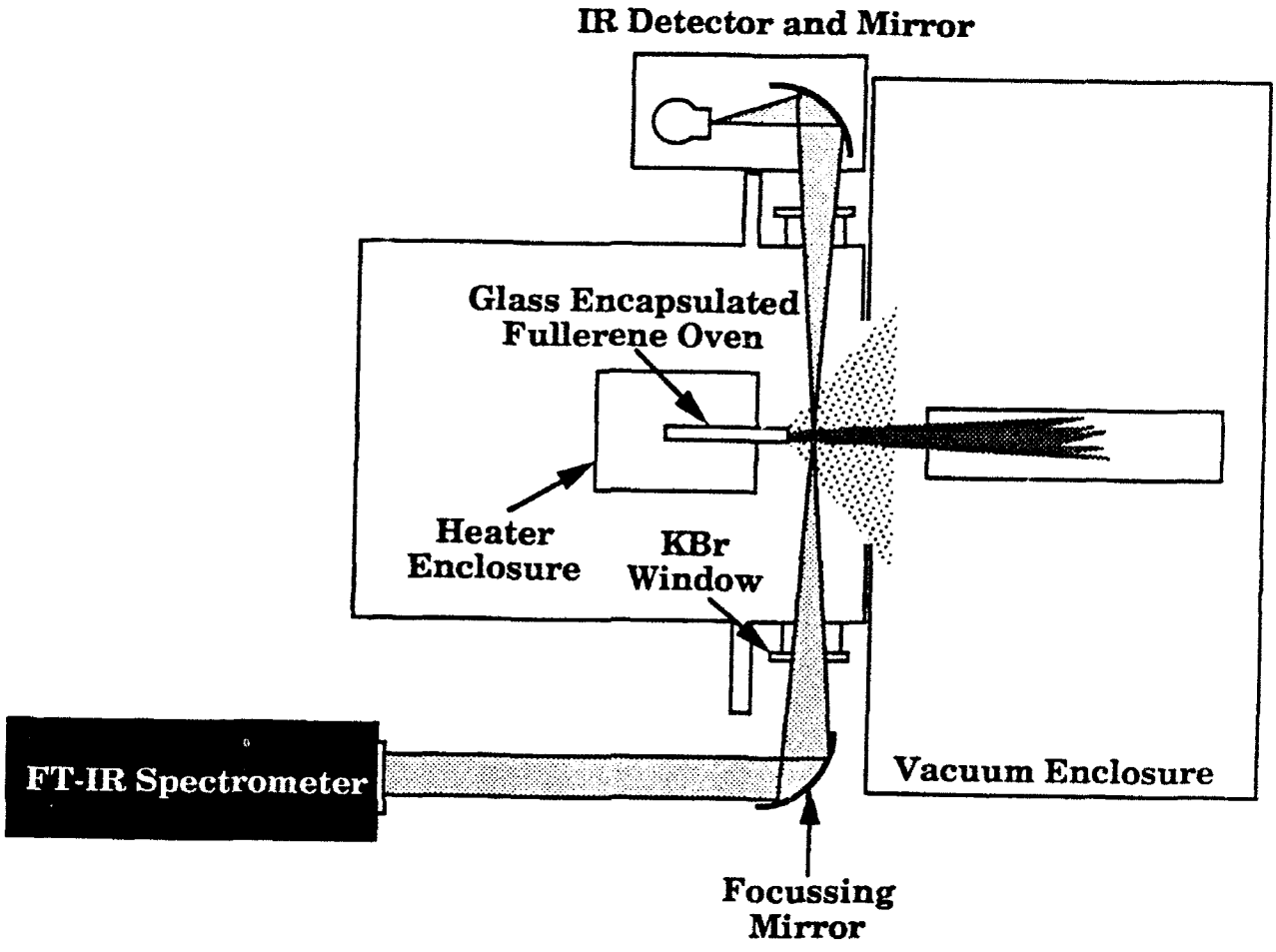

Fig. 9.2 Ion Engine Fullerene Source and FTIR Fullerene Detection Apparatus

oven. The IR detector was a liquid nitrogen cooled mercury cadmium telluride (MCT) photo conductive chip and amplifier, manufactured by Graseby Infrared. The IR output beam from the spectrometer was slightly diverging and had a gaussian intensity profile. This beam was initially 5 cm diameter, 55 cm from the focusing mirror (focal length = 30 cm) which gives focal spot of approximately .5 cm in diameter at the exit of the oven. Most of the beam's energy was confined to a diameter of about 2.5 cm around that spot. The window aperture diameter is 3.2 cm so some light was cut off of the beam entering and leaving the vacuum chamber through the KBr IR windows. The focal spot center was aligned with the axis of the molecular stream by a 6-axis translational/rotational mount attached to the vacuum chamber. The collection mirror and detector could be positioned independently on a common platform connected to the chamber by a 6-axis positioner.

The FTIR external optical system was crudely aligned using laser beams from within the spectrometer, followed by maximizing the detected IR signal by adjusting the position of both the final focussing mirror and detector position. The initial focussing mirror was positioned to be centered on both the output window and the centerline of the fullerene oven. Once the optics were aligned, the oven containing the fullerenes was heated in a programmed temperature profile to obtain a variety of fullerene concentrations and mass flow rates out of the glass fullerene chamber.

Fullerene detection tests consisted of taking transmission spectra at selected temperatures while heating the 80/20% mixture of C_{60}/C_{70}. The programmed temperature was stabilized and then held constant during the FTIR measurements. The total measurement time for each FTIR spectrum was kept to a minimum (1-2 minutes) to conserve the limited quantities of fullerenes available. A resolution of 4 cm^{-1} was chosen as a tradeoff between higher wavelength accuracy and longer scan time. Absorbance sensitivity is proportional to the square root of the number of individual FTIR scans that are added to generate a single, high sensitivity spectrum. The 4 cm^{-1} resolution was the lowest resolution (and fastest scan time) that allowed the fullerene absorbances to be fully resolved. At this resolution a measurement consists of typically 100 sequential scans (each less than 1 second) that are averaged to give a single detected transmission spectrum at each test temperature.

The sensitivity of a FTIR measurement can be calculated based on previous fullerene absorption measurements. At present, the best available calibration data comes from fullerene films. This data was obtained from the consultants at SRI, and it gives an absorbance value of 0.4/cm-torr of C_{60} vapor at 527 cm^{-1}. Thus a 1 micron pressure of C_{60} and a 10 cm pathlength for absorption would imply 4 milliabsorbance (mA) units peak height. The Bomem spectrometers have a noise level 0.4 mA for a single scan, so for 100 scans the noise level would be 0.06 mA (square root of number of scans). It is important to note the responsivity curve of the MCT detector, shown in Fig. 9.3. The detector-source combination is seen to be most sensitive in the central region of the spectrum, dropping off slowly at high wavenumbers (shorter wavelengths) and rapidly at smaller wavenumbers. In the case of fullerenes the sensitivity at 577 and 528 cm^{-1} is not great, and the 1429 cm^{-1} peak occurs in the same spectral region as atmospheric water vapor (in the beam outside the vacuum chamber). The 1183 cm^{-1} peak is the largest peak in a spectral region without interference, and it therefore most readily indicates the possible presence of C_{60}. Any indication at one wavenumber must be confirmed at the other wavenumbers in the proper proportion.

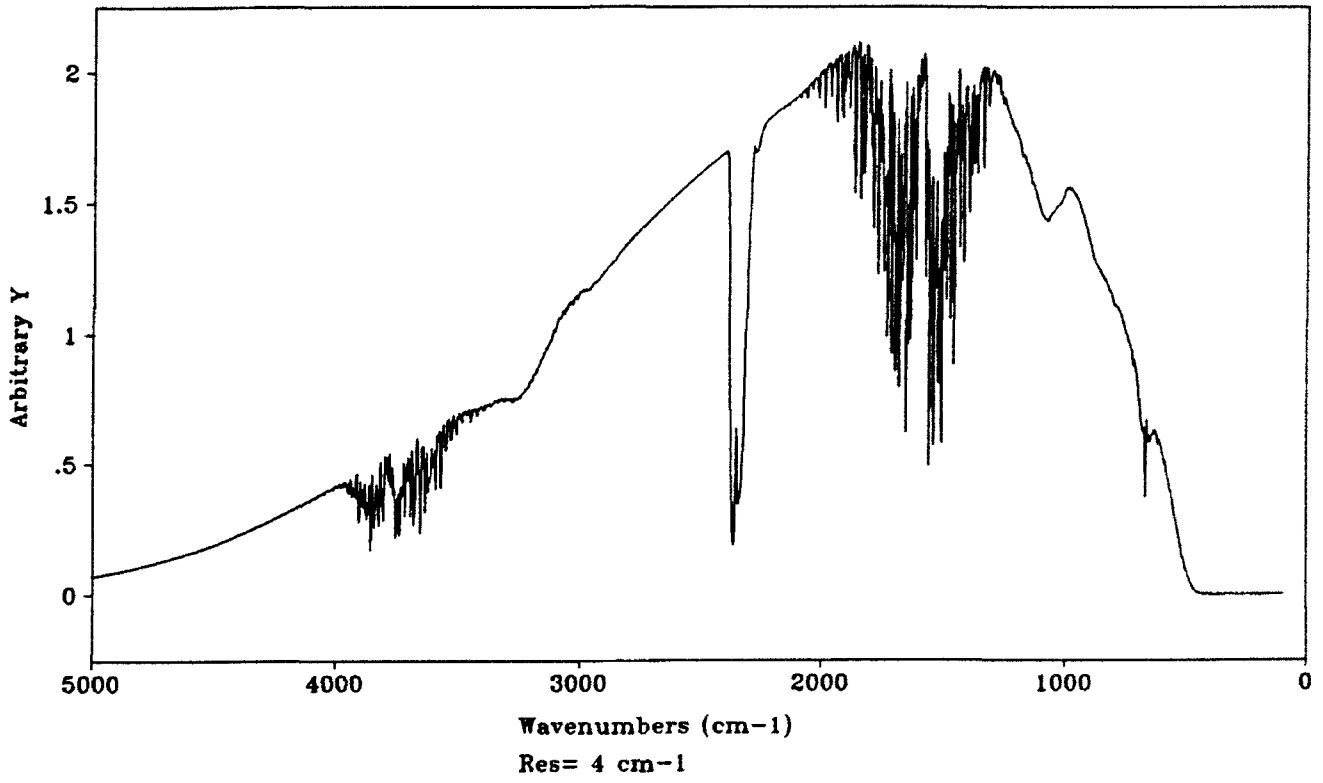

Fig. 9.3 Background Reference Spectrum Through Busek Vacuum Chamber

The geometry of the fullerene oven and vapor exhaust are another important characteristic of the FTIR measurement. The concentration-length product is the important factor; radiation is absorbed by the vapor over a pathlength of the absorbed beam as described by Beer's law. Lower concentrations can be detected by multipassing the absorbed beam. For the Busek apparatus of Fig. 9.2, the expected detection parameters can be assessed. The 1183 cm^{-1} peak that is most easily detected is down by a factor of three from the 527 cm^{-1} peak, and the pathlength through the exhaust may be as small as 3 cm, but even a pressure as low as 1 micron of C_{60} should be a factor of 10 above noise level. Oven pressures in the apparatus reach as high as 500 microns, but it is not known what the expansion factor is in the exhaust jet where the FTIR beam measures concentration.

9.3 Experimental Results and Analysis

Figure 9.4 shows the sequence of absorbance spectra for the testing period from an initially cold chamber, through high oven temperatures, to a final measurement of an oven cooled to less than 200°C. The most noticeable characteristics of the spectra are the water vapor and CO_2 that the IR beam passes through outside the vacuum chamber. The increasing, broad absorbance at 3200 cm^{-1} results from absorption by water ice inside the detector. Detection of species flowing from the fullerene oven is performed by using pre and post reference spectra to generate relative spectra during the tests so that the ambient molecular species, primarily CO_2 and H_2O, have been subtracted out. Only the top and bottom spectra show large changes in the concentration of other species than water and CO_2.

At an oven temperature of approximately 200°C there was a large increase in the vacuum chamber pressure as the fullerene sample exhibited outgassing typical of fresh fullerene samples, although the amount of outgassing was larger than seen previously. The oven temperature was maintained at 325°C until the pressure dropped to an acceptable level (10 microns). Figure 9.5 shows the spectrum of the evolving gas. This gas is clearly identified as diethyl ether (DEE) as shown by the feature match with its reference spectrum shown below. The DEE presumably originates from the solvent used to extract the fullerenes from their parent soot used by the manufacturer of this sample (Ulvick Industries).

Collected deposits from various locations in the vacuum chamber after previous experiments were found to contain only fullerenes, indicating that no breakdown of fullerenes was occurring. However, this test used a fullerene sample from a different manufacturer and had an unexpectedly large amount of outgassing that was measured as DEE by the FTIR system. The DEE contains oxygen and is unstable at the high temperatures later experienced in the chamber. The presence of oxygen could allow a variety of chemical reactions to take place, or even cause a breakdown of the fullerenes. The material remaining in the oven after these experiments was visibly unlike that of previous experiments. Whereas previously very little material remained after testing, after these experiments large, light blocks of material were found in the vaporization diameter chamber. For the measured spectra, it is assumed that the small changes in CO_2 and H_2O are due to changes in the ambient air conditions outside the reactor over the hours long testing period. Other species may also be present; Fig. 9.6 shows a correlation between a principle peak of acetylene (730 cm^{-1}) (Fig. 9.6 at top) and one of the lower-temperature spectra during the outgassing period of the sample.

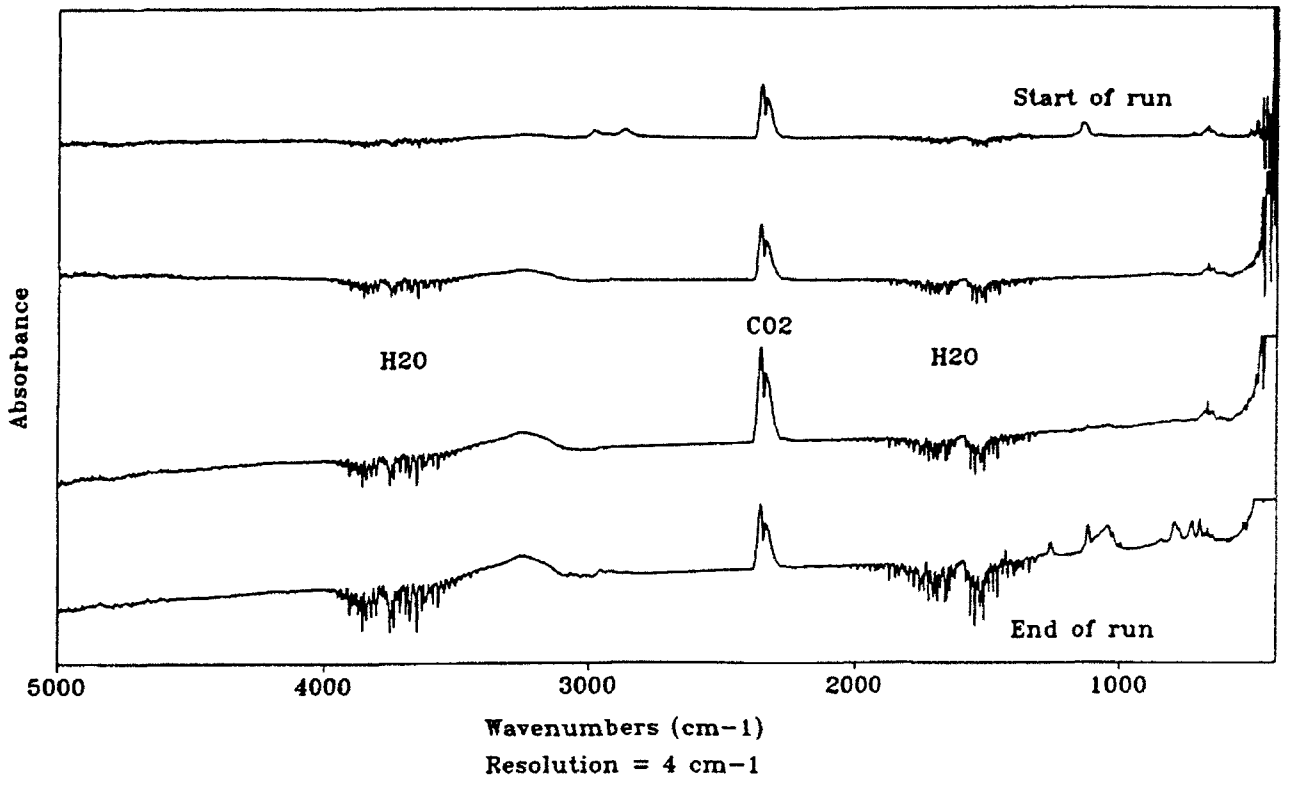

Fig. 9.4 Absorbance Spectra Vs. Time

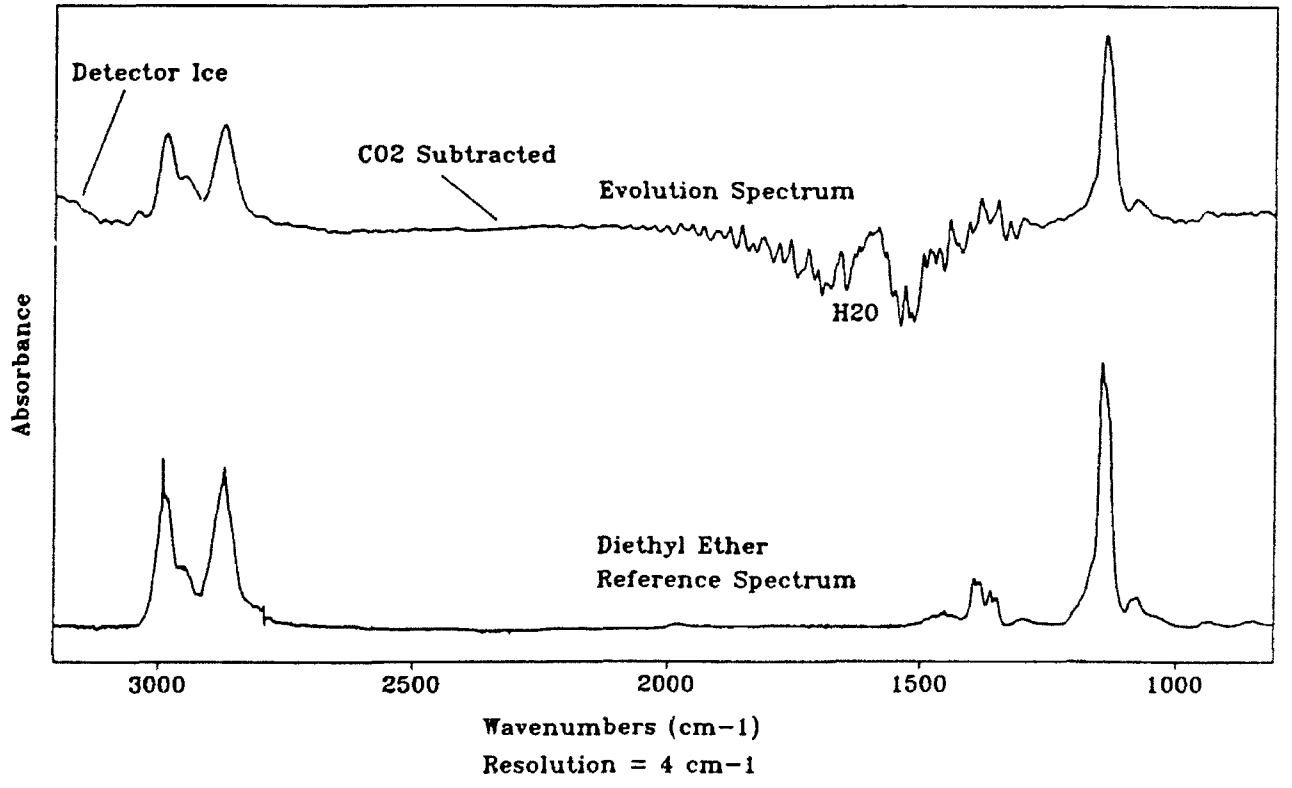

Fig. 9.5 Overlay of Diethyl Ether Reference and Evolved Solvent

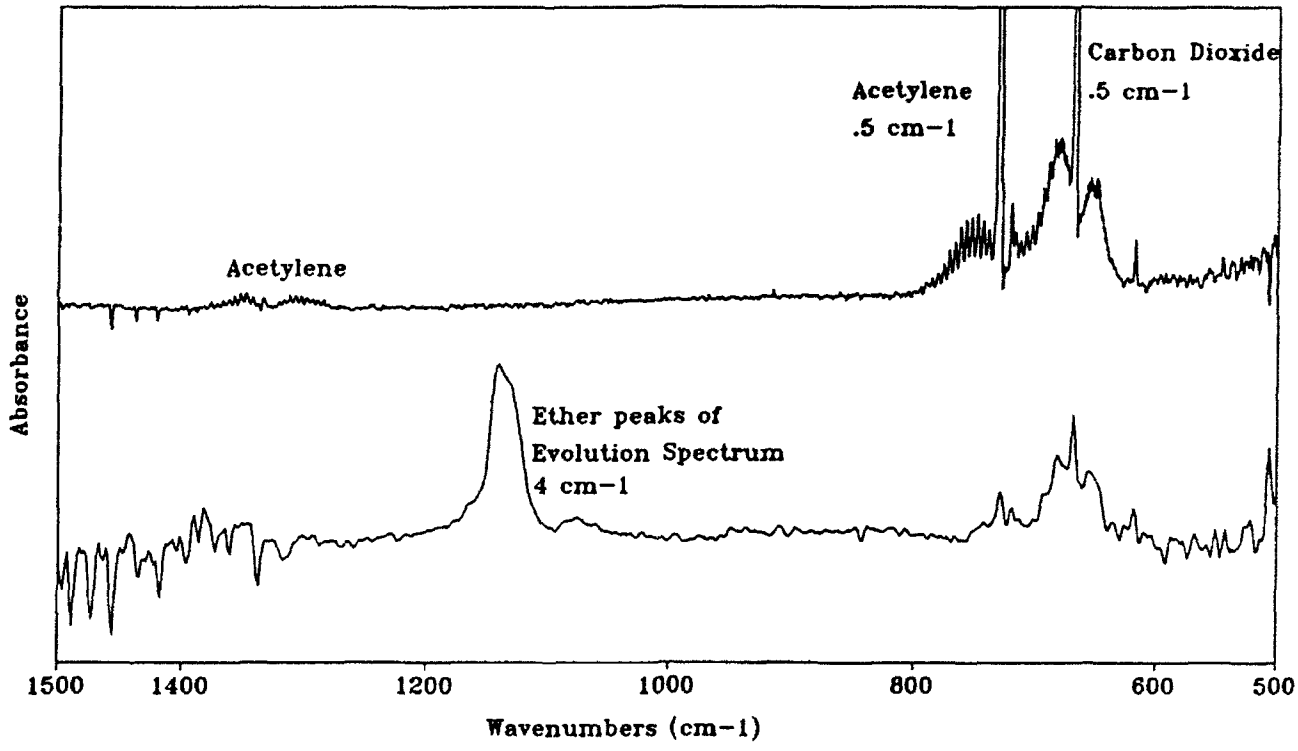

Fig. 9.6 Shows Solvent Evolution and Breakdown from Fullerene Sample

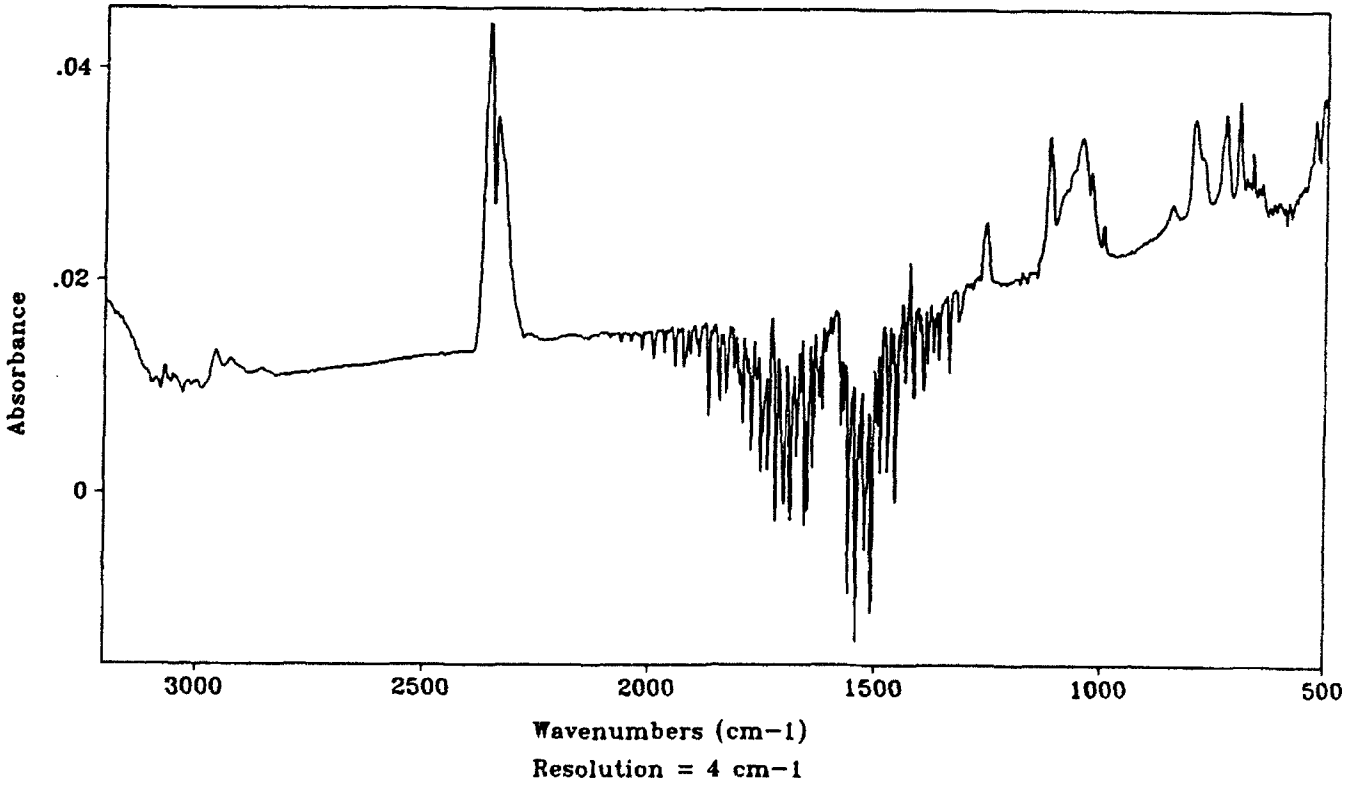

Fig. 9.7 Oven at Maximum Test Temperature

The fullerene oven was next heated to 600°C, the lowest temperature where the fullerene concentration in the oven exhaust stream was estimated to be observable, but no characteristic fullerene signature was seen. At a maximum oven temperature of 750°C the spectrum was as shown in Fig. 9.7. Although the ether absorbance has disappeared, there is no characteristic fullerene spectrum visible. Several times during heating a very weak peak at 1183 cm^{-1} could be seen when compared to the initial background reference, but since none of the other peaks could be seen it was concluded that this was due to noise. Spectra taken at lower temperatures also showed no signs of fullerenes using reference spectra taken after the sample had been baked out at lower temperatures.

Possible explanations for the lack of observed fullerene signature in the beam include expansion of the fullerene jet to too low a concentration, and misalignment of the IR beam. Since little mass loss from the vaporizer was seen during the latter part of the experiments, it seems probable that there were simply too few fullerenes exiting the nozzle. The experiment was originally designed to detect fullerenes immediately downstream of a 1 cm diameter orifice. Since the beam would pass through the exhaust close to the molecular flow orifice, it was thought that the concentration would be close to 1 micron pressure over a pathlength of a few centimeters. This would imply a noise level such that fullerenes could be detect d by a factor of 10 above noise level as discussed above, giving enough accuracy to detect minor breakdown products. As a result of last minute experimental changes for unrelated practical reasons, the orifice was made considerably smaller and placed further into the heating zone, 2.5 cm upstream of the first possible FTIR inspection location. This allowed the exhaust to expand and lower in concentration before it could be sampled. Misalignment also cannot be ruled out as an aggravating factor.

Although there was no immediate evidence of fullerenes during testing, careful post analysis showed the existence of the fullerene signature in a unexpected manner. An absorbance spectrum taken at the end of testing was examined using as a background the reference measurement taken before testing. The result, shown in Fig. 9.8 indicates the presence of the characteristic fullerenes absorbances. It is concluded that since there can be no fullerene vapors present at these test temperatures what has been measured is the deposition of fullerenes on the KBr windows along with the unknown solvents and impurities.

Reexamining the data at high temperature and using the appropriate reference data, Fig. 9.9 shows absorbance spectra taken as the oven heated up, first at 668°C and then at 700°C. At this time a thin brown film was observed on the inside surface of the KBr IR windows. Small absorbance peaks characteristic of C_{60} are seen to increase with time and temperature, indicating that a film is slowly depositing on the windows. In fact, the deposition continued as the chamber cooled. In the spectral region from 600 to 900 cm^{-1} absorbances can be seen that indicate species that are primarily aromatic nature, and there is an indication of aromatic absorbances just above 3000 cm^{-1}, though these higher wavenumber absorbances are much stronger when observing known aromatics. The CO_2 peak at 670 cm^{-1} is also visible, and low concentrations (ppm) of carbon monoxide were also incidentally detected in the room air. Absorptions in the region between 900 and 1200 cm^{-1} are probably due to the ether content of the film on the windows. The bands are shifted down as the ether is not free (as when we first observed DEE) but bonded in the film. The peak at 1250 cm^{-1} was not identified. These absorbance spectra clearly indicate the presence of fullerenes, marked by the proper four distinct absorbances, and they

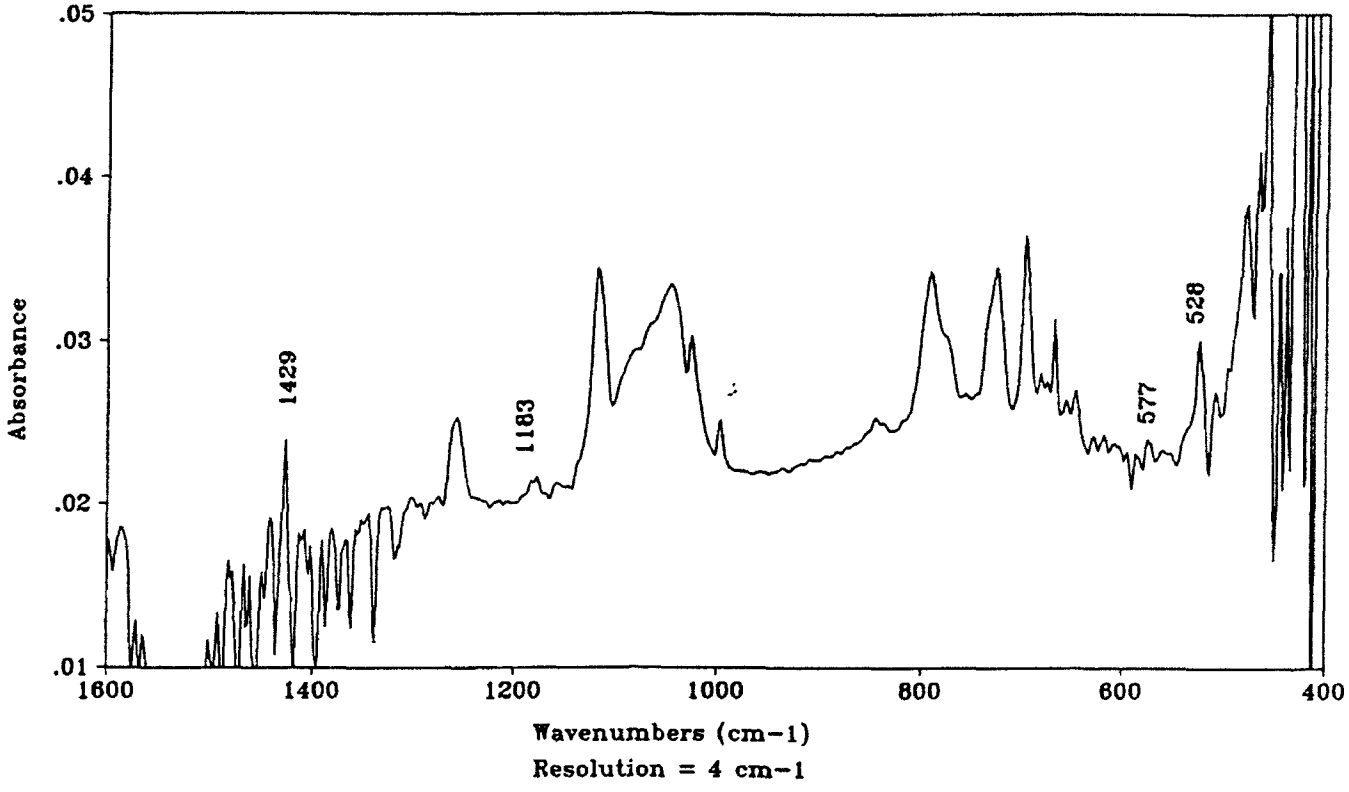

Fig. 9.8 Absorbance Spectrum of Post-Reference Background with Pre-Reference Background

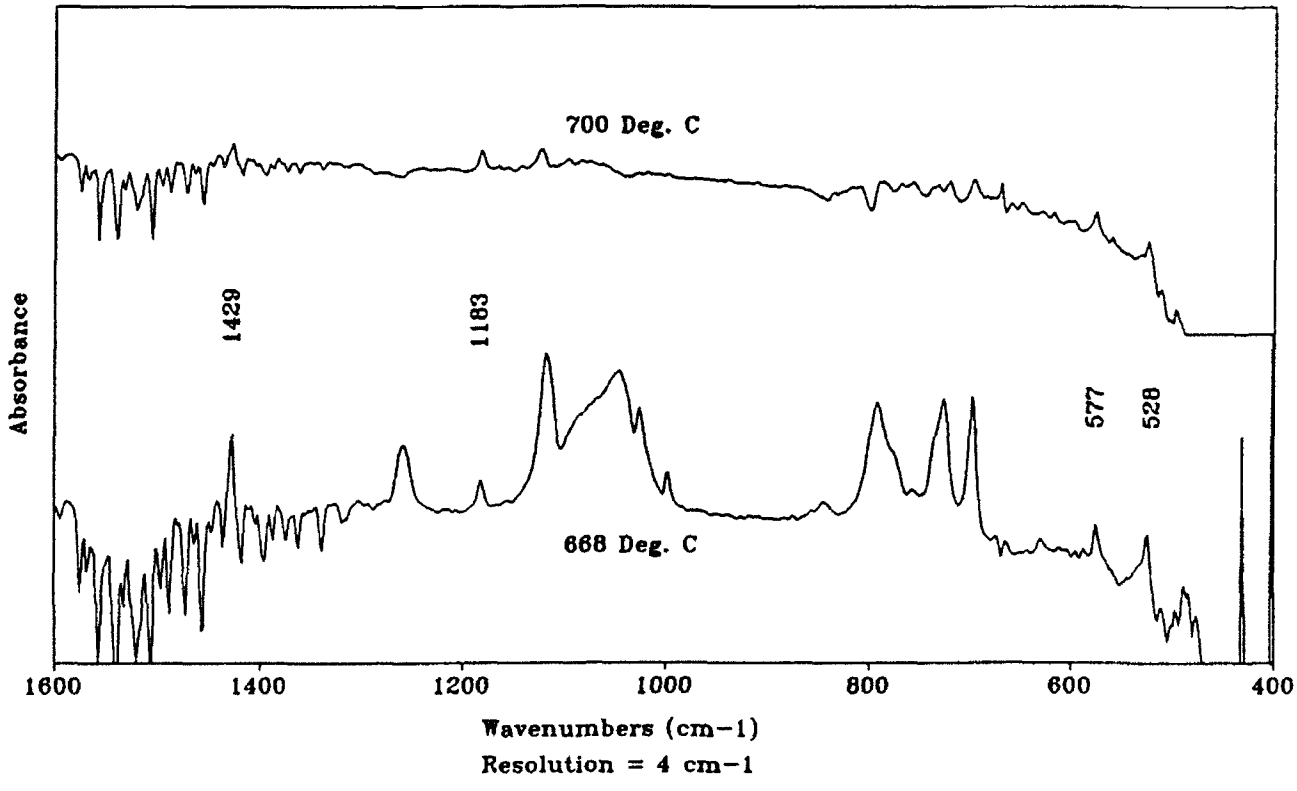

Fig. 9.9 Shows Deposition of C_{60} Film with Time and Temperature

demonstrate that the FTIR system can in fact detect the presence of fullerenes in a very sensitive manner.

9.4 Summary of FTIR Results

FTIR spectroscopy has been shown to be a sensitive detector of fullerenes that condensed on the KBr windows. The concentration-pathlength product of these vapors in the oven exhaust of the specific configuration that was accessible to the detection beam was not large enough to be detected. The cause of this low level of fullerenes in the detection volume could have been 1) depletion of vaporizable fullerenes in the reservoir (i.e., those infected by remainders of the solvent), 2) expansion of the exhaust jet into vacuum, or 3) misalignment of the detecting beam. A combination of the reasons seems the most likely explanation.

Fullerenes were detected, as were fullerene solvents and low concentrations (ppm) of carbon monoxide in the room air, indicating that the FTIR apparatus was working properly. Fortunately, analysis of the residues inside the vacuum tank demonstrated that there was no fragmentation of the fullerenes, so that FTIR monitoring of the breakdown products was a moot point for flow out of the oven. From these tests it is evident that the apparatus must be designed to allow direct access of the IR beam to the fullerene chamber and that this access permit significant pathlength (>5cm) for the measurement.

10.0 SPACECRAFT CONTAMINATION POTENTIAL

Condensation of plume-related C_{60} on spacecraft surfaces is a distinct possibility when fullerene is used as a propellant. Roughly speaking, the situation in this respect is similar to that for MPD systems using Lithium as a propellant, since the vapor pressures of these two materials are similar: at 400°C, P_v = 1.9 x 10^{-5} Torr of C_{60} and 8.9 x 10^5 for Li (down to 1.9 x 10^{-5} Torr at 370°C). Both will therefore condense on cool surfaces, although surface reactivity is likely to be less with C_{60}.

A quantitative evaluation of the deposition rate is not possible at this time due to lack of both, relevant data and reliable theory. Some data do exist for the case of Hg ion engines, and some semi-empirical correlation techniques were evolved in this connection, as reviewed recently by Samanta Roy and Hastings.[24] The charge-exchange ion current density or distance r(m) from the thruster exit (of radius r_b), when operating at a beam current I_b and propellant utilization factor η_p, using a propellant of molecular mass M (g/mol) and charge-exchange cross section σ_{CE} is given as

$$j_i = \frac{I_b^2(1-\eta_p)/\eta_p \sigma_{CE}\sqrt{M}\,10^{15}}{r_b\sqrt{T_n}} \frac{}{r^2}$$

where T_n is the neutral gas temperature (approximately the thruster wall temperature). This equation applies for angles of the order of 90° away from the beam. For greater angles (behind the thruster), Kaufman[25] has proposed an attenuation factor (exp (-1/2 $\cot^2\theta$), which somewhat overestimates the fluxes.

Consider a 2 Amp C_{60} ion beam, with η_u = 0.95. This high utilization factor is realistic for C_{60}, as shown by Torres.[16] The charge-exchange cross section of fullerene is not known, but we can estimate it[24] at between 10^{-18} and 10^{-19} m^2. At r = 5 m, and θ = 85°, the resulting j_i is equivalent to 0.1-1 monolayers/hr on a cold surface. An additional 1.5 monolayers/hr could be also collected directly as misdirected neutrals.

From data on C_{60} evaporation rate from $A\ell_2O_3$ surfaces, Samanta Roy has constructed a curve (Fig. 10.1) of surface temperature required to evaporate this arriving flux. Within the range considered, surface temperatures should be ~ 450 - 480 K. This could be somewhat reduced if the thruster is boom-mounted at r > 5 m.

More effective protection could be provided by shielding the thruster. A simple flat or cylindrical "shadow shield" could be quite effective in avoiding neutral flux at large backwards angles, since neutral (as well as charge-exchange ions) originate from the high-density region around the beam origin, and would not be coming from farther downstream. This shield could be kept cool enough by passive means to act as a cold trap for the C_{60}. The same approach could also be used against the slow charge-exchange ions which may be directed backwards, particularly if the shield is purposely maintained a few volts negative potential in order to selectively attract these ions (while keeping ambient electrons away).

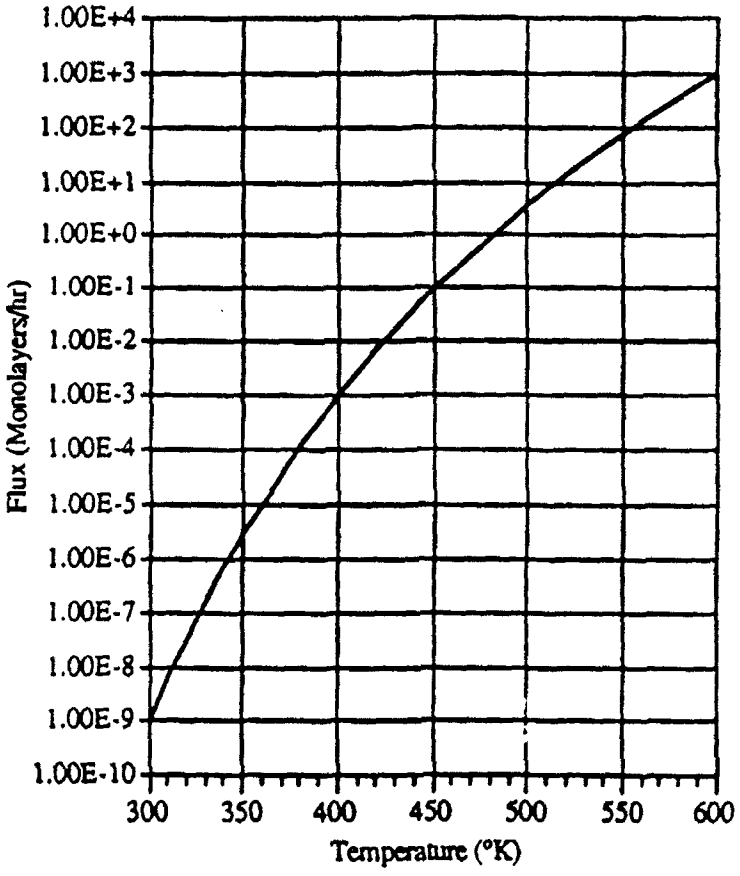

Fig. 10.1 Accumulation of C60 on $A\ell_2O_3$

(Reprinted from Ref. 24)

In summary, the C_{60} contamination issue is about as serious as the more familiar liquid-metal contamination issue. Given sufficient performance incentives, these problems should be amenable to engineering solutions, but much more data are required for proper evaluation.

11.0 CONCLUSIONS

The conclusions presented below are the same as those in Section 1.0 (Extended Abstract). They are reproduced here and expanded where appropriate.

All key objectives as set forth in the Phase I proposal were met and in most cases greatly exceeded. The salient overall conclusion is that the fullerene ion thruster is feasible and has the potential to fulfill its theoretical promise.

To prove the basic feasibility of the FIT concept, Busek designed and constructed balanced beam scale to measure fullerene mass flow rate, a fullerene vaporization and ionization chamber as well as simple acceleration grid which were used to perform a set of critical and unique experiments. The major accomplishments are as follows:

1) Fullerene compatibility with various metallic and dielectric materials was studied. Milligram quantities of fullerenes were evaporated from SST, molybdenum, alumina, boron nitride, aluminum nitride, and quartz substrates. Substrates and residue of fullerenes were analyzed. No reaction has been found with any materials although some substrates were visually stained. Containment of fullerene solids and vapor in SST vessels should be no problem. However, due to initial concerns expressed by SRI over SST catalyzed unknown fullerene reactions we selected quartz as the material for our fullerene flow train experiment.

2) FTIR spectroscopy was not able to detect highly diffused free molecular stream of fullerene vapor but it did detect fullerene condensation coating on IR windows and presence of solvents coming off the fullerenes during heating. Refinement of the optical access and application to denser vapor is likely to make this technique successful.

3) Preliminary assessment of spacecraft contamination by fullerene thruster effluent was carried out. The contamination is comparable to that projected for lithium. Concepts to reduce it include placement of the thruster on a boom and shrouding the exhaust by an electrified cone which traps ions and condenses fullerenes that deviate from proper trajectory.

4) Fullerene vapor generation and control was demonstrated. Samples of up to 9 grams were evaporated from a quartz vessel. Mass flow was measured real time by measuring mass loss rate of the sample and verified by pre and post test sample weight measurements. Mass closure within $\pm$ 8% was obtained in three short duration tests. A mass closure within 16% was obtained in a three hour test. As much as 7% of the initial sample remained as process residue not vaporizable at 700°C.

5) A discharge in fullerene vapor was established using 2% thoriated tungsten filament in a quartz chamber. A stable discharge voltage of approximately 190 volts was measured. Lowest discharge voltage obtained was approximately 60 volts which increased to 190 volts in steps of about 30 to 40 volts each time discharge was re-initiated. Graphite coating was found

on the cathode as well as possible thorium carbide. Possible explanation for high discharge voltage may be: (1) continuous forming of insulating fullerite layer that must be converted to graphite to maintain discharge, (2) formation of thorium carbide, and (3) high collisional losses, which is however unlikely but no collisional cross section data exist so it cannot be excluded. The coating is likely to lead to local high emission spots that become space charge limited and cause further increase in discharge voltage.

6) No fullerene fragmentation occurred due to vaporization, ionization, and acceleration as determined from samples collected in various parts of the system with the exception of an area in the back of the cathode where the deposit was found to be graphitic. This area was probably overheated by the high temperature cathode filament.

7) An ion beam of about 20 mA was recorded. The beam ion energy cost was estimated to be 915 eV/beam ion. Propellant utilization assuming single ionization was estimated to be 70%. These results are based on short duration tests and must be repeated to verify their accuracy.

This broad set of unique results reported above was achieved by the synergism of two DOD Phase I SBIR contracts. The first is the present, just completed fullerene ion thruster work, and the second is fullerene fueled SPT thruster program currently in progress. Knowledge so far gained in the SPT work is included here to present a more complete picture. It is hoped that this synergism will continue into the next phase of both programs.

REFERENCES

1. J.S. Sovey, et al., "The Evolutionary Development of High Specific Impulse Electric Thruster Technology," AIAA-92-1556, March 1992.

2. D.G. Fearn, "Factors Influencing the Integration of the UK-10 Ion Thruster System with a Spacecraft," AIAA Paper 87-1004 (1987).

3. V.K. Rawlin, "Operation of the J-Series Thruster Using Inert Gas," NASA TM-82977, AIAA 82-1929 (1982).

4. B.A. Free and J.D. Dunlop, "Battery-Powered Electric Propulsion for North-South Station Stationkeeping," COMSAT Technical Review CTR73/033, Vol. 3, Spring 1973, pp. 209-214.

5. R. Schreib, "Utility of Xenon Ion Stationkeeping,": Paper AIAA-86-1849, Presented at the AIAA/ASME/SAE, ASEE 22nd Joint Propulsion Conference, Huntsville, AL, 16-18 June 1986.

6. R.L. Poeschel, "Ion Propulsion for Communications Satellites," Paper IEPC-84-43, Presented at the JSASS/AIAA/DGLR 17th International Electric Propulsion Conference, Tokyo, Japan, May 1984.

7. J.R. Beattie, J.N. Matossian and R.R. Robson, "Status of Xenon Ion Propulsion Technology," AIAA Paper No. AIAA-87-1003(1987). Also, "High Power Xenon Ion Thrusters," AIAA-90-2540 (Beattie, J.A. and Matossian, J.N.).

8. J. Hermel, et al., "A Molecular, Ion Propelled, Orbit Transfer Vehicle, Paper AIAA-86-1394, Presented at the AIAA/ASME/SAE, ASEE 22nd Joint Propulsion Conference, Huntsville, AL, 16-18 June 1986.

9. T.L. Hardy and V.K. Rawlin, "Electric Propulsion Options for the SP-100 Reference Mission," National Aeronautics and Space Administration, Lewis Research Center, Cleveland, OH, NASA Technical Memorandum 88918, January 1987.

10. M.L. Day, T.S. Colbert and S.H. Max, "Intelsat VII Ion Propulsion Subsystem Implementation," AIAA 90-2550.

11. D. Lorentz, SRI International, Letter to V.J. Hruby, 7 August 1992.

12. J. Abrefah and D.R. Olander, "Vapor Pressure of Buckminsterfullerene," Appl. Phys. Lett. 69 (11), March 1992.

13. H.S. Chen, et al., "Thermodynamics of C_{60} in Pure O_2, N_2, and Ar," J. Phys. Chem. 1992, 96, 1016-1018, December 1991.

14. Y.K. Bae, et al., "Production, Characterization, and Deposition of Carbon Clusters," Symposium on Clusters and Cluster Assembed Materials Special Session on Buckminsterfullerene, Boston.

15. J.R. Beattie and J.N. Matossian, "Mercury Ion Thruster Technology," Final Report, NASA CR-174974, March 1989.

16. E.R. Torres, "Prediction of the Performance of an Ion Thruster Using Buckminsterfullerene as the Propellant," Master of Science Thesis, MIT, February 1993.

17. J. Brophy and C. Garner, "A 5,000 Hour Xenon Hollow Cathode Life Test," AIAA-91-2122, June 1991.

18. H. Miyoshi, et al., "Microwave Ion Thruster with Electron Cyclotron Resonance Discharge," AIAA-91-084.

19. G. Perrotta, et al., "Orbital Control and Nanoeuvering of Lightsats/Synchronous Satellites: Assessment of New Ion Propulsion Technologies, Based on the Electron Cyclotron Resonance Phenomenon, to Improve the Performances of Thrusters in the Millinewton Range," AIAA-91-121.

20. N.B. Colthup, L.H. Daly, and S.E. Wiberly, Introduction to Infrared and Raman Spectroscopy, Academic Press, New York, NY,(1990)

21. J.T. McKinnon, W.L. Bell, and R.M. Barkley, "Combustion Synthesis of Fullerenes", Combustion and Flame, **88**, 102-112, (1992).

22. C.I. Frum, R. Engleman Jr., et al., "The Infrared Emission Spectrum of Gas-Phase C_{60} (Buckminsterfullerene)," Chem. Phys. Lett., **176**, 6, 504-507, 1 Feb., (1991).

23. J.P. Hare, H.W. Kroto, and R. Taylor, "Preparation and UV/Visible Spectra of Fullerenes C_{60} and C_{70}," Chem. Phys. Lett., **177**, 4,5, 394-398, 1 March, (1991).

24. R.I. Samanta Roy and D.E. Hastings, "Electric Propulsion Contamination," AIAA-92-3560, July 1992.

25. H.R. Kaufman, "Charge-Exchange Plasma Generated by an Ion Thruster, NASA CR-134844, June 1975.